

**MECHANISM AND METAL SPECIFICITY OF ZINC-DEPENDENT
DEACETYLASES**

by

Samuel G. Gattis

A dissertation submitted in partial fulfillment
of the requirements for the degree of
Doctor of Philosophy
(Biological Chemistry)
in the University of Michigan
2010

Doctoral Committee:

Professor Carol A. Fierke, Chair
Professor William L. Smith
Associate Professor Ursula H. Jakob
Associate Professor Bruce A. Palfey
Associate Professor Raymond C. Trievel

© Samuel G. Gattis 2010
All rights reserved

ACKNOWLEDGEMENTS

Many people deserve acknowledgement for their hand in getting me to this point. First, I would like to thank Carol for being a truly great advisor. Learning how to be a scientist from you has been a real pleasure, and I am very grateful for the freedom you gave me to explore my ideas and the guidance you gave when I needed it. I also wish to thank the great members of the Fierke lab past and present, including Marcy, Stephanie, June, Jimmy, Terry, John, Nathan, Kristin, Andy, and others, who challenged me with spirited discussions, to say the least. No one can leave this lab without being able to critique and defend data, and that is a reflection on our great mentor and the colleagues we have. I also must thank my thesis committee, but especially Bruce, who was my original scientific mentor, and showed me my first enzyme assay – there was no turning back.

Thanks also go to my scientific collaborators. Marcy Hernick and Jim Penner-Hahn (Univ. of Michigan) contributed experiments and EXAFS analysis in Chapter 3 as noted, for which I am grateful. Saumen Chakraborty and Jody Lancia helped me get started in peptide synthesis described in Chapter 2. I also thank Dan Dowling of the University of Pennsylvania for allowing me to show his Fe-HDAC8 structure in the discussion of Chapter 5. Ted Huston (Univ. of Michigan) was invaluable in performing ICP-MS measurements used throughout this work.

I am also grateful to the tremendous support I received from my family, including my parents, who put me through undergrad and always supported a culture of education in our family. Even when they had no idea what I was doing, I always knew I had their support. I also have had the great privilege of marrying into another wonderful family, who have always been available for anything over the years.

Lastly, I must thank Sarah, for learning to live with me during these years, and for willing to sign up for another round of this at our next stop. I couldn't have done this without your support. When I wasn't sure anything was ever going to work out, I knew you were still a fan, and that was enough to keep me going. Thank you.

Best wishes,
Sam
April, 2010

TABLE OF CONTENTS

ACKNOWLEDGEMENTS.....	ii
LIST OF FIGURES.....	v
LIST OF TABLES.....	vii
LIST OF EQUATIONS.....	viii
ABSTRACT.....	ix
CHAPTER 1. INTRODUCTION.....	1
Biological zinc and iron sites.....	1
Lipid A biosynthesis.....	7
Transport and modification of Lipid A.....	11
Activation of immune system by LPS.....	12
Structure and mechanism of LpxC.....	14
LpxC inhibitors as antibiotics.....	21
Histone deacetylases.....	23
Histones and the nucleosome.....	24
Classes of histone deacetylases.....	27
HDAC inhibitors as therapeutics.....	28
HDAC8 structure and mechanism.....	28
Activity of HDAC8 affected by active site metal ion.....	32
Goals of this work.....	33
References.....	34
CHAPTER 2. MECHANISM OF LPXC PROBED BY MUTAGENESIS AND EXPRESSED PROTEIN LIGATION.....	46
Introduction.....	46
Materials and methods.....	50
Results.....	55
Discussion.....	63
References.....	68

CHAPTER 3. ACTIVATION OF ESCHERICHIA COLI UDP-3-O-(R-3-HYDROXYMYRISTOYL)-N-ACETYLGLUCOSAMINE DEACETYLASE BY Fe^{2+} YIELDS A MORE EFFICIENT ENZYME WITH ALTERED LIGAND AFFINITY.....70

Introduction.....	70
Materials and methods.....	73
Results.....	79
Discussion.....	95
References.....	102

CHAPTER 4. THE ACTIVE SITE METAL ION IN UDP-3-O-(R-3-HYDROXYMYRISTOYL)-N-ACETYLGLUCOSAMINE DEACETYLASE (LPXC) SWITCHES BETWEEN Fe^{2+} AND Zn^{2+} DEPENDING ON CELLULAR CONDITIONS.....107

Introduction.....	107
Materials and methods.....	110
Results.....	116
Discussion.....	124
References.....	132

CHAPTER 5. Fe^{2+} -DEPENDENT ACTIVITY OF HDAC8.....137

Introduction.....	137
Materials and methods.....	138
Results.....	143
Discussion.....	150
References.....	157

CHAPTER 6. SUMMARY, CONCLUSIONS, AND FUTURE DIRECTIONS....161

Summary and conclusions.....	161
Future directions.....	166
Concluding remarks.....	171
References.....	172

LIST OF FIGURES

Figure 1.1. Reactions catalyzed by selected zinc hydrolases.....	3
Figure 1.2. Mechanism of zinc proteases.....	4
Figure 1.3. Peptide deformylase pathway and mechanism.....	6
Figure 1.4. Gram-negative cell membrane.....	8
Figure 1.5. Lipid A biosynthetic pathway.....	10
Figure 1.6. Modification to Kdo ₂ -Lipid A.....	13
Figure 1.7. Topology and active site of LpxC.....	16
Figure 1.8. Proposed chemical mechanism of LpxC.....	19
Figure 1.9. Crystal structure of LpxC with tetrahedral mimic.....	20
Figure 1.10. Selected LpxC inhibitors.....	22
Figure 1.11. Structure of the nucleosome.....	25
Figure 1.12. Proposed mechanism of histone deacetylases.....	26
Figure 1.13. Selected HDAC inhibitors.....	29
Figure 1.14. Topology and active site of HDAC8.....	30
Figure 2.1. Proposed mechanisms for LpxC catalysis.....	48
Figure 2.2. Expressed protein ligation.....	49
Figure 2.3. Schematic of LpxC-Intein plasmid construction.....	51
Figure 2.4. Product binding of H265 mutants.....	58
Figure 2.5. Cysteine mutants in <i>E. coli</i> and <i>A. aeolicus</i> LpxC.....	60

Figure 2.6. Analogues used in EPL studies.....	60
Figure 2.7. Altered pH dependence in LpxC-pyrAla.....	62
Figure 3.1. LpxC reaction and structures.....	72
Figure 3.2. Activation of apo-LpxC by Zn ²⁺ or Fe ²⁺	81
Figure 3.3. Steady-state turnover catalyzed by EcLpxC.....	84
Figure 3.4. pH dependence of LpxC.....	84
Figure 3.5. XAS of Fe ²⁺ -EcLpxC.....	87
Figure 3.6. Dependence of LpxC activity on reducing agents.....	94
Figure 3.7. Native LpxC activity.....	96
Figure 3.8. Proposed mechanism of FeLpxC.....	99
Figure 4.1. Role LpxC in Lipid A biosynthesis.....	108
Figure 4.2. Metal content of EcC63A LpxC-ZZ isolated from <i>E. coli</i>	118
Figure 4.3. Native LpxC activity as a function of metal ²⁺ and oxygen exposure.....	121
Figure 4.4. Affinity of C63A-LpxC for Fe ²⁺ and Zn ²⁺	123
Figure 4.5. LpxC metal ion dissociation <i>in vitro</i>	123
Figure 4.6. Calculated Fe•LpxC fraction as a function of [Fe] _{free} and [Zn] _{free}	129
Figure 5.1. HeLa cell lysate is oxygen sensitive.....	144
Figure 5.2. Immunoprecipitated HDAC8 is oxygen sensitive.....	146
Figure 5.3. Inhibition by SAHA is dependent on the active site metal.....	148
Figure 5.4. HDAC8 metal affinity.....	149
Figure 5.5. Fe- and Zn-substituted HDAC8 structures are nearly indistinguishable.....	153
Figure 6.1. Possible LpxC chemical mechanisms.....	162
Figure 6.2. Analogues used in EPL studies.....	162

LIST OF TABLES

Table 2.1. Expressed protein ligation yields.....	49
Table 2.2. Effect of mutagenesis at H265 on LpxC catalysis.....	57
Table 2.3. Enzymatic activity of <i>A. aeolicus</i> LpxC substituted at H253 by EPL.....	62
Table 3.1. Steady-state activity parameters for EcLpxC	83
Table 3.2. XANES pre-edge areas.....	88
Table 3.3. Fitting results for Fe-LpxC.....	89
Table 3.4. LpxC molecular recognition parameters.....	92
Table 4.1. Metal stoichiometry of EcC63A LpxC-ZZ purified from <i>E. coli</i>	118
Table 4.2. Kinetic and thermodynamic parameters of LpxC-C63A.....	120
Table 4.3. Metal content of holo-LpxC-ZZ after incubation with <i>E. coli</i> lysates.....	120
Table 5.1. HDAC8 metal content from recombinant expression in <i>E. coli</i>	144
Table 5.2. SAHA inhibition constants.....	148

LIST OF EQUATIONS

Equation 3.1.....	75
Equation 3.2.....	75
Equation 3.3.....	76
Equation 3.4	77
Equation 4.1.....	113
Equation 4.2.....	113
Equation 4.3.....	114
Equation 4.4.....	122
Equation 4.5.....	122
Equation 5.1.....	142
Equation 5.2.....	143
Equation 5.3.....	155

ABSTRACT

**MECHANISM AND METAL SPECIFICITY OF ZINC-DEPENDENT
DEACETYLASES**

by

Samuel G. Gattis

Chair: Carol A. Fierke

Metal-dependent deacetylases catalyze a variety of essential reactions in nature, and it is estimated that over 10% of all human proteins require zinc for activity. However, most metalloamidases can be activated by a number of divalent metal ions. The metal functions as a catalytic cofactor in numerous classes of hydrolytic reactions by coordinating and polarizing a nucleophilic water and coordinating substrate.

One metal-dependent deacetylase, UDP-3-*O*-(*R*-3-hydroxymyristoyl)-*N*-acetylglucosamine deacetylase (LpxC), catalyzes the committed step in Lipid A biosynthesis. Lipid A is the major lipid component of the outer membrane in Gram-negative bacteria, and is essential for cell viability. Consequently, inhibitors of Lipid A biosynthesis are targets for the development of antibacterials.

Two chemical mechanisms consistent with the current data have been proposed: a glutamate that functions as both a general acid and general base with a conserved histidine functioning as an electrostatic catalyst, or a general acid/general base pair mechanism. Mutagenesis and expressed protein ligation experiments were performed to

distinguish between these mechanisms. LpxC was activated by a general acid analogue and inactive with a positively charged analogue, indicating the general acid/general base pair mechanism is most likely. The techniques developed here solve a persistent mechanistic question and have the potential to be applied to similar mechanistic questions in many other enzymes.

Additionally, the metal specificity of LpxC was explored. *In vitro*, Fe²⁺LpxC is more active than ZnLpxC. In addition, LpxC purified anaerobically from *E. coli* contains mainly bound Fe, although the bound Fe/Zn ratio varies with metal availability. Thermodynamic and kinetic studies of LpxC metal binding show that these results can be explained by thermodynamics without metal chaperones, as is observed in other metalloproteins. Another zinc-dependent deacetylase, histone deacetylase 8 (HDAC8), has a similar metal dependence. HDAC8 is more active with Fe²⁺ than Zn²⁺, and exhibits Fe²⁺-like activity *in vivo*, suggesting that many “Zn”-enzymes may in fact use either Fe or Zn cofactors *in vivo*. These results are important for understanding how best to inhibit the many clinically useful metalloprotein drug targets, as well as for understanding a potentially important new aspect of metal ion homeostasis and metalloprotein regulation.

CHAPTER 1. INTRODUCTION

Biological Zinc and Iron Sites

It is estimated that ~47% of all known proteins require a metal ion (1). After magnesium, zinc is the second most common metal, and it is thought over 10% of all the proteins in the human genome require zinc for activity (2-5). In many enzymes, zinc ions play a structural role by stabilizing protein structure, while in others the zinc activates catalysis as a catalytic or co-catalytic metal ion.

Among the first structural roles proposed for zinc was in a class of transcription factors now known as the 'zinc fingers' (6, 7). These proteins bind DNA to control transcription in response to stimuli, including in response to metal binding *in vitro*. The most abundant metal binding site in structural zinc ions is a Cys₂His₂ motif. These domains are characterized by the arrangement of (Tyr/Phe)-X-Cys-X₂₋₄-Cys-X₃-Phe-X₅-Leu-X₂-His-X_{3,5}-His, where X is a variable site (6). Classical Zn-fingers such as TFIIIA are characterized by an arrangement where the zinc ligands are shared between an α -helix and a β -sheet separated by a flexible linker. Because of their ability to specifically recognize DNA sequence elements, Zn-fingers have attracted attention as potential artificial transcriptional regulators (8).

Zinc also has several features that make it an ideal metal ion for catalyzing enzymatic reactions. Zinc is a strong lewis acid, meaning it readily accepts an electron pair. Zinc also has a full d¹⁰ electron configuration, and is therefore not redox-active.

Enzyme-bound zinc ions can catalyze a variety of hydrolytic reactions (Figure 1.1) by coordinating a nucleophilic water molecule, thereby lowering its pK_a for nucleophilic attack of a substrate at neutral pH. In addition, the catalytic zinc ion can also coordinate the substrate carbonyl to enhance the electrophilicity of the carbonyl carbon, thereby accelerating catalysis (9-11). The most common zinc ligand in catalytic sites is His, but Glu, Asp, and Cys are also common (12, 13). While zinc-dependent enzymes catalyze numerous types of hydrolytic reactions (Figure 1.1), among the first and most widely studied class is the metalloproteases, such as thermolysin, carboxypeptidase, and the matrix metalloproteases. These proteases catalyze the cleavage of peptide bonds in a variety of proteins important for regulatory processes in cells, and hence have been the targets of inhibitor development (14-16).

Carboxypeptidase A (CPA) is a prototypical metalloprotease and much of the structural and mechanistic work for this family of enzymes was done on CPA (14). As is typical for many zinc enzymes, CPA uses general acid/base chemistry to catalyze peptide bond hydrolysis, where glutamate 270 is the essential residue that fulfills both roles (Figure 1.2). The catalytic zinc ion, bound to a His₂Glu ligand set, coordinates a nucleophilic water molecule in the ground state as well as interacting with the carbonyl of the peptide bond to be cleaved by the enzyme. The zinc-bound water is deprotonated by Glu270, acting as a general base, as it attacks the carbonyl carbon, forming a tetrahedral intermediate. This species is stabilized by a positively charged Arg side chain as well as by the zinc ion. As the intermediate breaks down to form the products, the newly formed amino-terminus is protonated by Glu270, now acting as a general acid. This mechanism, with different residues playing the role of general acid, general base, and stabilization of

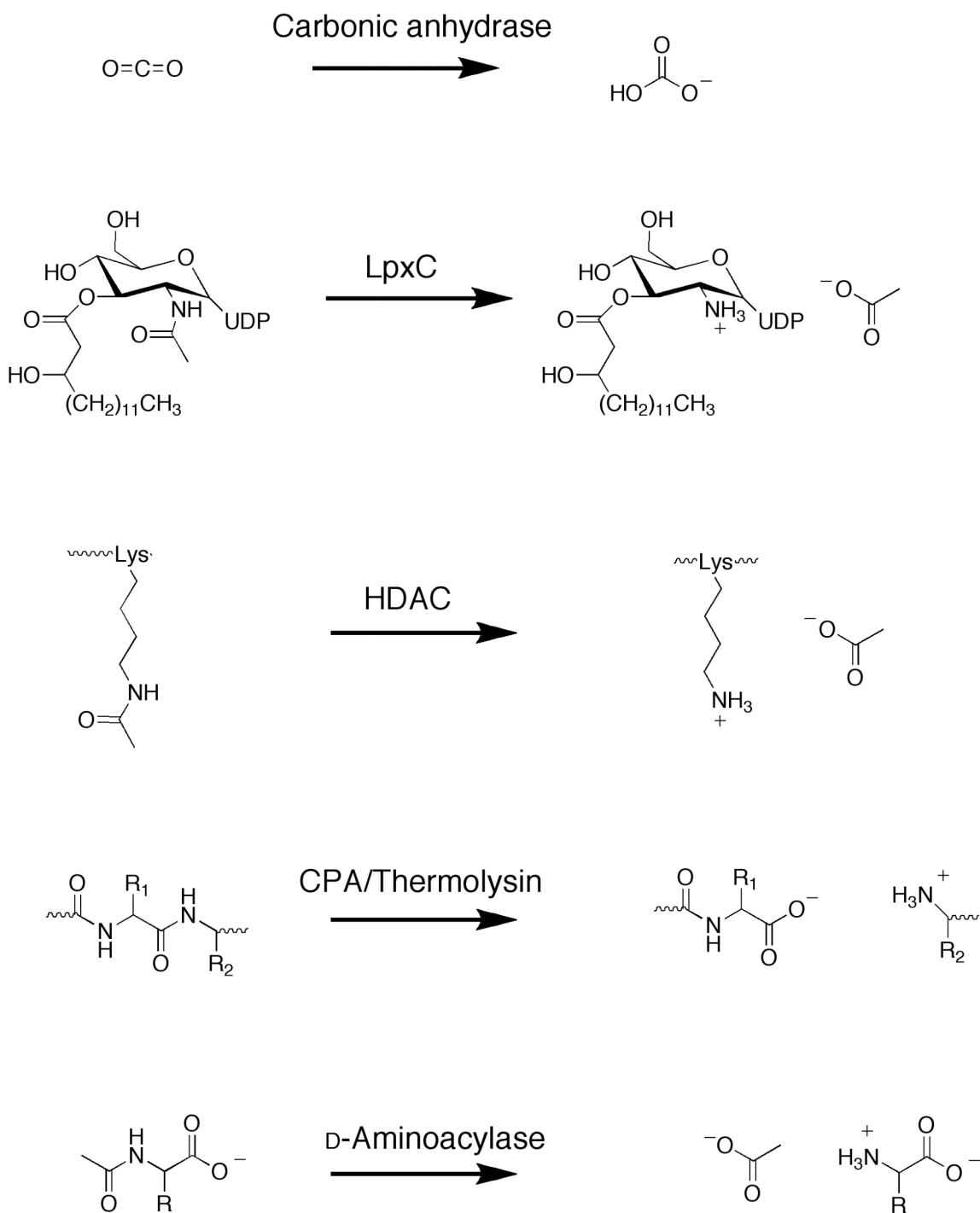


Figure 1.1: Reactions catalyzed by selected zinc hydrolases. The reactions catalyzed by CA (carbonic anhydrase), LpxC (UDP-3-*O*-(*R*-3-hydroxymyristoyl)-*N*-acetylglucosamine deacetylase), HDAC (histone deacetylase), CPA (carboxypeptidase) and thermolysin, and D-aminoacylase are shown as examples of zinc hydrolases.

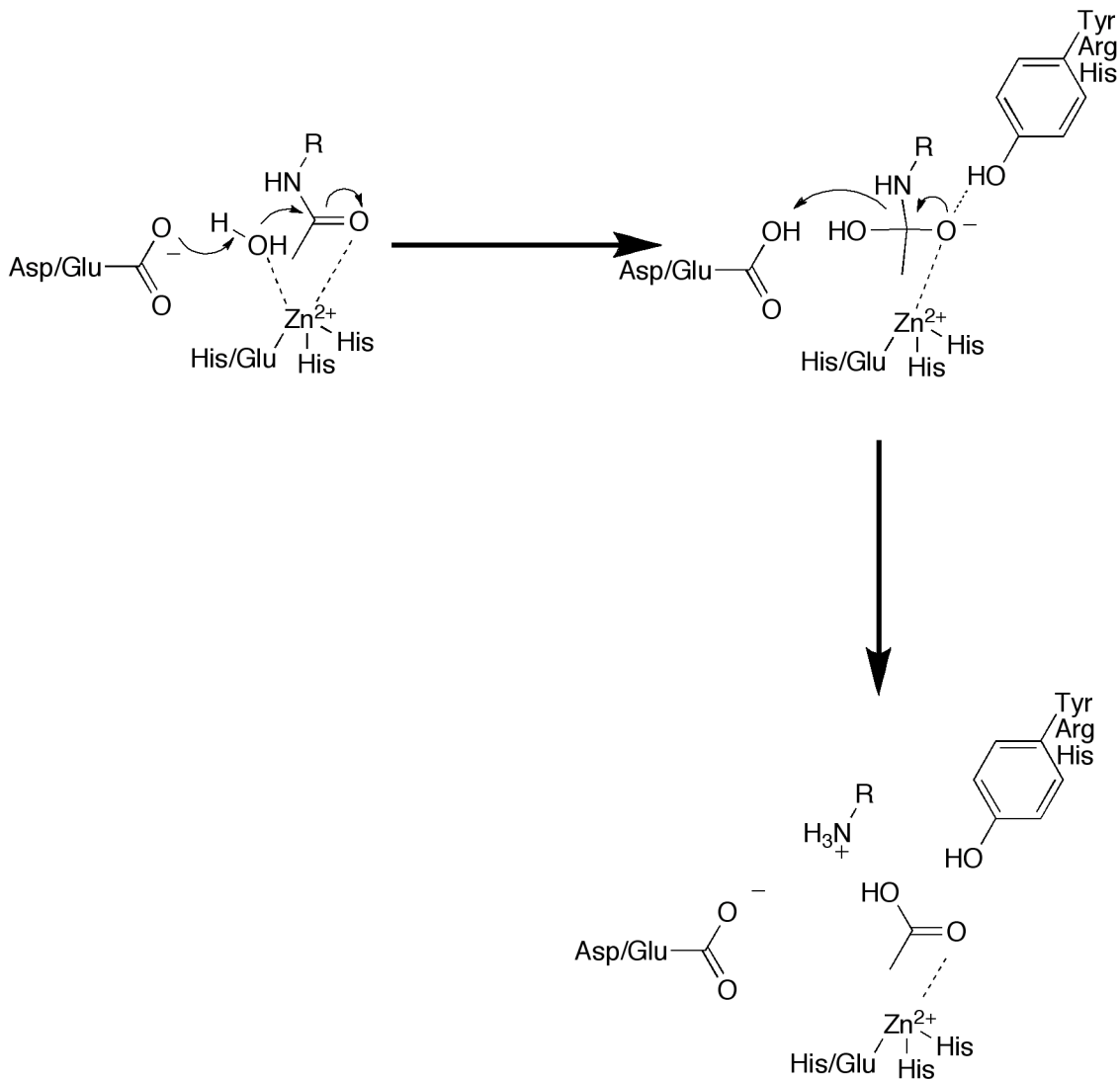


Figure 1.2: Mechanism of zinc proteases. In canonical zinc proteases such as carboxypeptidase A, peptide bond hydrolysis is activated by general acid/base catalysis. The catalytic zinc ion serves to position and coordinate the substrate carbonyl, as well as polarize the bound water molecule. An active site glutamate/aspartate is proposed to act as a general base, deprotonating the nucleophilic water as it attacks the carbonyl, forming a tetrahedral intermediate. The oxyanion is stabilized by a tyrosine, arginine, or histidine. Collapse of the tetrahedral intermediate forms the products, and the amine leaving group is protonated by the glutamate/aspartate, acting as a general acid.

the tetrahedral intermediate, is repeated throughout biology in zinc-dependent enzymes catalyzing a wide array of hydrolytic reactions.

With the exception of redox instability, Fe^{2+} is equally well suited to catalyze hydrolytic reactions of the type associated with zinc enzymes. Like zinc, Fe^{2+} can adopt a variety of coordination environments, and is stable from 4-6 ligands (9). In fact, Fe^{2+} can more readily adopt 5- or 6-coordinate states than Zn^{2+} , suggesting that iron would have advantages in stabilizing certain transition states compared to zinc. However, relatively few non-heme Fe-dependent hydrolases were identified until recently, when several Zn-dependent enzymes were reclassified as Fe-enzymes.

One of the most well-studied examples of an Fe-dependent hydrolase is peptide deformylase (PDF). PDF catalyzes the deformylation of N-formylated methionine in newly synthesized polypeptides in prokaryotes and some eukaryotic organelles, which is an essential step in protein synthesis (Figure 1.3) (17). Early work was hampered by highly unstable enzyme preparations, where activity was lost at room temperature with a $t_{1/2}$ of ~ 1 minute (18, 19). Additionally, although PDF was proposed to be a mononuclear metalloprotein, enzyme preparations contained variable amounts of metal ions, including Fe^{2+} and Zn^{2+} , calling into question the hypothesis that PDF was a Zn^{2+} -dependent enzyme (19). This problem was solved by the discovery that isolation of the enzyme sample in an anaerobic environment resulted in a completely stable enzyme (20), and thus PDF was labeled as an Fe^{2+} -dependent enzyme. Crystallographic and kinetic studies (21, 22) further illustrated that PDF is structurally and mechanistically similar to the canonical zinc proteases thermolysin and CPA, where a conserved glutamate (Glu133 in *E. coli*) is proposed to function as a general acid/base catalyst and Gln50 and the

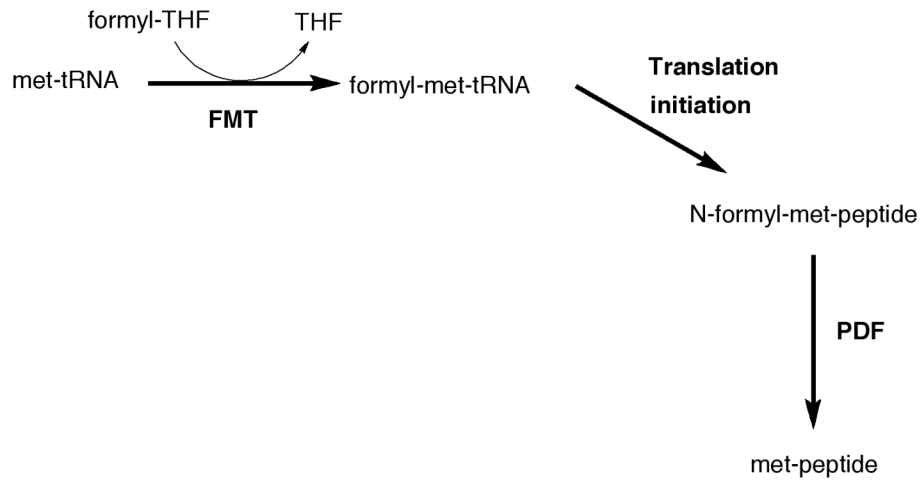
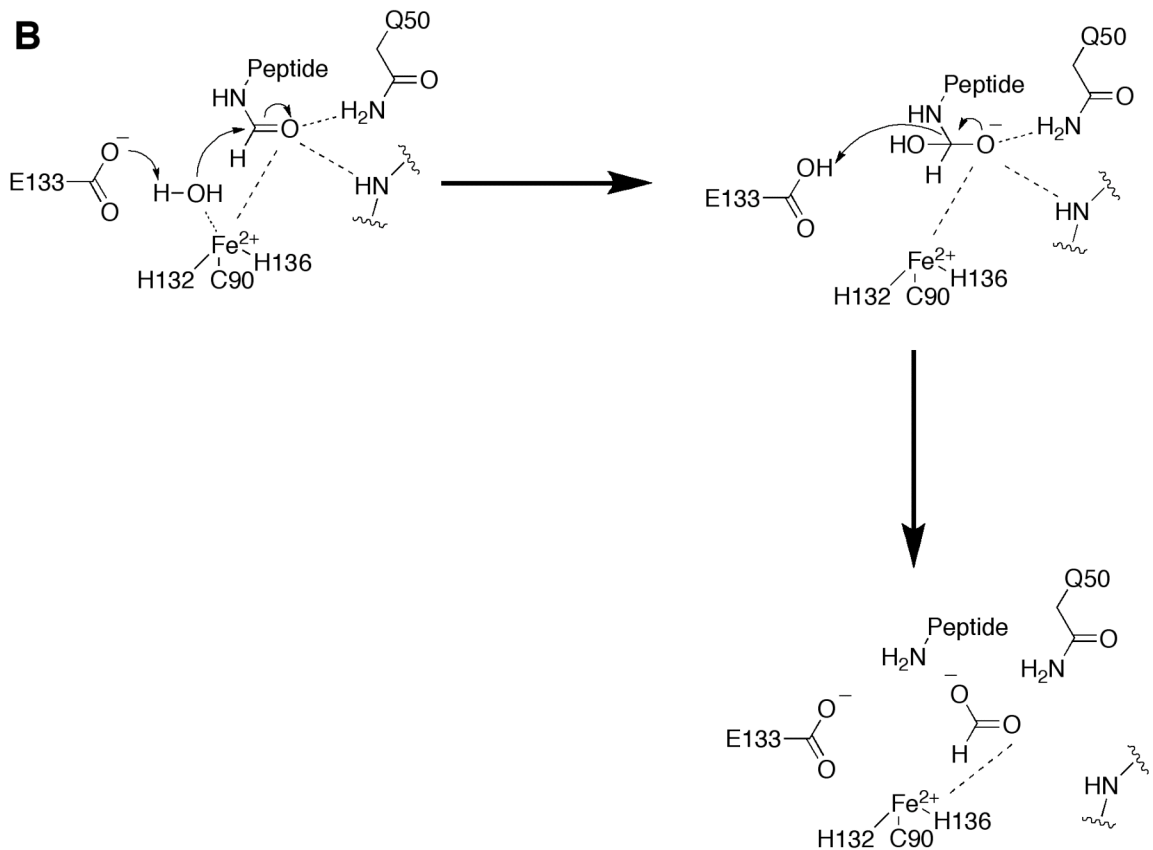
A**B**

Figure 1.3: Peptide deformylase pathway and mechanism. (A) Role of peptide deformylase (PDF) in prokaryotic peptide synthesis. (B) The proposed mechanism of *E. coli* PDF, which is analogous to the canonical zinc proteases, but is proposed to use Fe^{2+} as a metal cofactor.

backbone amide of Leu91 are proposed to stabilize the tetrahedral intermediate by hydrogen bonding (Figure 1.3).

Several other Fe^{2+} -hydrolases have been identified recently, including γ -carbonic anhydrase (23), S-ribosylhomocysteinase (24), methionyl aminopeptidase (25), cytosine deaminase (26, 27), and atrazine chlorohydrolase (28). Like PDF, both LuxS (S-ribosylhomocysteinase) and methionine aminopeptidase were originally classified as Zn^{2+} -enzymes, illustrating the overlap in metal binding sites and catalytic mechanisms between these two classes of enzymes. Currently, *N*-acetyl-D-glucosamine-6-phosphate deacetylase (NagA) shares many similarities to these enzymes but its native cofactor has not been conclusively demonstrated (29). Much of the confusion in studying these enzymes is due to the fact they can be activated *in vitro* by a variety of divalent metal ions. One possible conclusion from these findings may be that many divalent metallohydrolases may be activated by either Zn^{2+} or Fe^{2+} *in vivo* as well. Therefore, classifying these enzymes as exclusively Zn- or Fe-dependent may be confusing and erroneous. In future studies, evaluating the degree of possible metal ion promiscuity may be essential to understanding the enzymology of metalloproteins *in vitro* and *in vivo*.

LpxC: An Essential Zn-Dependent Deacetylase in Lipid A Biosynthesis

In Gram-negative bacteria, the outer-most layer of the cell envelope is predominantly comprised of lipopolysaccharides (LPS), which are anchored to the membrane through a core Lipid A component (Figure 1.4) (30-32). Lipid A biosynthesis is essential in nearly all Gram-negative bacteria, and understanding the enzymology of key steps in the pathway has been an active area of research (30, 31, 33, 34). In

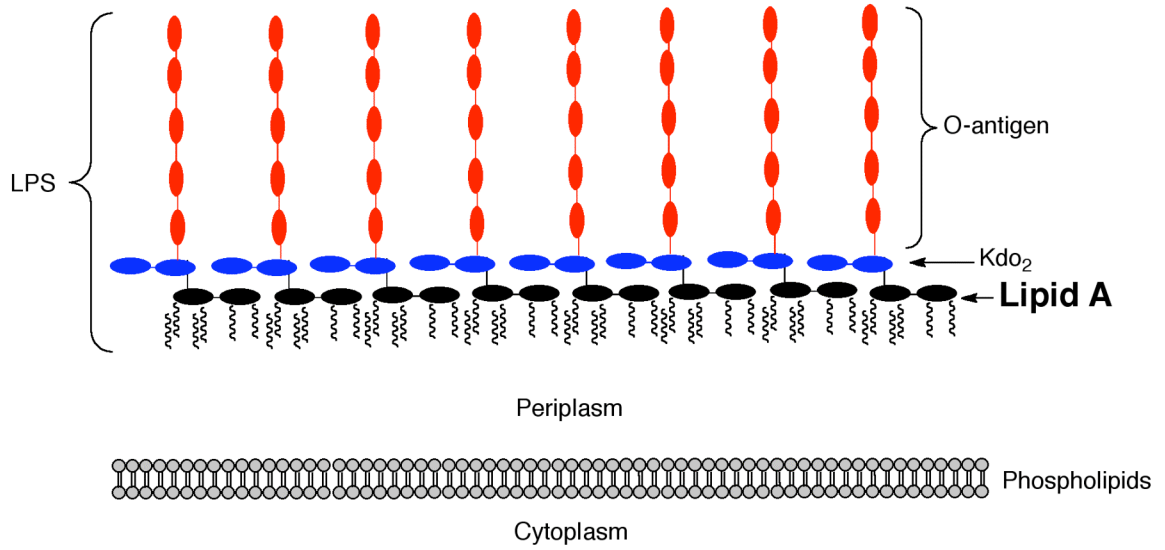


Figure 1.4: Gram-negative cell membrane. The major lipid species of the outermost layer of the cell envelope is Lipid A (black), which anchors the variable O-antigen/polysaccharide (red), forming the molecule known as lipopolysaccharide (LPS).

particular, the second and committed step, catalyzed by the Zn^{2+} -deacetylase LpxC, has been investigated over the past decade (35) and been a target for development of antimicrobials (36, 37).

The Lipid A Biosynthetic Pathway

The constitutive 9-step pathway for Lipid A biosynthesis is largely conserved in Gram-negative bacteria (Figure 1.5) and are similar to *E. coli*, where it is best characterized (31-33). The initial step is catalyzed by UDP-GlcNAc acyltransferase (LpxA), and is also the branch point between Lipid A and peptidoglycan biosynthesis (38). LpxA uses differing acyl chains depending on the organism, but has an absolute requirement for an acyl carrier protein (ACP) thioester donor (31, 38). An interesting feature of the LpxA reaction is that it has an unfavorable equilibrium constant (~ 0.01) (38), and the pathway is thus committed by the second step, the deacetylase LpxC.

LpxC catalyzes the second, committed step in Lipid A biosynthesis (35, 39, 40). LpxC has been described as a zinc-dependent enzyme (40), and is proposed to catalyze deacetylation of the myristoyl-UDP-acetylglucosamine substrate using acid/base chemistry (35). However, the precise chemical mechanism has not yet been determined. LpxC is discussed in greater detail below.

Following deacetylation, a second acyl transfer reaction is catalyzed by LpxD, again using a myristoyl-ACP thioester substrate (41), to generate UDP-2,3-diacetylglucosamine (Figure 1.5). The nucleotide is then cleaved by the phosphatase LpxH (42), yielding 2,3-diacetylglucosamine-1-phosphate, or Lipid X (Figure 1.5). Lipid X is then condensed with a second molecule of UDP-2,3-diacetylglucosamine, the LpxD

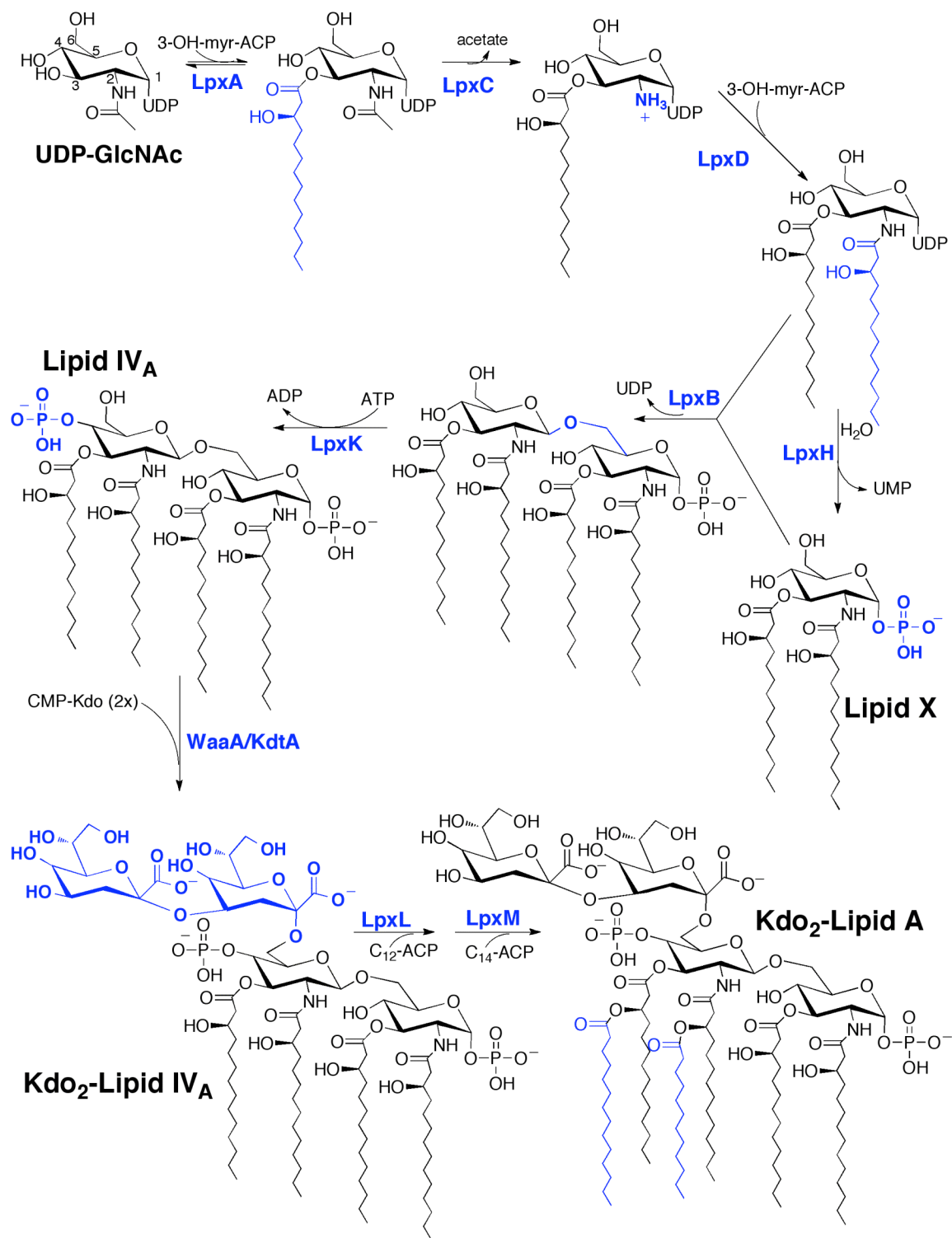


Figure 1.5: Lipid A biosynthetic pathway. The 9-step constitutive pathway in *E. coli* is widely conserved across Gram-negative bacteria (31).

product, catalyzed by LpxB (43, 44) to form a tetra-acylated disaccharide product (Figure 1.5). The kinase LpxK then catalyzes phosphorylation of the 4'-OH of the disaccharide, forming Lipid IV_A (45).

In *E. coli*, the next step involves transfer of multiple 3-deoxy-D-mannooctulosonic acid (Kdo) sugar moieties to Lipid IV_A (46). The Kdo transferase (kdtA) functions differently depending on the organism, where it may catalyze addition of 1, 2, or 3 Kdo molecules (46-48). The final acylation steps in the Lipid A pathway are catalyzed by LpxL and LpxM, termed the “late” acyltransferases, which recognize the presence of the Kdo moieties as a substrate requirement (49).

Transport and Modification of Lipid A

Kdo₂-Lipid A is synthesized at the cytoplasmic side of the inner membrane, but must be transported across the inner membrane and periplasm to be anchored outside of the outer membrane. Not all of the mechanisms in this transport step have been well characterized, but it is known that the ABC transporter MsbA is responsible for the first step, transport from the cytoplasmic side to the periplasm (50-52). MsbA is an ATP-dependent lipid flippase, which catalyzes flips-flop of the newly synthesized Kdo₂-Lipid A from the cytoplasm to the periplasmic side of the inner membrane. In the periplasm, the core Kdo disaccharide is lengthened by the addition of the O-antigen polysaccharide chain (31, 53), forming the molecule known as lipopolysaccharide (LPS). LPS is then shuttled across the periplasm by the essential protein LptA (54). The outer membrane protein RlpB then transports LPS from the periplasm to the outer surface of the outer membrane (55). The mechanisms by which these transporters function have yet to be determined in detail.

Lipid A also undergoes significant modifications that vary by organism and have effects on virulence and susceptibility to antibiotics (31, 34, 56). Several of the possible modifications are shown in (Figure 1.6). For example, in *E. coli* and *S. typhimurium*, the enzyme ArnT transfers a 4-amino-4-deoxy-L-arabinose (L-Ara4N) modification to the 4' position. Deletion of ArnT results in a loss of the modification and an increased susceptibility in both organisms to antimicrobial peptides like polymyxin (57). The outer membrane palmitoyl transferase PagP catalyzes addition of a palmitoyl group to one of the hydroxymyristoyl chains (Figure 1.6), and is transcriptionally repressed unless activated by low Mg^{2+} or certain other conditions (58). Modification of Lipid A by PagP also confers resistance to antimicrobial peptides and is required for infection by *Legionella pneumophila* and *Bordetella bronchiseptica* (59, 60). In *Francisella tularensis*, deletions of the inner membrane phosphatases LpxE and LpxF have been shown to greatly decrease virulence, with the potential to create strains suitable for use as vaccines (34). Biochemical characterization and manipulation of Lipid A modifications may be a promising avenue in the future fight against Gram-negative bacterial infections.

Activation of the immune system by LPS

Lipid A is also referred to as “endotoxin” because of its ability to stimulate inflammatory responses via binding to extracellular receptors (31). In animal cells, Lipid A is initially bound to CD14 on the cell surface. The bound lipid A is then recognized by toll-like receptor 4 (TLR4). Activation of TLR4 stimulates the NF- κ B pathway, leading to upregulation of IL1- β and TNF- α , as well as co-stimulatory molecules for the immune system. When clearing a local infection, these events are appropriate. However, in sepsis, where an infection spreads throughout the body, overproduction of these factors

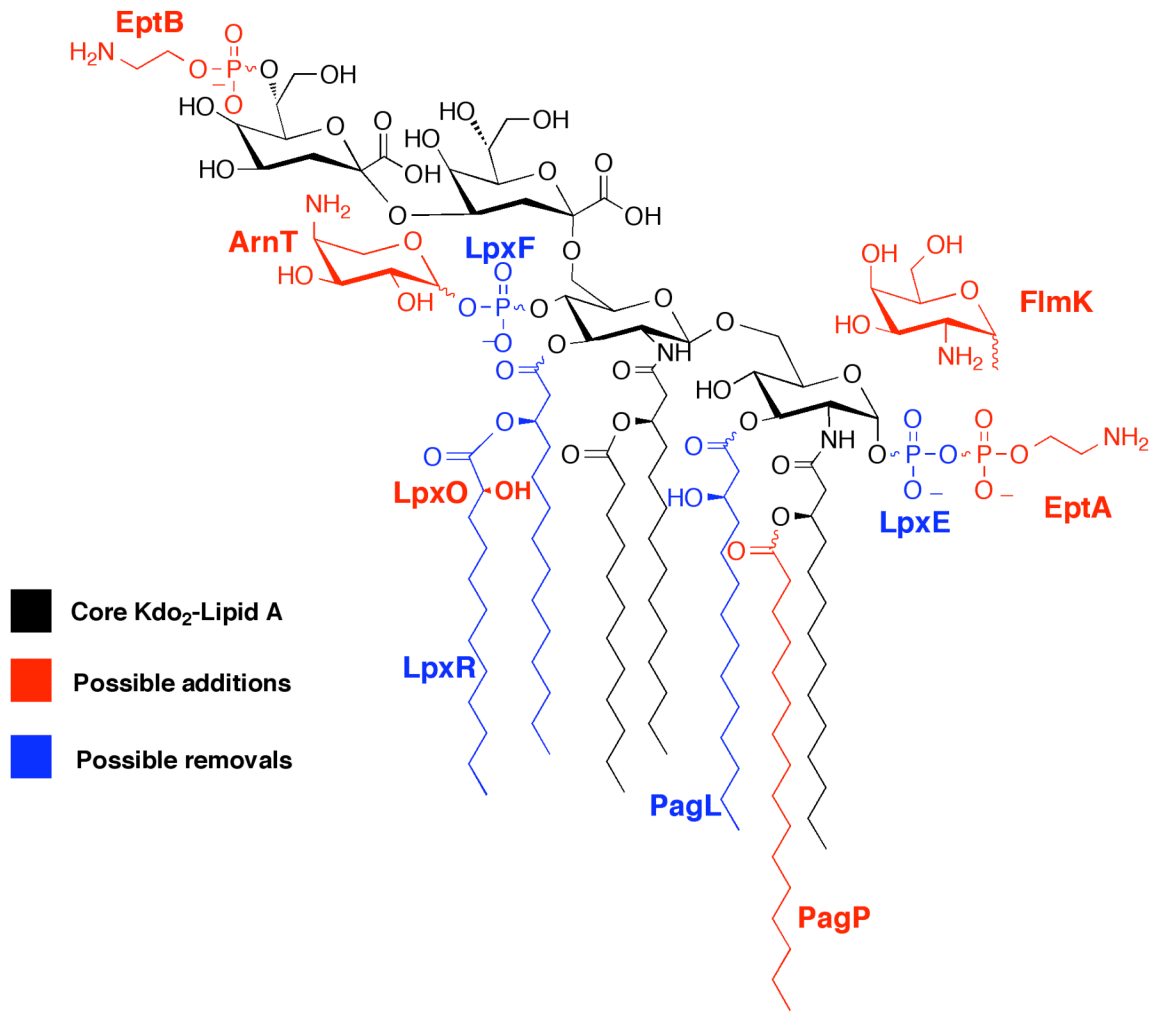


Figure 1.6: Modifications to Kdo₂-Lipid A. Possible modifications to Kdo₂-Lipid A in *E. coli*, *S. typhimurium*, or *F. novicida*.

leads to an overwhelming inflammatory response that can result in blood vessel damage, multiple organ failure, and death (61). Therefore, inhibitors of lipid A biosynthesis may have an advantage in limiting Gram-negative sepsis in addition to functioning as antibacterials (62).

LpxC: M^{2+} -dependent deacetylase essential for Lipid A biosynthesis

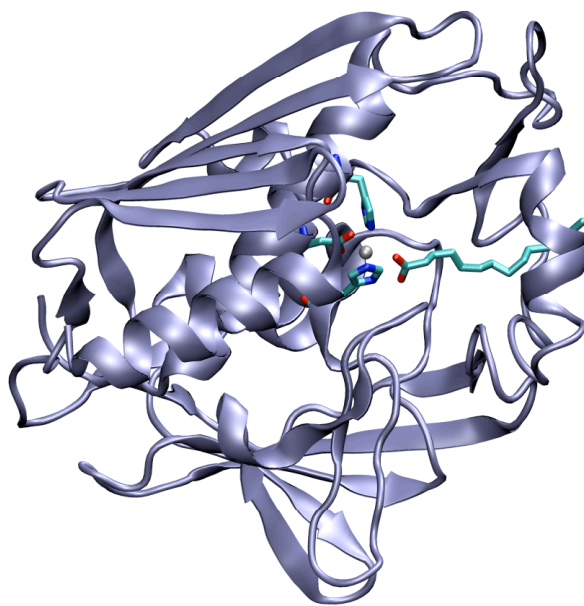
As described above, LpxC catalyzes the second, but committed step in lipid A biosynthesis, and is a metal-dependent deacetylase. The role of LpxC in Lipid A biosynthesis was originally identified on the basis of genetic evidence, where mutations to the *envA* gene caused hypersensitivity to antibiotics and a lowered ratio of LPS:protein in the outer membrane (63). The *envA* gene was later identified as the second step in lipid A biosynthesis, the deacetylation of UDP-3-*O*-(*R*-3-hydroxymyristoyl)-*N*-acetylglucosamine, and renamed LpxC (39).

LpxC was identified as a metalloenzyme on the basis of several factors (40). The first suggestion came from observation that LpxC activity was inhibited by hydroxamates, which are classic Zn-enzyme inhibitors. Later, activity was observed to be reversibly lost upon incubation with chelators such as EDTA. Next, apo-enzyme, generated by stripping the metal by chelation, was activated by a single divalent metal ion, and inhibited by excess metal, which has been observed in other zinc hydrolases (64). Finally, benchtop purification from *E. coli* grown in rich media yielded an enzyme that contained 1 – 3 bound zinc ions, and determined by inductively coupled plasma mass spectrometry (ICP-MS) elemental analysis. Based upon these results, LpxC was classified a Zn^{2+} -dependent deacetylase.

The zinc binding site in LpxC was probed by mutagenesis (65), X-ray absorption spectroscopy (66), and crystallography (67), and was identified as a His₂AspH₂O ligand set (Figure 1.7). The structure of LpxC revealed a novel protein fold, consisting of two domains connected by a 16-residue linker. Each domain has identical topology, consisting of a 5-stranded β -sheet and 2 α -helices, but with minimal sequence identity, suggesting gene duplication followed by divergent evolution. The structure also identified an $\sim 15\text{\AA}$ -long hydrophobic tunnel, in which a palmitate group was unexpectedly found. A separate structure with the substrate analogue TU-514 confirms that this tunnel accommodates the lipid portion of the substrate (68, 69), while a more basic pocket binds the UDP moiety (70). A crystal structure of LpxC from *Pseudomonas aeruginosa* has also been solved, and was found to be structurally homologous to the previously solved structures (71).

LpxC catalysis has been studied in great detail, but questions still remain about the precise chemical mechanism. Like the canonical zinc-hydrolases discussed above, such as carboxypeptidase and thermolysin, LpxC catalysis was proposed to proceed via a general acid/base mechanism. Based on the crystal structure and previous work, two residues were suggested as potential acid/base catalysts: His265 and Glu78 (Figure 1.7). Mutation of either residue to alanine resulted in a significant decrease in activity; in *E. coli* the E78A mutation decreased k_{cat}/K_M by 400-fold relative to the wild-type enzyme, while the H265A mutant decreased k_{cat}/K_M 2190-fold (72). In *A. aeolicus*, these residues were similarly found to be essential, with the H265A (H253 in *A. aeolicus*) and E78A (E73) mutants exhibiting a 167-fold decrease and a 41-fold decrease respectively (72, 73). This difference may be due to several reasons, including: a change

A



B

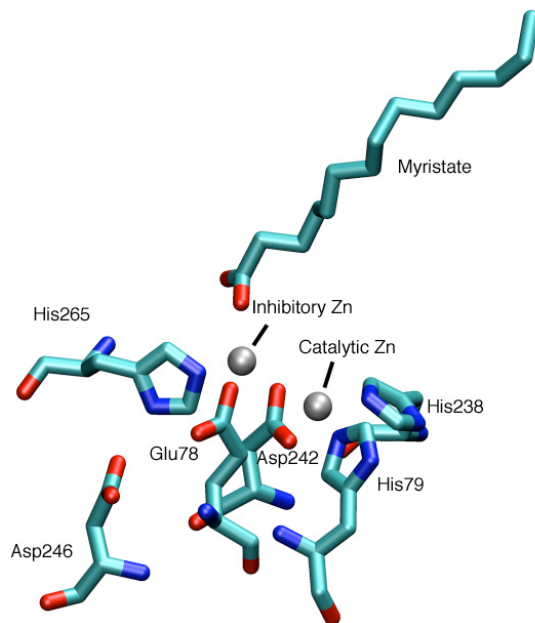


Figure 1.7: Topology and active site of LpxC. (A) Overall structure and (B) active site residues. Figures derived from PDB file 1P42 using VMD.

in rate limiting step (i.e., hydrolysis is not rate limiting in WT AaLpxC), or the EcLpxC mutants have greater structural perturbations than the AaLpxC mutants, resulting in a larger decrease in catalytic activity. The k_{cat}/K_M exhibits a bell-shaped dependence on pH, suggesting at least two ionizations are essential for catalysis, consistent with an acid/base mechanism (72, 73). When E78 is mutated to alanine, $\text{pK}_{\text{a}1}$ is lost, suggesting that the step accelerated by deprotonation (i.e., the general base) is linked to E78 (72, 73). However, determining the identity of $\text{pK}_{\text{a}2}$ has been more difficult. Mutation of the other essential active site residue, H265, to alanine results in a loss of activity but does not abolish $\text{pK}_{\text{a}2}$, suggesting that other enzyme groups could also be observed in that pH range. NMR experiments determined the pK_{a} of H253 in the *A. aeolicus* enzyme to be 7.6 ± 0.1 (69), which is difficult to definitively assign to the published $\text{pK}_{\text{a}2}$ of 8.4 ± 0.2 (73) under k_{cat}/K_M conditions. However, separate measurements published later measured $\text{pK}_{\text{a}2}$ to be 7.9 ± 0.3 (72), which is nearly equivalent to the H253 pK_{a} determined by NMR. Another possibility is that $\text{pK}_{\text{a}2}$ reflects the ionization of the metal-water, which is consistent with the increase in $\text{pK}_{\text{a}2}$ when Zn^{2+} is substituted with Co^{2+} or Fe^{2+} (72, 74). However, ^{67}Zn NMR experiments revealed that while a titratable group at high pH had a pK_{a} between 7.8 and 8.2, this ionization was not observed in the H265A mutant, disfavoring assignment of $\text{pK}_{\text{a}2}$ to the metal-water (75). The ^{67}Zn NMR results suggest that if H265 is not $\text{pK}_{\text{a}2}$, the ionizing group must be in the vicinity of both H265 and the catalytic zinc ion. It is also difficult to be certain how well NMR experiments done at cryogenic temperatures can be extrapolated to experiments at $30^\circ - 50^\circ \text{C}$. The cumulative results are most consistent with assignment of $\text{pK}_{\text{a}2}$ to H265, but that this pK_{a}

is coupled to other ionization of another group, such as ZnOH₂, preventing a definitive assignment.

Two mechanisms have been proposed for the LpxC-catalyzed reaction (72, 73) (Figure 1.8). In both mechanisms, E78 is proposed to function as a general base catalyst, deprotonating the metal-bound water as the metal-water nucleophile reacts with the substrate carbonyl carbon. The catalytic zinc ion functions to polarize and lower the pK_a of the bound water molecule, coordinate the substrate carbonyl, and stabilize the developing oxyanion in the transition state and tetrahedral intermediate. A major difference between the two mechanisms is the role of H265. In the first proposed mechanism, H265 is essential because it serves to stabilize the oxyanion in the developing transition state and the tetrahedral intermediate. As the tetrahedral intermediate collapses, protonated E78 functions as a general acid catalyst by protonating the amine leaving group, forming the products myr-UDP-glucosamine and acetate. In the second proposed mechanism, E78 still functions as the general base, deprotonating the water, but the tetrahedral intermediate is stabilized by forming a hydrogen bond with T191. In this alternative mechanism, H265 is essential because in addition to providing charge stabilization of the transition state, it is the general acid, protonating the leaving group amine as the intermediate collapses (Figure 1.8).

Several pieces of evidence suggest the second proposal, the general acid/base pair mechanism, is the most likely. First, H265 forms a hydrogen bond with D246, and mutation of D246 to alanine (D246A) leads to a ~1200-fold loss in $k_{\text{cat}}/K_{\text{M}}$ (72). This type of His-Asp charge relay (Figure 1.8 and 1.9) is frequently observed for histidines that mediate proton transfer reactions (76). A crystal structure was solved with a

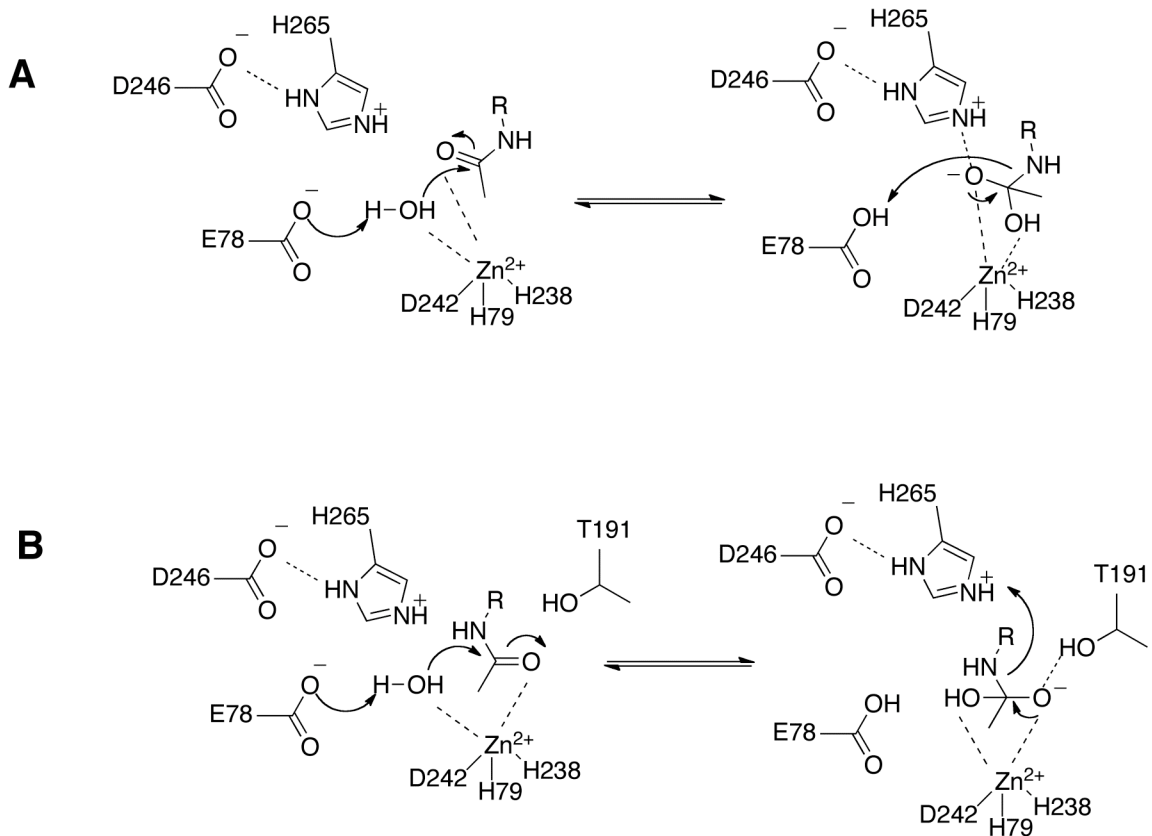


Figure 1.8: Proposed chemical mechanisms of LpxC. The two mechanisms most consistent with the current data differ mainly in the role of H265, while E78 is proposed to function as either the general base (A) or the general acid/base (B). In (A) H265 is an electrostatic catalyst analogous to a metalloprotease-like mechanism, while in (B) H265 functions as the general acid.

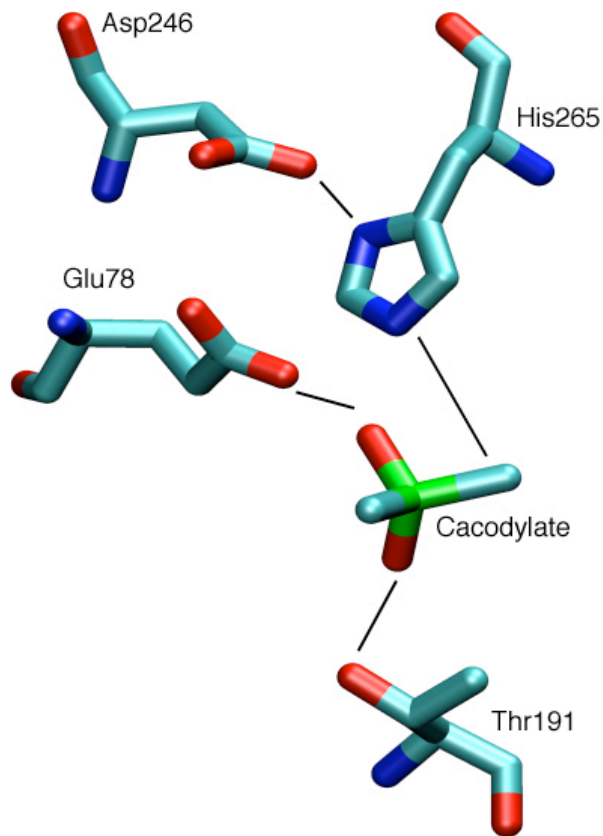
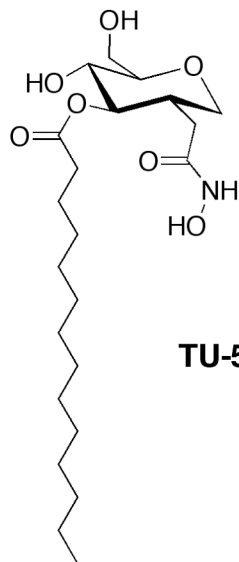


Figure 1.9: Crystal structure of LpxC with tetrahedral mimic. When crystallized with the tetrahedral intermediate mimic cacodylate ($\text{As}(\text{CH}_3)_2\text{O}_2\text{H}$), E78 is closest to one of the oxygen groups, while H265 is closer to the methyl group, analogous to the amine leaving group. T191 is observed to contact the second oxygen group, as expected if it were to stabilize the oxyanion intermediate. Derived from PDB file 1YHC and VMD.

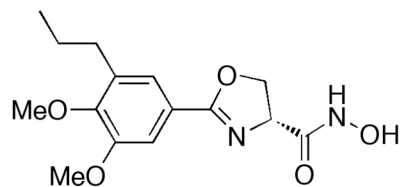
tetrahedral mimic, cacodylate (Figure 1.9), which placed the CH₃ (equivalent to the amine leaving group) closest to H265 (72), further suggesting it is more likely to be the general acid. T191 was suggested to be important for electrostatic stabilization by crystallography (72), in which it is observed to form a hydrogen bond with the tetrahedral mimic, and mutagenesis, in which the T191A mutation resulted in a loss of activity (77). Nonetheless, these data are suggestive, not conclusive, and further experiments are needed to conclusively differentiate between the two proposed mechanisms. A detailed understanding of the chemical mechanism is essential for design and optimization of antibacterials that target LpxC.

LpxC inhibitors as antibacterials

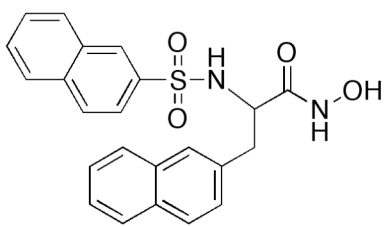
LpxC is essential for Lipid A biosynthesis in Gram-negative bacteria, and consequently it has emerged as an attractive drug target for the development of novel antibiotics. Because LpxC is a metalloenzyme, most of the compounds that target LpxC use chelating groups to introduce at least one high-affinity interaction between the compound and the protein (37). Some of the first compounds identified were hydroxamic acids (36, 40, 78), which are canonical zinc-chelating groups (Figure 1.10). Further development of these early compounds was hindered by their inability to target a broad spectrum of Gram-negative bacteria – while compounds such as L-161,240 had antibiotic activity comparable to ampicillin in *E. coli*, they were ineffective against *Pseudomonas aeruginosa* and other pathogens, possibly because they do not penetrate the outer membrane (78). L-161,240 does not inhibit *A. aeolicus* LpxC, suggesting subtle differences in the active site may be important for drug development (79). Subsequent efforts yielded a series of sulfonamide-based compound from British Biotech, such as



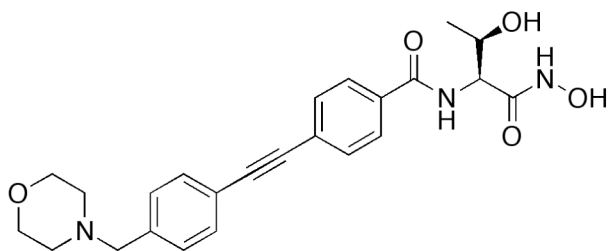
TU-514



L-161,240



BB-78485



CHIR-090

Figure 1.10: Selected LpxC inhibitors.

BB-78485 (71, 80). The sulfonamides such as BB-78485 were somewhat more promising, and had a broader spectrum of antibacterial activity, but again in pathogenic bacteria were not found to be effective enough for further development (80). Attempts have been made to improve on these early results (81-83), but have been hampered by concern in the industry about developing “niche” antibiotics. Most recently, the compound CHIR-090 (Chiron corporation) has shown promise as a lead compound (84-86). CHIR-090 has a K_i of 1 nM in *A. aeolicus* LpxC, and exhibits behavior typical of a slow, non-covalent tight-binding inhibitor (84). Importantly, CHIR-090 exhibits antibacterial activity against both *E. coli* and *P. aeruginosa* at 1 $\mu\text{g/mL}$ in a disk diffusion assay, comparable to ciprofloxacin (84).

The success of CHIR-090 suggests that targeting LpxC may be a viable strategy for developing a novel class of antibiotics. Further mechanistic studies will be key to the success of this strategy in developing a potent, broad spectrum inhibitor of Lipid A biosynthesis.

Histone deacetylases

Although a genome contains the blueprint for all the proteins in a cell, the content of the proteome can be orders of magnitude greater due to the numerous potential post translational modifications (PTMs) (87). These modifications include phosphorylation, methylation, sulfation, prenylation, biotinylation, ubiquitination, and acetylation. Acetylation is a common PTM that was first characterized in histones, but has since been shown to be widespread in eukaryotic proteins (88-92). Acetylation occurs on the ϵ -amino position of lysines, and is catalyzed by members of the histone acetyl transferase (HAT) family, using acetyl-CoA as the acetate donor (88, 93, 94). This modification is

regulated in part by the competing activity of the histone deacetylase (HDAC) family, although some effort is being made to rename these proteins KDACs (lysine deacetylases) to recognize the broader range of substrates now known (95). HDACs catalyze deacetylation by multiple mechanisms using multiple cofactors, depending on the isozyme (35, 91, 96). Given the ubiquity of acetylation and its importance in regulating protein function, aberrant acetylation has been implicated in several diseases including cancer, neurodegenerative diseases, and inflammation (97-101).

Histones and the nucleosome

Cellular DNA is packaged in chromatin, a highly regulated structure composed of discrete units known as nucleosomes (102). The nucleosome is composed of two basic elements: DNA, and the histone octamer, an eight-protein complex composed of two copies each of the 4 histones H2A, H2B, H3, and H4. Crystal structures of the nucleosome have been solved (103, 104), showing 146 base-pairs of DNA wrapped around each histone octamer (Figure 1.11). The histone N-terminal tails are flexible and exposed to solvent, while the cores of the proteins are well-structured and mainly α -helical. Chromatin structure, access to DNA, and therefore gene expression, is in part regulated by modifications to the N-terminal histone tails, in a manner that has been termed “the histone code” (105-107). Possible histone modifications include phosphorylation, methylation, ubiquitination, and acetylation.

Although acetylation has been most closely associated with histones, many non-histone proteins are also regulated by ϵ -amino acetylation of lysine, including transcription factors, nuclear receptors, cytoskeletal proteins, DNA repair enzymes, heat shock proteins, and others (89, 90, 92), with at least 195 acetylated proteins found by one

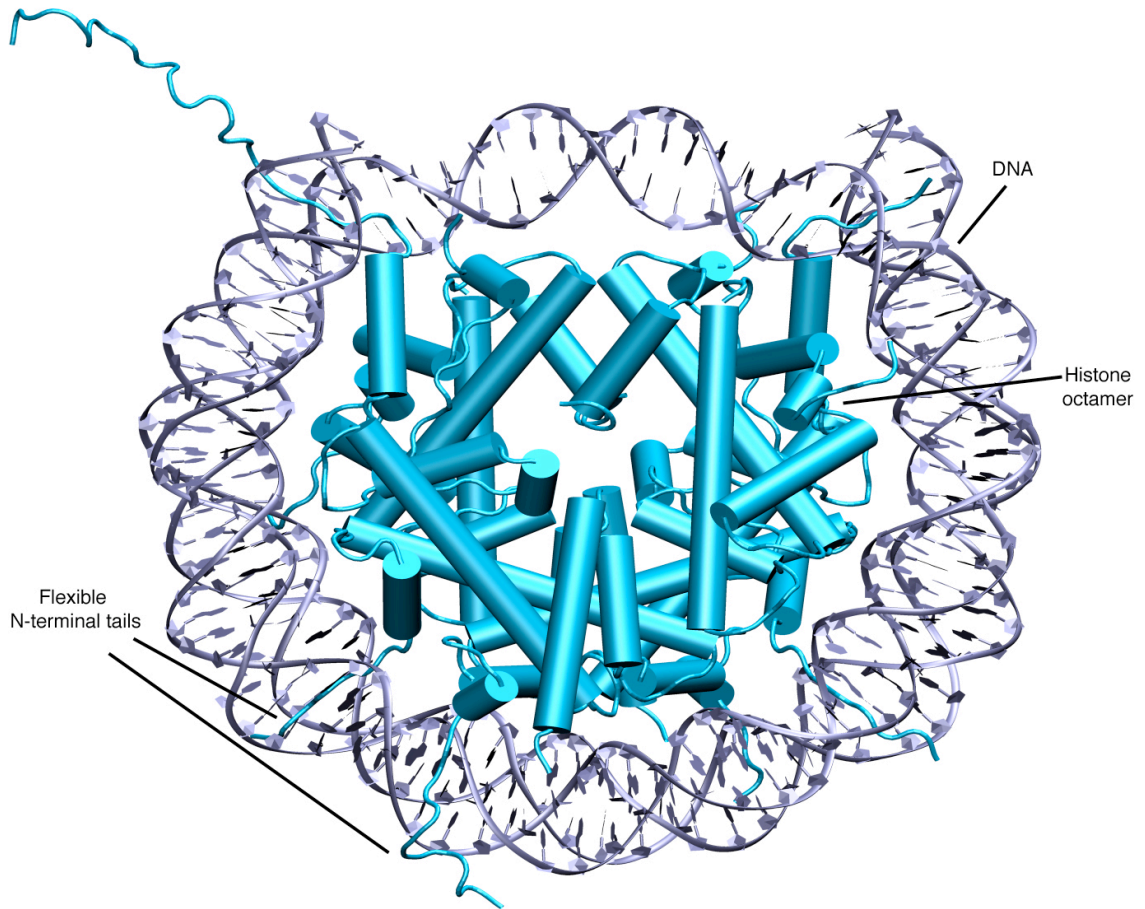


Figure 1.11: Structure of the nucleosome. DNA is wrapped around 2 copies each of H2A, H2B, H3, and H4 (the histone octamer). Gene expression is regulated in part by post translational modifications on the N-terminal histone tails. Derived from PDB file 1AOI and VMD.

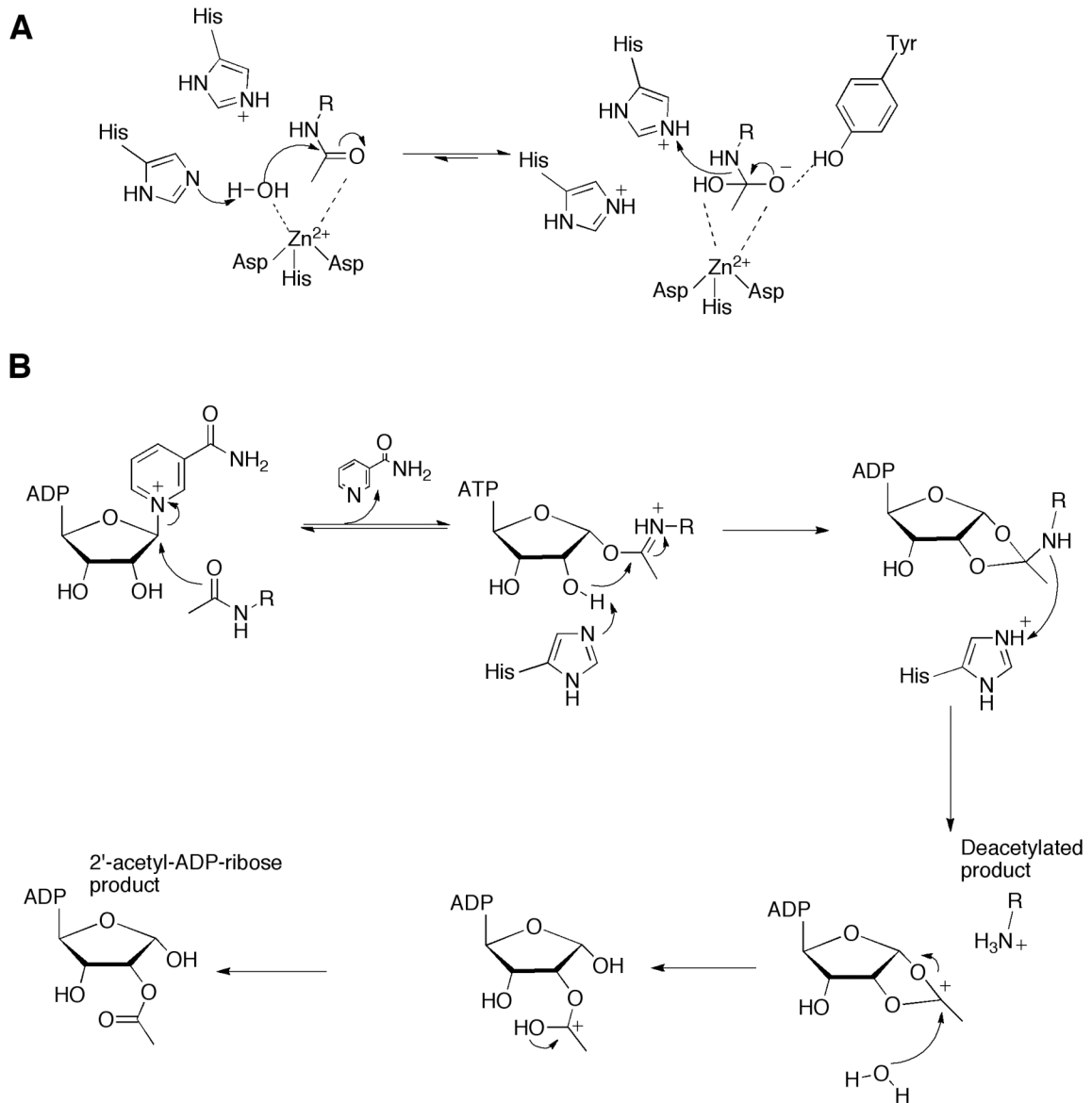


Figure 1.12: Proposed mechanisms of histone deacetylases. (A) Mechanism of metal-dependent histone deacetylases (class 1, 2, and 4) is proposed to proceed via a general acid/base pair. (B) NAD^+ -dependent (class 3) deacetylases have an unusual mechanism and yield a novel ADP-ribose metabolite.

proteomics survey (92). Acetylation can regulate these proteins in a variety of ways, including increasing/decreasing enzymatic activity, changing protein structure, or altering the favorability of protein-protein interactions. The ubiquity and wide-ranging regulatory effects of acetylation may be comparable to the much better studied phosphorylation (88).

4 Classes of Histone Deacetylases

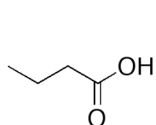
Histone deacetylases (HDACs) have been divided into 4 classes by phylogeny (91, 96, 108), where class 1, 2, and 4 HDACs are classic metal-dependent hydrolases, and are proposed to use a Zn^{2+} cofactor. However, the class 3 enzymes share little sequence homology and utilize a unique NAD^+ -dependent mechanism (Figure 1.12). The metal dependent HDACs are subdivided on the basis of sequence homology to the archetypal yeast HDAC, Rpd3. Class 1 HDACs (HDAC 1, 2, 3, and 8) are the most similar to Rpd3, and consist mainly of a single catalytic metallohydrolase domain. The class 2 HDACs (HDAC 4, 5, 6, 7, 9, and 10) are more similar to yeast Hda1. The class 2 enzymes are somewhat larger (~2-fold longer polypeptides) and contain an additional domain with variable motifs, such as zinc-finger regions or transcription factor binding elements (91, 108). Class 4 presently consists of only HDAC11, which is most similar to the class 1 enzymes but is divergent enough to have been deemed a novel class on the basis of sequence (31% identical and 41% similar to Rpd3, compared 43/65% for HDAC8, the most divergent class 1 HDAC) (91, 109).

The class 3 HDACs are also referred to as the Sir2 family or sirtuins in mammals, by homology to the yeast enzyme Sir2 (96). In addition to their unique mechanism (Figure 1.12), sirtuins have attracted great interest because of their implication in aging.

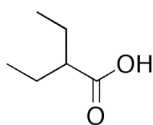
Calorie restriction has been observed to increase lifespan in several model organisms, and sirtuins have been implicated as essential for this process, prompting great interest in potential therapies targeted at sirtuins (96, 110-112).

HDAC inhibitors as potential therapeutics

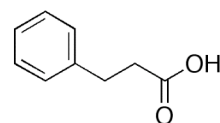
Acetylation of histones and other proteins plays a key role in regulating gene expression and other vital cell functions. Therefore, compounds that alter the balance of acetylation and deacetylation may be useful in treating diseases where an imbalance exists, such as cancer, neurodegenerative diseases, and inflammation (97-101). Numerous HDAC inhibitors have been synthesized (Figure 1.13), including carboxylates, hydroxamates, benzamides, epoxyketones, and cyclic peptides (90). The carboxylates, hydroxamates, and benzamides function by chelating the active site metal ion, while the epoxyketones and cyclic peptides bind due mainly to contacts with the protein. The hydroxamate inhibitors have generally been found to have the tightest affinity, and one, suberoylanalide hydroxamic acid (SAHA, Zolinza) has been approved by the FDA for the treatment of cutaneous T-cell lymphoma (113). Compounds that function by chelating the active site metal, such as SAHA, broadly inhibit all class 1, 2, and 4 HDACs, but not the NAD⁺-dependent class 3 enzymes. However, recent efforts to develop isozyme-specific HDAC inhibitors have yielded some success (114), suggesting the promise of more targeted treatments for specific diseases. For example, a pimelic diphenylamide HDAC3-specific inhibitor (106) has shown promise for the treatment of Friedrich's Ataxia, a disease related to silencing of a single gene, frataxin (115-117).



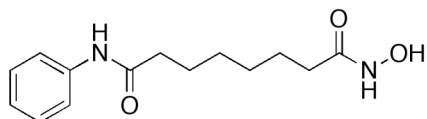
Butyric acid



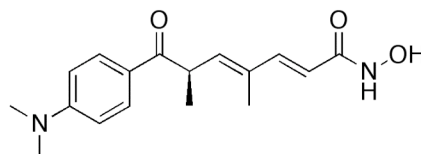
Valproic acid



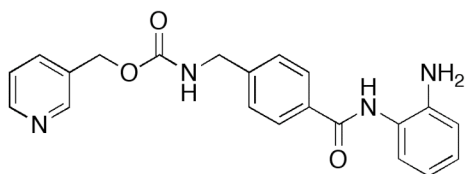
Phenylbutyric acid



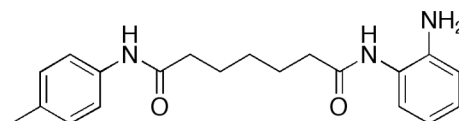
Suberoylanilide hydroxamic acid (SAHA)



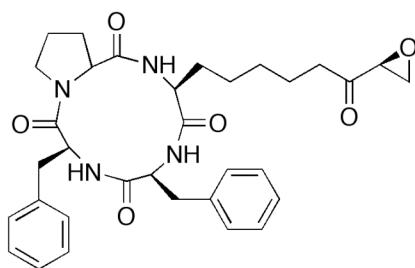
Trichostatin A (TSA)



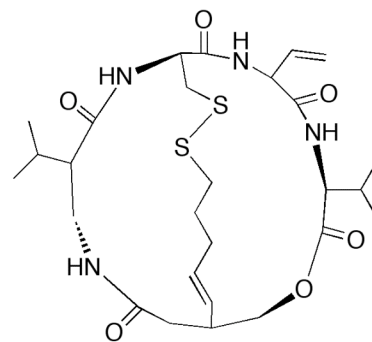
MS-275



Pimelic diphenylamide 106



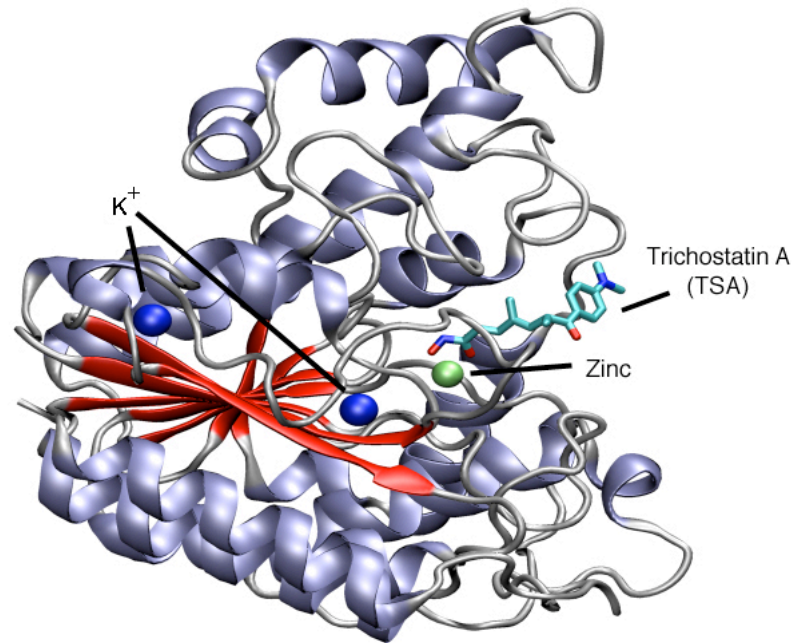
Trapoxin (TPX)



Depsipeptide

Figure 1.13: Selected HDAC inhibitors. Metal dependent histone deacetylase (HDAC) inhibitors include carboxylates, hydroxamates, benzamides, epoxyketones, and cyclic peptides.

A



B

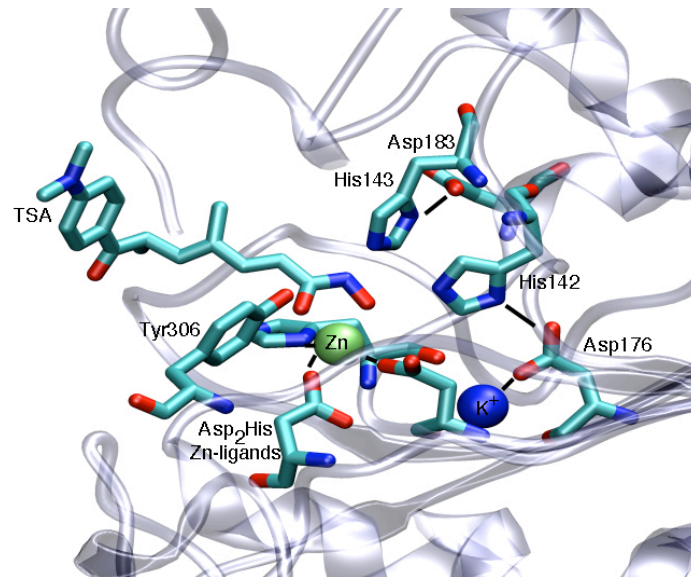


Figure 1.14: Topology and active site of HDAC8. (A) HDAC8 colored by secondary structure. (B) Active site residues of HDAC8. Figures derived from PDB file 1T64 and VMD.

The class 1 histone deacetylase 8 (HDAC8)

HDAC8 is a class 1 histone deacetylase and is the best biochemically characterized human HDAC isozyme. HDAC8 has both nuclear and cytoplasmic localization, and is expressed preferentially in the cytosol of smooth muscle cells (118, 119). HDAC8 also associates with smooth muscle α -actin and is essential for smooth muscle cell contractility (120), and is regulated by phosphorylation at serine 39 by protein kinase A (121). HDAC8 has also been validated as an anticancer target in neuroblastoma and other cancers (122-124) despite the fact that little is known about its *in vivo* substrates.

HDAC8 was the first mammalian HDAC crystal structure to be solved (125, 126), and this structure is similar to that of the thermophilic bacterial histone deacetylase-like protein (HDLP) from *A. aeolicus* solved earlier (127). HDAC8 has a single $\alpha+\beta$ domain and a HisAsp₂ zinc coordination sphere, with a hydroxamate inhibitor that binds the zinc in a bidentate manner in the original structures (Figure 1.14). Interestingly, two monovalent ion sites were also observed in the crystal structures. The active site is located at the end of a hydrophobic tunnel; subsequent structures revealed that the acetyl-lysine binds in this tunnel, while the remainder of the peptide substrate binds the surface of HDAC8 (128).

A chemical mechanism for HDAC deacetylation was proposed on the basis of the crystal structure of HDLP (127) (Figure 1.12). A pair of catalytic histidines (H142 and H143, HDAC8 numbering) were proposed to act as a general acid/base catalyst pair, while Y306 was proposed to donate a hydrogen bond to stabilize the oxyanion tetrahedral intermediate. More recent evidence has suggested that HDAC8 is more likely to function

via a single general acid/base metalloprotease mechanism, where H143 is the general acid/base and H142 assists by electrostatic stabilization (129), (Gantt and Fierke, unpublished). Investigation of the dependence of activity on monovalent cations (MVC) found that HDAC8 is both activated and inhibited by MVCs at two distinct sites (129). The activating MVC site is located more than 20Å away from the active site, while the inhibitory MVC is coordinated by D176, which also forms a hydrogen bond with H142. The time-dependent increase in activity observed upon binding the activating MVC suggests that this site stabilizes the active conformation of the enzyme. The $K_{1/2}$ for K^+ -activation and inhibition of HDAC8 are 3.4 and 26 mM, respectively, suggesting that HDAC8 is likely to be bound to potassium *in vivo*, but could be modulated by changes in intracellular cation levels.

Activity of HDAC8 is affected by the active site metal

Class 1, 2, and 4 HDACs have been suggested to be Zn-dependent enzymes *in vivo*, but the identity of the active site metal has a large impact on the activity and ligand affinity of this enzyme. Like many metallohydrolases, HDAC8 is activated by a variety of divalent metal ions, where k_{cat}/K_M values for deacetylation of a fluorescently-labeled peptide substrate show the following trend: $Co^{2+} > Fe^{2+} > Zn^{2+} > Ni^{2+} > Mn^{2+}$ (130). The reaction with the non-physiological fluorescent substrate has low k_{cat}/K_M values ($10^2 - 10^3 M^{-1}s^{-1}$) and high K_M (0.1 – 1 mM) values (130) compared to values typically observed in metallohydrolases, where k_{cat}/K_M is frequently close to the diffusion controlled limit (131). Therefore, it is reasonable to hypothesize that $K_M \approx K_D^{substrate}$ and $k_{cat} \approx k_{hydrolysis}$, for these substrates. Although the metal-dependent HDACs have all been proposed to use Zn^{2+} , the higher activity of Fe^{2+} relative to Zn^{2+} (2.8-fold in k_{cat}/K_M) is intriguing

given the high levels of readily exchangeable iron suggested in mammalian cells (132-134). Furthermore, HDAC8 purified recombinantly from *E. coli* contains 8-fold more iron than zinc, and the deacetylase activity in *E. coli* cell lysates from recombinant expression is oxygen-sensitive, consistent with an Fe²⁺-enzyme (130). Further work is needed to determine the metal cofactor that activates HDAC8 *in vivo*.

Goals of this work

The following chapters describe my advances in understanding the catalytic mechanism and metal-dependence of two medically important deacetylases, LpxC and HDAC8. For LpxC, two chemical mechanisms are consistent with the published data: either a single general acid/base (E78), or a general acid/base pair (E78/H265) mechanism. Differentiating between these two mechanisms for any enzyme is difficult given the readily available methods. Differentiation of these two roles is especially difficult when the residue in question is a histidine, which can function either as an electrostatic catalyst or as a general acid, and few options for detailed probing are provided by mutagenesis within the 20 amino acids. In this work, I will resolve this mechanistic question in LpxC by combining mutagenesis with expressed protein ligation, which allows incorporation of unnatural amino acids (135, 136).

Furthermore, I will develop methods to analyze the metal ions bound to a specific protein in a cell. I will then combine these methods with measurements of metal affinity to identify the metal ion bound to LpxC and HDAC8 in cells and to analyze metal ion selectivity by proteins. These findings shed light on our understanding of metalloprotein selectivity *in vivo*, and illuminate the potential for a new regulatory mechanism controlled by metal-switching in cells.

REFERENCES

- (1) Andreini, C., Bertini, I., Cavallaro, G., Holliday, G. L., and Thornton, J. M. (2008) Metal ions in biological catalysis: from enzyme databases to general principles. *Journal of Biological Inorganic Chemistry* 13, 1205-1218.
- (2) Berg, J. M., and Shi, Y. (1996) The galvanization of biology: a growing appreciation for the roles of zinc. *Science* 271, 1081-1085.
- (3) Finney, L. A., and O'Halloran, T. V. (2003) Transition metal speciation in the cell: Insights from the chemistry of metal ion receptors. *Science* 300, 931-936.
- (4) Hoovers, J. M. N., Mannens, M., John, R., Blik, J., Vanheyningen, V., Porteous, D. J., Leschot, N. J., Westerveld, A., and Little, P. F. R. (1992) High-Resolution Localization of 69 Potential Human Zinc Finger Protein Genes - a Number Are Clustered. *Genomics* 12, 254-263.
- (5) Andreini, C., Banci, L., Bertini, I., and Rosato, A. (2006) Counting the zinc-proteins encoded in the human genome. *Journal of Proteome Research* 5, 196-201.
- (6) Berg, J. M., and Merkle, D. L. (1989) On the Metal-Ion Specificity of Zinc Finger Proteins. *Journal of the American Chemical Society* 111, 3759-3761.
- (7) Coleman, J. E. (1992) Zinc proteins: enzymes, storage proteins, transcription factors, and replication proteins. *Annu Rev Biochem* 61, 897-946.
- (8) Klug, A. (2005) Towards therapeutic applications of engineered zinc finger proteins. *FEBS Lett* 579, 892-894.
- (9) Lippard, S. J., Berg, J.M. (1994) *Principles of Bioinorganic Chemistry*, University Science Books, Mill Valley, California.
- (10) Frausto da Silva, J. J. R., Williams, R.J.P. (2001) *The Biological Chemistry of the Elements*, Oxford University Press, New York.
- (11) Holm, R. H., Kennepohl, P., and Solomon, E. I. (1996) Structural and functional aspects of metal sites in biology. *Chemical Reviews* 96, 2239-2314.
- (12) Alberts, I. L., Nadassy, K., and Wodak, S. J. (1998) Analysis of zinc binding sites in protein crystal structures. *Protein Science* 7, 1700-1716.
- (13) Auld, D. S. (2001) Zinc coordination sphere in biochemical zinc sites. *Biometals* 14, 271-313.

- (14) Christianson, D. W., and Lipscomb, W. N. (1989) Carboxypeptidase-A. *Accounts of Chemical Research* 22, 62-69.
- (15) Lipscomb, W. N., and Strater, N. (1996) Recent advances in zinc enzymology. *Chemical Reviews* 96, 2375-2433.
- (16) Wilcox, D. E. (1996) Binuclear metallohydrolases. *Chemical Reviews* 96, 2435-2458.
- (17) Meinnel, T., Mechulam, Y., and Blanquet, S. (1993) Methionine as Translation Start Signal - a Review of the Enzymes of the Pathway in Escherichia-Coli. *Biochimie* 75, 1061-1075.
- (18) Adams, J. M. (1968) On Release of Formyl Group from Nascent Protein. *Journal of Molecular Biology* 33, 571-&.
- (19) Rajagopalan, P. T., Datta, A., and Pei, D. (1997) Purification, characterization, and inhibition of peptide deformylase from Escherichia coli. *Biochemistry* 36, 13910-13918.
- (20) Rajagopalan, P. T., and Pei, D. (1998) Oxygen-mediated inactivation of peptide deformylase. *J Biol Chem* 273, 22305-22310.
- (21) Rajagopalan, P. T. R., Grimme, S., and Pei, D. H. (2000) Characterization of cobalt(II)-substituted peptide deformylase: Function of the metal ion and the catalytic residue Glu-133. *Biochemistry* 39, 779-790.
- (22) Chan, M. K., Gong, W., Rajagopalan, P. T., Hao, B., Tsai, C. M., and Pei, D. (1997) Crystal structure of the Escherichia coli peptide deformylase. *Biochemistry* 36, 13904-13909.
- (23) Zimmerman, S. A., and Ferry, J. G. (2008) The beta and gamma classes of carbonic anhydrase. *Current Pharmaceutical Design* 14, 716-721.
- (24) Zhu, J. G., Dizin, E., Hu, X. B., Wavreille, A. S., Park, J., and Pei, D. H. (2003) S-ribosylhomocysteinase (LuxS) is a mononuclear iron protein. *Biochemistry* 42, 4717-4726.
- (25) Chai, S. C., Wang, W. L., and Ye, Q. Z. (2008) FE(II) is the native cofactor for Escherichia coli methionine aminopeptidase. *J Biol Chem* 283, 26879-26885.
- (26) Ireton, G. C., McDermott, G., Black, M. E., and Stoddard, B. L. (2002) The structure of Escherichia coli cytosine deaminase. *Journal of Molecular Biology* 315, 687-697.
- (27) Ireton, G. C., Black, M. E., and Stoddard, B. L. (2003) The 1.14 angstrom crystal structure of yeast cytosine deaminase: Evolution of nucleotide salvage enzymes and implications for genetic chemotherapy. *Structure* 11, 961-972.

- (28) Seffernick, J. L., McTavish, H., Osborne, J. P., de Souza, M. L., Sadowsky, M. J., and Wackett, L. P. (2002) Atrazine chlorohydrolase from *Pseudomonas* sp strain ADP is a metalloenzyme. *Biochemistry* 41, 14430-14437.
- (29) Hall, R. S., Xiang, D. F., Xu, C. F., and Raushel, F. M. (2007) N-acetyl-D-glucosamine-6-phosphate deacetylase: Substrate activation via a single divalent metal ion. *Biochemistry* 46, 7942-7952.
- (30) Raetz, C. R. H. (2002) Biosynthesis, secretion and function of Gram-negative endotoxin - A potent lipid activator of innate immunity. *Faseb Journal* 16, A521-A521.
- (31) Raetz, C. R., and Whitfield, C. (2002) Lipopolysaccharide endotoxins. *Annu Rev Biochem* 71, 635-700.
- (32) Raetz, C. R. (1993) Bacterial endotoxins: extraordinary lipids that activate eucaryotic signal transduction. *J Bacteriol* 175, 5745-5753.
- (33) Wyckoff, T. J. O., Raetz, C. R. H., and Jackman, J. E. (1998) Antibacterial and anti-inflammatory agents that target endotoxin. *Trends in Microbiology* 6, 154-159.
- (34) Raetz, C. R., Guan, Z., Ingram, B. O., Six, D. A., Song, F., Wang, X., and Zhao, J. (2008) Discovery of new biosynthetic pathways: the lipid A story. *J Lipid Res.*
- (35) Hernick, M., and Fierke, C. A. (2005) Zinc hydrolases: the mechanisms of zinc-dependent deacetylases. *Arch Biochem Biophys* 433, 71-84.
- (36) Jackman, J. E., Fierke, C. A., Tumey, L. N., Pirrung, M., Uchiyama, T., Tahir, S. H., Hindsgaul, O., and Raetz, C. R. (2000) Antibacterial agents that target lipid A biosynthesis in gram-negative bacteria. Inhibition of diverse UDP-3-O-(r-3-hydroxymyristoyl)-n-acetylglucosamine deacetylases by substrate analogs containing zinc binding motifs. *J Biol Chem* 275, 11002-11009.
- (37) White, R. J., Margolis, P. S., Trias, J., and Yuan, Z. Y. (2003) Targeting metalloenzymes: a strategy that works. *Current opinion in pharmacology* 3, 502-507.
- (38) Anderson, M. S., Bull, H. G., Galloway, S. M., Kelly, T. M., Mohan, S., Radika, K., and Raetz, C. R. (1993) UDP-N-acetylglucosamine acyltransferase of *Escherichia coli*. The first step of endotoxin biosynthesis is thermodynamically unfavorable. *J Biol Chem* 268, 19858-19865.
- (39) Young, K., Silver, L. L., Bramhill, D., Cameron, P., Eveland, S. S., Raetz, C. R., Hyland, S. A., and Anderson, M. S. (1995) The envA permeability/cell division gene of *Escherichia coli* encodes the second enzyme of lipid A biosynthesis. UDP-3-O-(R-3-hydroxymyristoyl)-N-acetylglucosamine deacetylase. *J Biol Chem* 270, 30384-30391.

- (40) Jackman, J. E., Raetz, C. R., and Fierke, C. A. (1999) UDP-3-O-(R-3-hydroxymyristoyl)-N-acetylglucosamine deacetylase of *Escherichia coli* is a zinc metalloenzyme. *Biochemistry* 38, 1902-1911.
- (41) Kelly, T. M., Stachula, S. A., Raetz, C. R., and Anderson, M. S. (1993) The *firA* gene of *Escherichia coli* encodes UDP-3-O-(R-3-hydroxymyristoyl)-glucosamine N-acyltransferase. The third step of endotoxin biosynthesis. *J Biol Chem* 268, 19866-19874.
- (42) Babinski, K. J., and Raetz, C. R. H. (1998) Identification of a gene encoding a novel *Escherichia coli* UDP-2,3-diacylglucosamine hydrolase. *Faseb Journal* 12, A1288-A1288.
- (43) Bulawa, C. E., and Raetz, C. R. H. (1984) The Biosynthesis of Gram-Negative Endotoxin - Identification and Function of Udp-2,3-Diacylglucosamine in *Escherichia-Coli*. *Journal of Biological Chemistry* 259, 4846-4851.
- (44) RAY, B. L., Painter, G., and Raetz, C. R. H. (1984) The Biosynthesis of Gram-Negative Endotoxin - Formation of Lipid a Disaccharides from Monosaccharide Precursors in Extracts of *Escherichia-Coli*. *Journal of Biological Chemistry* 259, 4852-4859.
- (45) RAY, B. L., and Raetz, C. R. H. (1987) The Biosynthesis of Gram-Negative Endotoxin - a Novel Kinase in *Escherichia-Coli* Membranes That Incorporates the 4'-Phosphate of Lipid-A. *Journal of Biological Chemistry* 262, 1122-1128.
- (46) Clementz, T., and Raetz, C. R. (1991) A gene coding for 3-deoxy-D-manno-octulosonic-acid transferase in *Escherichia coli*. Identification, mapping, cloning, and sequencing. *J Biol Chem* 266, 9687-9696.
- (47) White, K. A., Kaltashov, I. A., Cotter, R. J., and Raetz, C. R. H. (1997) A monofunctional 3-deoxy-D-manno-octulosonic acid (Kdo) transferase and a Kdo kinase in extracts of *Haemophilus influenzae*. *Journal of Biological Chemistry* 272, 16555-16563.
- (48) Belunis, C. J., Mdluli, K. E., Raetz, C. R. H., and Nano, F. E. (1992) A Novel 3-Deoxy-D-Manno-Octulosonic Acid Transferase from *Chlamydia-Trachomatis* Required for Expression of the Genus-Specific Epitope. *Journal of Biological Chemistry* 267, 18702-18707.
- (49) Brozek, K. A., and Raetz, C. R. H. (1990) Biosynthesis of Lipid-a in *Escherichia-Coli* - Acyl Carrier Protein-Dependent Incorporation of Laurate and Myristate. *Journal of Biological Chemistry* 265, 15410-15417.
- (50) Zhou, Z. M., White, K. A., Polissi, A., Georgopoulos, C., and Raetz, C. R. H. (1998) Function of *Escherichia coli* MsbA, an essential ABC family transporter, in lipid A and phospholipid biosynthesis. *Journal of Biological Chemistry* 273, 12466-12475.

- (51) Dawson, R. J. P., and Locher, K. P. (2007) Structure of the multidrug ABC transporter Sav1866 from *Staphylococcus aureus* in complex with AMP-PNP. *Febs Letters* 581, 935-938.
- (52) Dawson, R. J. P., and Locher, K. P. (2006) Structure of a bacterial multidrug ABC transporter. *Nature* 443, 180-185.
- (53) Reeves, P. R., Hobbs, M., Valvano, M. A., Skurnik, M., Whitfield, C., Coplin, D., Kido, N., Klena, J., Maskell, D., Raetz, C. R. H., *et al.* (1996) Bacterial polysaccharide synthesis and gene nomenclature. *Trends in Microbiology* 4, 495-503.
- (54) Sperandio, P., Cescutti, R., Villa, R., Di Benedetto, C., Candia, D., Deho, G., and Polissi, A. (2007) Characterization of *lptA* and *lptB*, two essential genes implicated in lipopolysaccharide transport to the outer membrane of *Escherichia coli*. *Journal of Bacteriology* 189, 244-253.
- (55) Braun, M., and Silhavy, T. J. (2002) Imp/OstA is required for cell envelope biogenesis in *Escherichia coli*. *Molecular Microbiology* 45, 1289-1302.
- (56) Raetz, C. R. H., Reynolds, C. M., Trent, M. S., and Bishop, R. E. (2007) Lipid A modification systems in gram-negative bacteria. *Annual Review of Biochemistry* 76, 295-329.
- (57) Trent, M. S., Ribeiro, A. A., Lin, S. H., Cotter, R. J., and Raetz, C. R. H. (2001) An inner membrane enzyme in *Salmonella* and *Escherichia coli* that transfers 4-amino-4-deoxy-L-arabinose to lipid A - Induction in polymyxin-resistant mutants and role of a novel lipid-linked donor. *Journal of Biological Chemistry* 276, 43122-43131.
- (58) Bader, M. W., Sanowar, S., Daley, M. E., Schneider, A. R., Cho, U. S., Xu, W. Q., Klevit, R. E., Le Moual, H., and Miller, S. (2005) Recognition of antimicrobial peptides by a bacterial sensor kinase. *Cell* 122, 461-472.
- (59) Robey, M., O'Connell, W., and Cianciotto, N. P. (2001) Identification of *Legionella pneumophila* *rcp*, a *pagP*-like gene that confers resistance to cationic antimicrobial peptides and promotes intracellular infection. *Infection and Immunity* 69, 4276-4286.
- (60) Preston, A., Maxim, E., Toland, E., Pishko, E. J., Harvill, E. T., Caroff, M., and Maskell, D. J. (2003) *Bordetella bronchiseptica* *PagP* is a Bvg-regulated lipid A palmitoyl transferase that is required for persistent colonization of the mouse respiratory tract. *Molecular Microbiology* 48, 725-736.
- (61) Opal, S. M. (2007) The host response to endotoxin, antilipopolysaccharide strategies, and the management of severe sepsis. *Int J Med Microbiol* 297, 365-377.

- (62) Manocha, S., Feinstein, D., and Kumar, A. (2002) Novel therapies for sepsis: antiendotoxin therapies. *Expert Opinion on Investigational Drugs* 11, 1795-1812.
- (63) Beall, B., and Lutkenhaus, J. (1987) Sequence-analysis, transcriptional organization, and insertional mutagenesis of the envA gene of Escherichia coli. *Journal of Bacteriology* 169, 5408-5415.
- (64) Hernick, M., and Fierke, C. A. (2005) Zinc hydrolases: The mechanisms of zinc-dependent deacetylases. *Archives of Biochemistry and Biophysics* 433, 71-84.
- (65) Jackman, J. E., Raetz, C. R., and Fierke, C. A. (2001) Site-directed mutagenesis of the bacterial metalloamidase UDP-(3-O-acyl)-N-acetylglucosamine deacetylase (LpxC). Identification of the zinc binding site. *Biochemistry* 40, 514-523.
- (66) McClure, C. P., Rusche, K. M., Peariso, K., Jackman, J. E., Fierke, C. A., and Penner-Hahn, J. E. (2003) EXAFS studies of the zinc sites of UDP-(3-O-acyl)-N-acetylglucosamine deacetylase (LpxC). *Journal of Inorganic Biochemistry* 94, 78-85.
- (67) Whittington, D. A., Rusche, K. M., Shin, H., Fierke, C. A., and Christianson, D. W. (2003) Crystal structure of LpxC, a zinc-dependent deacetylase essential for endotoxin biosynthesis. *Proc Natl Acad Sci USA* 100, 8146-8150.
- (68) Coggins, B. E., Li, X. C., McClerren, A. L., Hindsgaul, O., Raetz, C. R. H., and Zhou, P. (2003) Structure of the LpxC deacetylase with a bound substrate-analog inhibitor. *Nature Structural Biology* 10, 645-651.
- (69) Coggins, B. E., McClerren, A. L., Jiang, L., Li, X., Rudolph, J., Hindsgaul, O., Raetz, C. R. H., and Zhou, P. (2005) Refined Solution Structure of the LpxC-TU-514 Complex and pKa Analysis of an Active Site Histidine: Insights into the Mechanism and Inhibitor Design. *Biochemistry* 44, 1114-1126.
- (70) Gennadios, H. A., and Christianson, D. W. (2006) Binding of uridine 5'-diphosphate in the "basic patch" of the zinc deacetylase LpxC and implications for substrate binding. *Biochemistry* 45, 15216-15223.
- (71) Mochalkin, I., Knafels, J. D., and Lightle, S. (2008) Crystal structure of LpxC from Pseudomonas aeruginosa complexed with the potent BB-78485 inhibitor. *Protein Sci* 17, 450-457.
- (72) Hernick, M., Gennadios, H. A., Whittington, D. A., Rusche, K. M., Christianson, D. W., and Fierke, C. A. (2005) UDP-3-O-((R)-3-hydroxymyristoyl)-N-acetylglucosamine deacetylase functions through a general acid-base catalyst pair mechanism. *J Biol Chem* 280, 16969-16978.

- (73) McClerren, A. L., Zhou, P., Guan, Z., Raetz, C. R., and Rudolph, J. (2005) Kinetic analysis of the zinc-dependent deacetylase in the lipid A biosynthetic pathway. *Biochemistry* 44, 1106-1113.
- (74) Hernick, M., Gattis, S. G., Penner-Hahn, J. E., and Fierke, C. A. Activation of E. coli UDP-3-O-(R-3-hydroxymyristoyl)-N-acetylglucosamine deacetylase by Fe²⁺ yields a more efficient enzyme with altered ligand affinity. *Biochemistry*.
- (75) Lipton, A. S., Heck, R. W., Hernick, M., Fierke, C. A., and Ellis, P. D. (2008) Residue Ionization in LpxC Directly Observed by (67)Zn NMR Spectroscopy. *J Am Chem Soc*.
- (76) Hedstrom, L. (2002) Serine protease mechanism and specificity. *Chemical Reviews* 102, 4501-4523.
- (77) Hernick, M., and Fierke, C. A. (2006) Catalytic Mechanism and Molecular Recognition of E. coli UDP-3-O-(R-3-Hydroxymyristoyl)-N-acetylglucosamine Deacetylase Probed by Mutagenesis. *Biochemistry* 45, 15240-15248.
- (78) Onishi, H. R., Pelak, B. A., Gerckens, L. S., Silver, L. L., Kahan, F. M., Chen, M. H., Patchett, A. A., Galloway, S. M., Hyland, S. A., Anderson, M. S., *et al.* (1996) Antibacterial agents that inhibit lipid A biosynthesis. *Science* 274, 980-982.
- (79) Jackman, J. E., Fierke, C. A., Tumey, L. N., Pirrung, M., Uchiyama, T., Tahir, S. H., Hindsgaul, O., and Raetz, C. R. H. (2000) Antibacterial agents that target lipid A biosynthesis in Gram-negative bacteria - Inhibition of diverse UDP-3-O-(R-3-hydroxymyristoyl)-N-acetylglucosamine deacetylases by substrate analogs containing zinc binding motifs. *Journal of Biological Chemistry* 275, 11002-11009.
- (80) Clements, J. M., Coignard, F., Johnson, I., Chandler, S., Palan, S., Waller, A., Wijkmans, J., and Hunter, M. G. (2002) Antibacterial activities and characterization of novel inhibitors of LpxC. *Antimicrobial Agents and Chemotherapy* 46, 1793-1799.
- (81) Pirrung, M. C., Tumey, L. N., McClerren, A. L., and Raetz, C. R. H. (2003) High-throughput catch-and-release synthesis of oxazoline hydroxamates. Structure-activity relationships in novel inhibitors of Escherichia coli LpxC: In vitro enzyme inhibition and antibacterial properties. *Journal of the American Chemical Society* 125, 1575-1586.
- (82) Li, X. C., Uchiyama, T., Raetz, C. R. H., and Hindsgaul, O. (2003) Synthesis of a carbohydrate-derived hydroxamic acid inhibitor of the bacterial enzyme (LpxC) involved in lipid A biosynthesis. *Organic Letters* 5, 539-541.
- (83) Pirrung, M. C., Tumey, L. N., Raetz, C. R. H., Jackman, J. E., Snehathala, K., McClerren, A. L., Fierke, C. A., Gantt, S. L., and Rusche, K. M. (2002) Inhibition

of the antibacterial target UDP-(3-O-acyl)-N- acetylglucosamine deacetylase (LpxC): Isoxazoline zinc amidase inhibitors bearing diverse metal binding groups. *Journal of Medicinal Chemistry* 45, 4359-4370.

- (84) McClerren, A. L., Endsley, S., Bowman, J. L., Andersen, N. H., Guan, Z., Rudolph, J., and Raetz, C. R. (2005) A slow, tight-binding inhibitor of the zinc-dependent deacetylase LpxC of lipid A biosynthesis with antibiotic activity comparable to ciprofloxacin. *Biochemistry* 44, 16574-16583.
- (85) Mdluli, K. E., Witte, P. R., Kline, T., Barb, A. W., Erwin, A. L., Mansfield, B. E., McClerren, A. L., Pirrung, M. C., Tumey, L. N., Warrenner, P., *et al.* (2006) Molecular validation of LpxC as an antibacterial drug target in *Pseudomonas aeruginosa*. *Antimicrobial Agents and Chemotherapy* 50, 2178-2184.
- (86) Barb, A. W., Jiang, L., Raetz, C. R., and Zhou, P. (2007) Structure of the deacetylase LpxC bound to the antibiotic CHIR-090: Time-dependent inhibition and specificity in ligand binding. *Proc Natl Acad Sci USA* 104, 18433-18438.
- (87) Walsh, C. T. (2006) *Posttranslational Modifications of Proteins: Expanding Nature's Inventory*, Roberts and Co. Publishers, Greenwood Village.
- (88) Kouzarides, T. (2000) Acetylation: a regulatory modification to rival phosphorylation? *EMBO J* 19, 1176-1179.
- (89) Glozak, M. A., Sengupta, N., Zhang, X., and Seto, E. (2005) Acetylation and deacetylation of non-histone proteins. *Gene* 363, 15-23.
- (90) Drummond, D. C., Noble, C. O., Kirpotin, D. B., Guo, Z., Scott, G. K., and Benz, C. C. (2005) Clinical development of histone deacetylase inhibitors as anticancer agents. *Annu Rev Pharmacol Toxicol* 45, 495-528.
- (91) Yang, X. J., and Seto, E. (2008) The Rpd3/Hda1 family of lysine deacetylases: from bacteria and yeast to mice and men. *Nat Rev Mol Cell Biol* 9, 206-218.
- (92) Kim, S. C., Sprung, R., Chen, Y., Xu, Y., Ball, H., Pei, J., Cheng, T., Kho, Y., Xiao, H., Xiao, L., *et al.* (2006) Substrate and functional diversity of lysine acetylation revealed by a proteomics survey. *Mol Cell* 23, 607-618.
- (93) Hassig, C. A., and Schreiber, S. L. (1997) Nuclear histone acetylases and deacetylases and transcriptional regulation: HATs off to HDACs. *Current opinion in chemical biology* 1, 300-308.
- (94) Yang, X. J., and Seto, E. (2007) HATs and HDACs: from structure, function and regulation to novel strategies for therapy and prevention. *Oncogene* 26, 5310-5318.

- (95) Allis, C. D., Berger, S. L., Cote, J., Dent, S., Jenuwien, T., Kouzarides, T., Pillus, L., Reinberg, D., Shi, Y., Shiekhhattar, R., *et al.* (2007) New nomenclature for chromatin-modifying enzymes. *Cell* 131, 633-636.
- (96) Blander, G., and Guarente, L. (2004) The Sir2 family of protein deacetylases. *Annu Rev Biochem* 73, 417-435.
- (97) Glozak, M. A., and Seto, E. (2007) Histone deacetylases and cancer. *Oncogene* 26, 5420-5432.
- (98) Lin, H. Y., Chen, C. S., Lin, S. P., Weng, J. R., and Chen, C. S. (2006) Targeting histone deacetylase in cancer therapy. *Med Res Rev*.
- (99) Witt, O., Deubzer, H. E., Milde, T., and Oehme, I. (2009) HDAC family: What are the cancer relevant targets? *Cancer Lett* 277, 8-21.
- (100) Saha, R. N., and Pahan, K. (2005) HATs and HDACs in neurodegeneration: a tale of disconcerted acetylation homeostasis. *Cell Death Differ*.
- (101) Grabiec, A. M., Tak, P. P., and Reedquist, K. A. (2008) Targeting histone deacetylase activity in rheumatoid arthritis and asthma as prototypes of inflammatory disease: should we keep our HATs on? *Arthritis Res Ther* 10, 226.
- (102) Kornberg, R. D., and Lorch, Y. (1999) Twenty-five years of the nucleosome, fundamental particle of the eukaryote chromosome. *Cell* 98, 285-294.
- (103) Luger, K., Mader, A. W., Richmond, R. K., Sargent, D. F., and Richmond, T. J. (1997) Crystal structure of the nucleosome core particle at 2.8 Å resolution. *Nature* 389, 251-260.
- (104) Luger, K., and Richmond, T. J. (1998) DNA binding within the nucleosome core. *Curr Opin Struct Biol* 8, 33-40.
- (105) Strahl, B. D., and Allis, C. D. (2000) The language of covalent histone modifications. *Nature* 403, 41-45.
- (106) Kouzarides, T. (2007) Chromatin modifications and their function. *Cell* 128, 693-705.
- (107) Jenuwein, T., and Allis, C. D. (2001) Translating the histone code. *Science* 293, 1074-1080.
- (108) de Ruijter, A. J., van Gennip, A. H., Caron, H. N., Kemp, S., and van Kuilenburg, A. B. (2003) Histone deacetylases (HDACs): characterization of the classical HDAC family. *Biochem J* 370, 737-749.

- (109) Gao, L., Cueto, M. A., Asselbergs, F., and Atadja, P. (2002) Cloning and functional characterization of HDAC11, a novel member of the human histone deacetylase family. *Journal of Biological Chemistry* 277, 25748-25755.
- (110) Sinclair, D. A., Lin, S. J., and Guarente, L. (2006) Life-span extension in yeast. *Science* 312, 195-196.
- (111) Chen, D., and Guarente, L. (2007) SIR2: a potential target for calorie restriction mimetics. *Trends in Molecular Medicine* 13, 64-71.
- (112) Guarente, L. (2001) SIR2 and aging--the exception that proves the rule. *Trends Genet* 17, 391-392.
- (113) Mann, B. S., Johnson, J. R., Cohen, M. H., Justice, R., and Pazdur, R. (2007) FDA approval summary: vorinostat for treatment of advanced primary cutaneous T-cell lymphoma. *Oncologist* 12, 1247-1252.
- (114) Balasubramanian, S., Verner, E., and Buggy, J. J. (2009) Isoform-specific histone deacetylase inhibitors: the next step? *Cancer Lett* 280, 211-221.
- (115) Chou, C. J., Herman, D. M., and Gottesfeld, J. M. (2008) Pimelic diphenylamide 106 is a slow, tight-binding inhibitor of class I histone deacetylases. *J Biol Chem*.
- (116) Herman, D., Jenssen, K., Burnett, R., Soragni, E., Perlman, S. L., and Gottesfeld, J. M. (2006) Histone deacetylase inhibitors reverse gene silencing in Friedreich's ataxia. *Nat Chem Biol* 2, 551-558.
- (117) Rai, M., Soragni, E., Jenssen, K., Burnett, R., Herman, D., Coppola, G., Geschwind, D. H., Gottesfeld, J. M., and Pandolfo, M. (2008) HDAC inhibitors correct frataxin deficiency in a Friedreich ataxia mouse model. *PLoS One* 3, e1958.
- (118) Van den Wyngaert, I., de Vries, W., Kremer, A., Neefs, J. M., Verhasselt, P., Luyten, W., and Kass, S. U. (2000) Cloning and characterization of human histone deacetylase 8. *Febs Letters* 478, 77-83.
- (119) Waltregny, D., de Leval, L., Glenisson, W., Tran, S. L., North, B. J., Bellahcene, A., Weidle, U., Verdin, E., and Castronovo, V. (2004) Expression of histone deacetylase 8, a class I histone deacetylase, is restricted to cells showing smooth muscle differentiation in normal human tissues. *American Journal of Pathology* 165, 553-564.
- (120) Waltregny, D., Glénisson, W., Tran, S. L., North, B. J., Verdin, E., Colige, A., and Castronovo, V. (2005) Histone deacetylase HDAC8 associates with smooth muscle alpha-actin and is essential for smooth muscle cell contractility. *Faseb J* 19, 966-968.

- (121) Lee, H., Rezai-Zadeh, N., and Seto, E. (2004) Negative regulation of histone deacetylase 8 activity by cyclic AMP-dependent protein kinase A. *Mol Cell Biol* 24, 765-773.
- (122) Nakagawa, M., Oda, Y., Eguchi, T., Aishima, S., Yao, T., Hosoi, F., Basaki, Y., Ono, M., Kuwano, M., Tanaka, M., *et al.* (2007) Expression profile of class I histone deacetylases in human cancer tissues. *Oncol Rep* 18, 769-774.
- (123) Balasubramanian, S., Ramos, J., Luo, W., Sirisawad, M., Verner, E., and Buggy, J. J. (2008) A novel histone deacetylase 8 (HDAC8)-specific inhibitor PCI-34051 induces apoptosis in T-cell lymphomas. *Leukemia* 22, 1026-1034.
- (124) Oehme, I., Deubzer, H. E., Wegener, D., Pickert, D., Linke, J. P., Hero, B., Kopp-Schneider, A., Westermann, F., Ulrich, S. M., von Deimling, A., *et al.* (2009) Histone deacetylase 8 in neuroblastoma tumorigenesis. *Clin Cancer Res* 15, 91-99.
- (125) Somoza, J. R., Skene, R. J., Katz, B. A., Mol, C., Ho, J. D., Jennings, A. J., Luong, C., Arvai, A., Buggy, J. J., Chi, E., *et al.* (2004) Structural snapshots of human HDAC8 provide insights into the class I histone deacetylases. *Structure* 12, 1325-1334.
- (126) Vannini, A., Volpari, C., Filocamo, G., Casavola, E. C., Brunetti, M., Renzoni, D., Chakravarty, P., Paolini, C., De Francesco, R., Gallinari, P., *et al.* (2004) Crystal structure of a eukaryotic zinc-dependent histone deacetylase, human HDAC8, complexed with a hydroxamic acid inhibitor. *Proc Natl Acad Sci USA* 101, 15064-15069.
- (127) Finnin, M. S., Donigian, J. R., Cohen, A., Richon, V. M., Rifkind, R. A., Marks, P. A., Breslow, R., and Pavletich, N. P. (1999) Structures of a histone deacetylase homologue bound to the TSA and SAHA inhibitors. *Nature* 401, 188-193.
- (128) Dowling, D. P., Gantt, S. L., Gattis, S. G., Fierke, C. A., and Christianson, D. W. (2008) Structural Studies of Human Histone Deacetylase 8 and Its Site-Specific Variants Complexed with Substrate and Inhibitors (dagger) (,) (double dagger). *Biochemistry* 47, 13554-13563.
- (129) Gantt, S. L., Joseph, C. G., and Fierke, C. A. (2009) Activation and inhibition of histone deacetylase 8 by monovalent cations. *J Biol Chem*.
- (130) Gantt, S. L., Gattis, S. G., and Fierke, C. A. (2006) Catalytic activity and inhibition of human histone deacetylase 8 is dependent on the identity of the active site metal ion. *Biochemistry* 45, 6170-6178.
- (131) Fersht, A. R. (1999) *Structure and Mechanism in Protein Science: A Guide to Enzyme Catalysis and Protein Folding*, W. H. Freeman and Company, New York.

- (132) Epsztejn, S., Kakhlon, O., Glickstein, H., Breuer, W., and Cabantchik, Z. I. (1997) Fluorescence analysis of the labile iron pool of mammalian cells. *Analytical Biochemistry* 248, 31-40.
- (133) Petrat, F., de Groot, H., and Rauen, U. (2001) Subcellular distribution of chelatable iron: a laser scanning microscopic study in isolated hepatocytes and liver endothelial cells. *Biochem J* 356, 61-69.
- (134) MacKenzie, E. L., Iwasaki, K., and Tsuji, Y. (2008) Intracellular iron transport and storage: from molecular mechanisms to health implications. *Antioxid Redox Signal* 10, 997-1030.
- (135) Muir, T. W., Sondhi, D., and Cole, P. A. (1998) Expressed protein ligation: A general method for protein engineering. *Proc Natl Acad Sci U S A* 95, 6705-6710.
- (136) Muir, T. W. (2003) Semisynthesis of proteins by expressed protein ligation. *Annu Rev Biochem* 72, 249-289.

CHAPTER 2.

MECHANISM OF LPXC PROBED BY MUTAGENESIS AND EXPRESSED PROTEIN LIGATION

Introduction

Despite the high degree of interest in LpxC as a drug target, the mechanism of deacetylation catalyzed by LpxC remains unresolved. A complete understanding of the mechanism is a critical step in design and optimization of potential antibiotics (1-5).

Several chemical mechanisms for LpxC catalysis have been proposed (see Chapter 1 for a thorough discussion), with two competing mechanisms most consistent with the published data (6-8). The first proposed mechanism is similar to the mechanism of most metalloproteases, in which a single residue functions as both a general acid and a general base catalyst. As shown in Figure 2.1A, the catalytic metal ion (presumed to be Zn) coordinates a water molecule. The water is deprotonated by the active site base, Glu78 (*E. coli* numbering), as it attacks the carbonyl carbon of the substrate acetyl group. A tetrahedral intermediate is formed, where the oxyanion is stabilized by interaction with the positively charged His265, as well as with Zn^{2+} and other groups. Breakdown of the intermediate is catalyzed by protonation of the amine leaving group by E78 to form the products, free acetate and UDP-3-*O*-(*R*-3-hydroxymyristoyl)-glucosamine.

A second proposed mechanism differs mainly in the role of His265. As shown in Figure 2.1B, Glu78 still functions as a general base to activate the nucleophilic water, but

H265, rather than stabilizing the tetrahedral intermediate by a positive charge in the active site, functions as a general acid to protonate the glucosamine leaving group to accelerate breakdown of the tetrahedral intermediate. Both mechanisms are consistent with the published data, which have demonstrated that Glu78 and His265 are both essential for LpxC catalysis (6, 8). The dependence of k_{cat}/K_M on pH in LpxC catalysis shows a bell-shaped dependence, and mutagenesis of Glu78 to alanine has demonstrated that pK_{a1} reflects ionization of that residue. However, identifying the second ionizing group has been more difficult due to complications from the metal-water pK_a and potentially other groups. In particular, NMR measurements of the protonation state of H265 have called into question whether ionization of His265 adequately accounts for the second ionization (9). Nonetheless, a variety of evidence supports the role of His265 as a general acid. Mutation of His265 to Ala decreases activity 2190-fold. Additionally, mutation of the group that forms a hydrogen bond with H265, Asp246, has a similar effect (8). Such Asp/His dyads are often associated with proton transfer reactions (10). Finally, crystal structures of LpxC with a tetrahedral mimic, cacodylate, reveal that His265 is closer to the CH_3 (equivalent to the leaving group amine), while Glu78 is close to one of the oxygen groups (equivalent to the nucleophilic water). This structure suggests that H265 is positioned to protonate the leaving group rather than stabilize the oxyanion intermediate (8). Since the evidence for either mechanism is inconclusive, further experiments are needed to define the role of His265. Therefore, I sought to develop methods to probe the function of His265, including mutagenesis and expressed protein ligation.

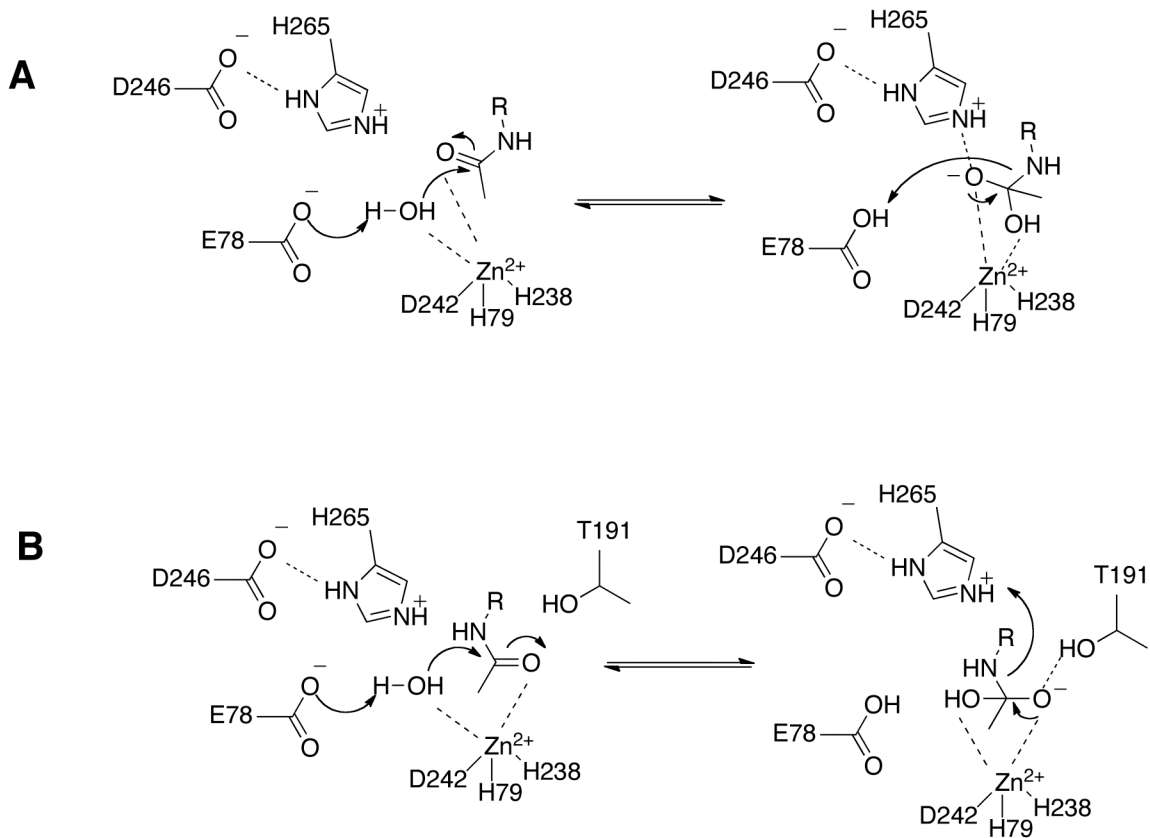


Figure 2.1: Proposed mechanisms for LpxC catalysis LpxC is proposed to function either using a single general acid/base residue (A), or via a general acid/general base pair (B). R = myristoyl-UDP-glucose. Numbering is for *E. coli* LpxC.

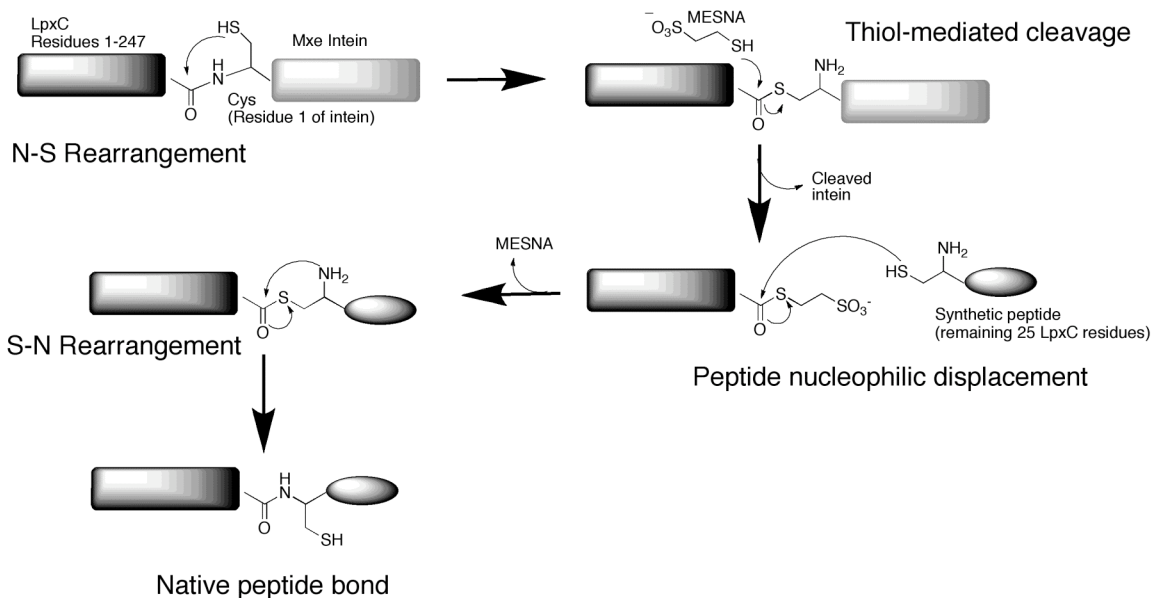


Figure 2.2: Expressed protein ligation. LpxC-intein fusion protein undergoes spontaneous N-S rearrangement. Addition of thiol nucleophile (mercaptoethane sulfonic acid, MESNA) leads to cleavage of intein from LpxC, followed by addition of peptide. Cys1 of the peptide attacks the carbonyl carbon of the thioester, followed by S-N rearrangement to form a native peptide bond and full length LpxC.

Table 2.1: Expressed protein ligation yields

EPL Preparation Step ^a	Approximate Yield (mg/L or %) ^b
Purified LpxC-Mxe fusion	20 – 40
Refolded LpxC-Mxe fusion	15 – 30 (~75%)
Cleavage of LpxC from Mxe	4 – 8 (~50%)
Ligation to C-terminal peptide	2 – 4 (~50%)
Refolding of full-length protein	~1 – 2 (~50%)

^a Each step outlined in preparation of semisynthetic-LpxC, as outlined in Materials and Methods, is listed along with typical yields

^b Approximate yields, in mg/L of cell growth and mole percent.

Expressed protein ligation is a technique that allows the incorporation of unnatural groups into an otherwise native protein (reviewed in (11-14), shown in Figure 2.2). This method greatly augments traditional site-directed mutagenesis, which is limited to the 20 natural amino acids, due to the ability to incorporate a wide range of chemical groups outside those observed in nature. In LpxC, our specific question is whether His265 functions solely as an electrostatic catalyst to stabilize the oxyanion intermediate, or also functions as a general acid by protonating the leaving group amine. By introducing amino acids that contain a side-chain structurally similar to histidine but have an altered pKa value or charge, we propose to specifically test this hypothesis. EPL allows for a much more comprehensive structure-activity analysis of enzyme function.

Materials and methods

General methods, site-directed mutagenesis, and plasmid construction

All solutions were prepared in “metal-free” plastic ware with reagents without extraneous metal ions, as verified by ICP-MS (Dr. Ted Huston, University of Michigan). Reagents were of the highest quality available from Sigma-Aldrich, unless noted. Site-directed mutations were prepared using Quik-Change site-directed mutagenesis kits (Stratagene). For construction of the LpxC-Intein fusion plasmid (Figure 2.3), a BspQ1 (isoschizomer of Sap1) site was inserted in the pAaLpxC plasmid after residue 246 (pAaLpxC-BspQ1) using the Quik-Change method (Stratagene). Both the pAaLpxC-BspQ1 and the pTXB1 (NEB) plasmids were digested sequentially by BspQ1 and Nde1 with gel purification (Promega) after each digestion. The isolated LpxC fragment was ligated with the BspQ1/Nde1-digested pTXB1 vector using T4 DNA ligase (NEB) to create the new vector pAaLpxC-Mxe. The LpxC-Mxe portion of the plasmid was then

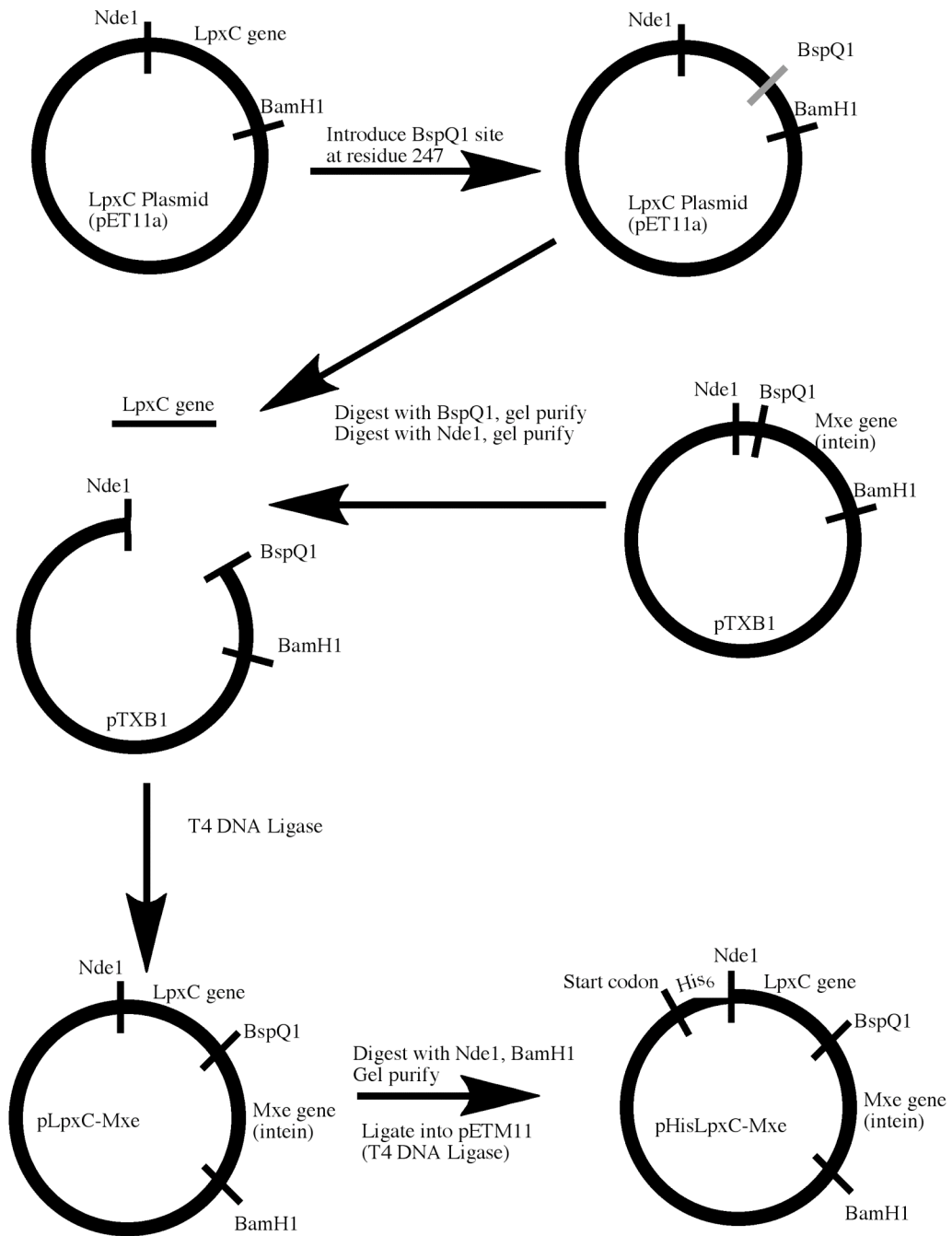


Figure 2.3: Schematic of LpxC-intein plasmid construction.

moved into a vector containing an N-terminal His₆-tag. The pAaLpxC-Mxe plasmid and the pETM11 plasmid (Novagen) were both digested by NdeI/BamHI, gel purified, and then ligated together using T4 DNA ligase, creating the vector pAaHisLpxC-Mxe. All sequences were verified by the University of Michigan DNA sequencing core.

Activity assays

¹⁴C-labeled LpxC substrate, UDP-3-*O*-(*R*-3-hydroxymyristoyl)-*N*-acetylglucosamine, was prepared by enzymatic synthesis as previously described (8, 15, 16). Briefly, a 1 mL reaction containing 40 mM HEPES, pH 8, 1 mg/mL bovine serum albumin, 1 mM methylmethane thiosulfonate, 54 μM myristoylated acyl carrier protein (myr-ACP), and 6.94 μM ¹⁴C-UDP-*N*-acetylglucosamine (PerkinElmer). To this was added 20 μL of ~20 mg/mL LpxA protein, and the reaction was incubated at 30°C for 30 min. The ACP and LpxA plasmids were the generous gifts of Chris Walsh (Harvard Medical School) and Chris Raetz (Duke University). The reaction was loaded onto ~2 mL DEAE resin followed by a SepPak C18 cartridge (Waters), pre-equilibrated in 50 mM bis-tris pH 6. The reaction mixtures were washed with 0.2 M NaCl and then water, followed by elution with MeOH. The dried product was dissolved in 20 mM bis-tris, pH 6, analyzed by TLC (described below) and quantified by scintillation counting.

LpxC activity was assayed as previously described (8, 15, 16). Briefly, LpxC (0.5 – 1 nM) was added to a 130 μL mixture of substrate (200 nM UDP-myristoyl-*N*-acetylglucosamine, unless noted otherwise) and assay buffer (20 mM bistrispropane, pH 7.5, 1 mg/mL BSA) at 30° C (*E. coli*) or 60° (*A. aeolicus*) unless noted otherwise. After various times, 20 μL aliquots were withdrawn and quenched in 8 μL 1.25 M NaOH, which also cleaves the myristate substituent for ease of separation. Samples were

neutralized with 80:20 iPrOH:1.5 M CH₃COOH, dried, dissolved in 14 μL 20 mM bis-tris pH 6, and spotted on PEI-cellulose TLC plates (EMD Biosciences). TLC plates were developed in 0.1 M guanidinium HCl and exposed to film overnight. Films were developed and used to guide the cutting of TLC plates to separate product and substrate followed by scintillation counting. For activity assays of crude lysates of *E. coli* expressing *A. aeolicus* LpxC mutants, a 5 mL culture of LB media was inoculated with a single colony of *E. coli* containing the pET21a-derived WT AaLpxC or a mutant plasmid and grown at 37° C until OD₆₀₀ = 0.6, then lowered to 30°C and expressed by induction with addition of 1 mM IPTG. Cells were lysed with FastBreak (Promega) and assayed as described above at 60°C after addition of 10 μL lysate containing LpxC. At 60°C, endogenous *E. coli* deacetylase activity is not observed.

Product affinity

Product affinity for LpxC mutants was assayed by ultrafiltration as described (16). Briefly, the concentration of product (¹⁴C-UDP-3-O-(R-3-hydroxymyristoyl)-glucosamine) was held constant (30 nM) while the enzyme was varied from 0 to 80 μM. The LpxC•product complexes were generated by incubating substrate and enzyme for 30 minutes at 30° C to allow for product formation and ligand equilibration. Mixtures were then transferred to ultrafiltration devices (Amicon 30K MWCO) and centrifuged to separate free and bound product (<20% volume change), which were quantified by scintillation counting. A binding isotherm was fit to the data to determine the dissociation constant (K_D).

Protein purification

Recombinant WT Aa- and EcLpxC and site-directed mutants were purified as described (8, 17). The His₆-LpxC-Mxe fusion protein (intein construct) was purified from inclusion bodies. The pAaHisLpxC-Mxe plasmid was transformed into BL21(DE3) cells, and grown at 37° C until OD₆₀₀ = 0.6. Expression was then induced by addition of IPTG (1 mM) and incubated for 4-6 hours at 37°. Cells were harvested by centrifugation and resuspended in 0.1 M Hepes pH 7.5, 2 mM TCEP (25 mL per liter of cell growth). Cells were lysed by a microfluidizer (Microfluidics), and the insoluble fraction was pelleted at 18,000 rpm (SS-34 rotor). The soluble fraction was discarded, and the pellet was resuspended in 0.1 M Hepes, 8 M urea, 2 mM TCEP, pH 7.5 (denaturing buffer). The denatured lysate was then applied to a Ni-NTA-sepharose column (~50 mL), washed with denaturing buffer plus 25 mM imidazole (5 column volumes), then eluted by a linear gradient of 25 mM – 1 M imidazole in denaturing buffer (10 column volumes). Fractions were analyzed by SDS-PAGE, and pure LpxC-Mxe was pooled and concentrated. Approximately 20-40 mg of pure, insoluble LpxC-Mxe per liter of cell growth was obtained (Table 2.1).

Intein cleavage and ligation

The purified fusion protein (approximately 10 mL of 50 – 100 μM) was then refolded by dialysis against 4L of 0.1 M Hepes pH 7.5, 2 mM TCEP overnight at 4°C. Precipitated protein that did not refold solubly was removed by centrifugation, and the LpxC-Mxe protein was cleaved by addition of 40 mM mercaptoethane sulfonic acid (MESNA) and incubation overnight at 4°C. Approximately 50 – 70% cleavage efficiency is observed. The resulting LpxC fragment (first 247 amino acids) precipitated, and was isolated by centrifugation. The protein was dissolved in denaturing buffer.

Ligation to the C-terminal peptide was performed in denaturing buffer by the addition of 10 mM MESNA and 1 mM peptide to ~70 μ M LpxC at 4°C for 16-24 hours. Full length LpxC was then refolded by dialysis as described, but at room temperature. Contaminating LpxC-Mxe or cleaved Mxe, which contain a C-terminal chitin binding domain, were removed by passing over a Chitin-sepharose column. Each step was verified by SDS-PAGE, and the final product was confirmed by mass spectrometry (Michigan Proteome Consortium). The pure protein was chelated to obtain apo-enzyme and reconstituted with stoichiometric metal as previously described (8, 15, 16).

Peptide synthesis

A peptide corresponding to residues 247-271 of *A. aeolicus* LpxC (CSFRGGHSLNVKLVKELAKKQKLTR) were made by peptide synthesis, where the His265 position was varied to test reactivity. These peptides do not contain the final 11 amino acids of AaLpxC, corresponding to a previously studied truncation construct used for crystallographic studies (18) for ease of peptide synthesis and crystallography. The WT control peptide using histidine (Bachem) and the 1-methyl histidine (RSP amino acids) peptide were synthesized using standard solid-phase peptide synthesis (19) on an Applied Biosystems 433 A automated synthesizer. All other peptides were commercially synthesized by Elim Biopharmaceuticals (pyrazole) or AnaSpec (pyridyl alanine). Peptides were purified on a reverse phase C18 column with a 0-70% linear acetonitrile gradient in H₂O/0.1% TFA or were used as synthesized (>70% pure).

Results

Active site His mutants suggest greater role than electrostatic catalyst

To examine the role of His265 in LpxC catalysis, several mutations were prepared and analyzed. Mutation to alanine was previously shown to decrease the activity of *E. coli* LpxC by over 2000-fold (8). As shown in Table 2.3, this contrasts with mutation to glutamine or arginine, which decreases activity ~600-fold and 170-fold, respectively. The majority of this effect is seen in k_{cat} , while K_{M} was increased only 7.5-, 3.1-, and 4.2-fold for the Ala, Gln, and Arg mutants, respectively. The rate acceleration observed upon changing the catalytic metal (Chapter 3), as well as the previously observed solvent isotope effect of 2 for k_{cat} in LpxC (8), suggests that hydrolysis is a rate-contributing parameter for k_{cat} wild-type LpxC. Furthermore, the significant decreases in k_{cat} with modest changes in K_{M} for the mutants argue that chemistry is the rate limiting step in k_{cat} . Assays with AaLpxC mutants reveal that H265A decreased $k_{\text{cat}}/K_{\text{M}}$ 167-fold (8), and a screen of the activity of mutations at H265 (R, E, Q, D, F, N) in cell extracts demonstrate that the activities of all of these mutant enzymes are decreased by >500-fold compared to WT. Expression, as determined by SDS-PAGE, was approximately equivalent to WT. These results demonstrate that adding back a positive charge at H265 only increases activity ~10-fold relative to the catalytically inactive H265A, which suggests that charge stabilization of the developing transition state and the tetrahedral intermediate is not the only role of H265. However, the positive charge added by site-directed mutagenesis may not be properly positioned in the active site to maximally stabilize the oxyanion due to differences in the size and shape of different amino acids.

To determine the effect of mutagenesis at H265 on interactions with the substrate, product binding assays were performed. Product affinity assays as a function of pH previously showed the H265A mutation destabilizes product affinity (Figure 2.4) (16). In

Table 2.2: Effect of mutagenesis at H265 on LpxC catalysis.

Enzyme ^a		k_{cat} (min^{-1})	K_M (μM)	k_{cat}/K_M ($\text{min}^{-1}\mu\text{M}^{-1}$)	Fold decrease (k_{cat}/K_M)
EcLpxC	WT ^b	90 ± 2	0.19 ± 0.01	460 ± 10	—
	H265A ^b	0.30 ± 0.05	1.4 ± 0.5	0.21 ± 0.04	2200
	H265Q	0.46 ± 0.08	0.60 ± 0.15	0.77 ± 0.07	600
	H265R	2.21 ± 0.39	0.82 ± 0.38	2.71 ± 0.86	170
AaLpxC	WT ^b	ND ^d	ND ^d	65 ± 11	—
	H253A ^b	ND ^d	ND ^d	0.39 ± 0.04	170
				Lysate screen^c (nM min^{-1})	Fold decrease (activity)
	WT			157	—
	H253R			0.11 ± 0.08	1400
	H253E			0.11 ± 0.02	1400
	H253Q			0.28 ± 0.04	560
	H253D			0.24 ± 0.11	650
	H253F			<0.08	>2000
	H253N			0.20 ± 0.07	790

^a Enzyme reconstituted 1:1 with Zn^{2+} was assayed at pH 7.5 at 30°C (EcLpxC) or 60°C (AaLpxC).

^b Obtained from reference (8).

^c Deacetylase activity (aerobic conditions) in BL21(DE3)pLysS cell lysates transformed with the plasmid indicated.

^d ND, not determined.

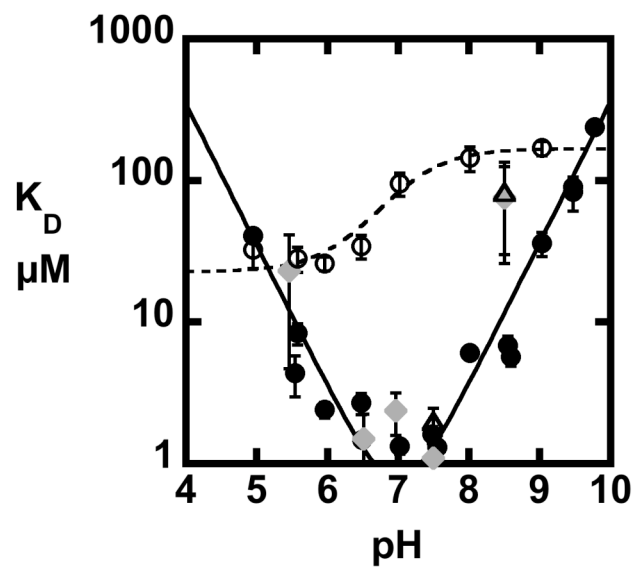


Figure 2.4: Product binding of H265 mutants. Product binding versus pH for WT (closed circles, black line), H265A (open circles, dashed line), H265Q (gray diamonds), and H265R (open triangles).

contrast, EcLpxC H265R and H265Q bind product with similar affinity to WT LpxC (Figure 2.4), suggesting that restoring hydrogen bonding capability is sufficient to bind product, and disfavoring the possibility that the mutants are less active due to a large perturbation in the active site structure. However, to better analyze the role of the catalytic histidine, more precise structure-activity probes are required. Therefore, expressed protein ligation (EPL) was developed in order to make more subtle modifications at H265.

Determination of optimal ligation site in LpxC

The only required sequence element for a protein made by EPL is at the ligation site, where the chemistry dictates that the first amino acid at the ligation site must be a cysteine (11-14). Therefore, various cysteine mutants were created to determine where this sequence alteration would introduce the smallest effect on activity. In the *E. coli* enzyme, cysteine substitutions near the C-terminus (K260, K262, S263, Figure 2.5) all decreased activity >10-fold. In *A. aeolicus* LpxC, several cysteine mutations near the C-terminus caused a <2-fold decrease in activity (Figure 2.5), and the Y247 site was chosen for peptide ligation. To reduce the length of the synthetic peptide, a truncated sequence was used ($\Delta 11$) that had previously been characterized (18). Therefore, AaLpxC Y247C- $\Delta 11$ was used as the WT control for intein experiments.

Highest activity with general acid mimic

In order to probe the role of H265, histidine analogues were substituted at this position using EPL. The three analogues used for these studies are shown in Figure 2.6. 1-methyl histidine (MeHis) was chosen because it is only one CH₃-group larger than WT histidine, but has a positive charge at the N1-nitrogen when protonated, as shown in

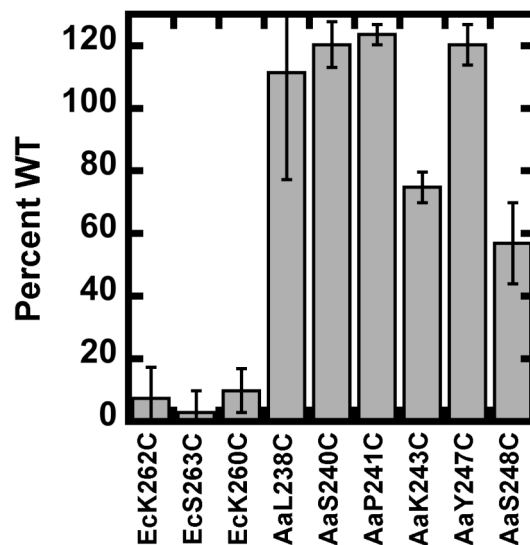


Figure 2.5: Cysteine mutants in *E. coli* and *A. aeolicus* LpxC. *E. coli* LpxC is sensitive to additional cysteine residues near the C-terminus, while *A. aeolicus* LpxC is minimally affected at several sites.

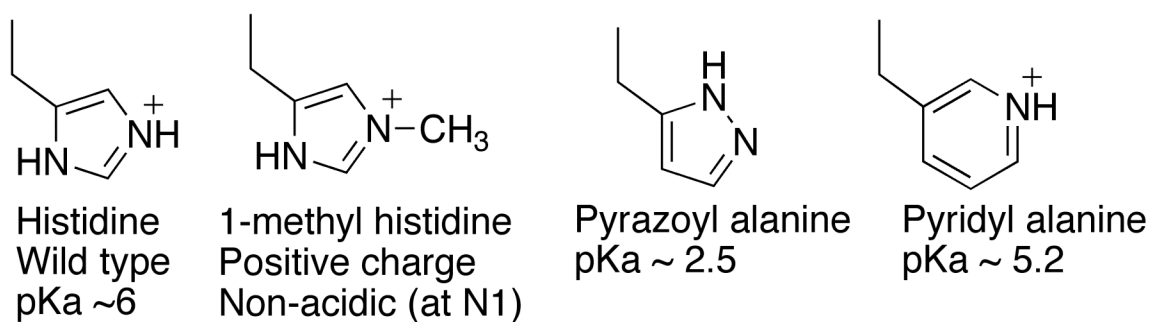


Figure 2.6: Analogues used in EPL studies.

Figure 2.6. The methylimidazole side-chain N3 pK_a is ~7.4, suggesting it will be ~50% protonated at pH 7.5. The presence of the methyl group prevents any acid/base chemistry at that nitrogen. It is possible for the imidazole ring to rotate, such that the N3 nitrogen would be positioned near the substrate and function as the general acid, but it is expected that hydrogen bonding to D246, as shown in Figure 2.1, will favor the wild-type conformation. The second two analogues were chosen as histidine-mimics with altered pK_a values compared to histidine (pK_a ~6-7). The pyrazole analogue is nearly isosteric with histidine, but has a much lower pK_a (~2.5). At pH 7.5, the fraction of protonated pyrazole is ~10⁻⁵, limiting its role as either a general acid or electrostatic catalyst. The third analogue chosen is pyridyl-alanine (pyrAla). PyrAla is a 6-membered ring versus the 5-membered imidazole ring, but both are aromatic and contain an acidic nitrogen. The pyridyl nitrogen has a lower pK_a value of ~5.2, compared to ~6 for imidazole. Like histidine, the pK_a value of PyrAla is well-positioned to be both an acidic residue as well as have a significant fraction protonated at neutral pH. Therefore, pyrAla-LpxC is predicted to be active but exhibit an altered pH profile if H265 functions as a general acid.

If electrostatic stabilization is the primary role of H265, MeHis would be expected to catalyze deacetylation with activity similar to WT. As shown in Table 2.3, the activity of LpxC containing the MeHis analogue at residue 265 is 15-fold below WT when substituted with Co²⁺ at 30°C and 110-fold below WT when substituted with Zn²⁺ at 37°C, indicating more than electrostatic stabilization is required for full activity (the alanine mutant is decreased 167-fold). In fact, this is an upper limit, as some fraction of the methyl-histidine could rotate to protonate the leaving group with the N3 nitrogen as

Table 2.3: Enzymatic activity of *A. aeolicus* LpxC substituted at H253 by EPL.

Enzyme (H253)	k_{cat}/K_M^b ($\mu\text{M}^{-1}\text{min}^{-1}$)	Fold decrease
WT ^a	0.63 ± 0.03	—
MeHis	0.04 ± 0.02	15.8
Pyrazole	<0.01	>60
PyrAla	0.54 ± 0.07	1.17

^a Wild-type (WT) is AaLpxC-Y247C- Δ 11, the background protein in all EPL studies as described in Materials and Methods.

^b V/K calculated at 200 nM substrate at pH 7.5, 30°C using 1:1 Co^{2+} .

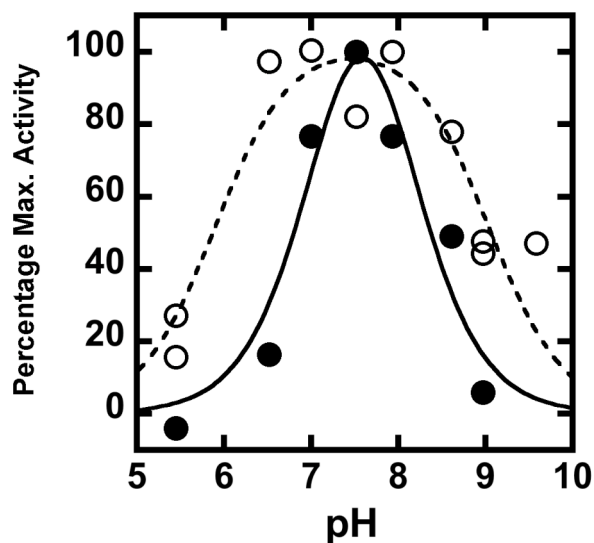


Figure 2.7: Altered pH dependence of LpxC-pyrAla. LpxC-pyrAla (closed circles) or WT AaLpxC-Y247- Δ 11 (open circles) reconstituted with 1:1 Co^{2+} and assayed at 30°C with 0.2 μM substrate as described in Materials and Methods. Y-axis depicts normalized k_{cat}/K_M measurements.

discussed above. LpxC-pyrazole has activity close to the lower limit for detection under the assay conditions used at pH 7.5, consistent with the prediction it cannot serve as a general acid. Importantly, the activity of LpxC-pyrAla is within 1.1 fold of WT, strongly suggesting that a general acid at H265 is required. Activity was tested over the pH range of 5.5 to 10.4, and Co^{2+} -LpxC-pyrAla exhibited an altered pH profile in which $\text{pK}_{\text{a}2}$ is shifted approximately 1 pH unit from 9.0 ± 0.2 to 8.0 ± 0.4 (Figure 2.7), consistent with the 1 pH unit difference between the pK_{a} values of histidine and pyrAla if H265 was serving as a general acid. These data indicate that electrostatic interactions modestly stabilize the transition state and tetrahedral intermediate; however, this does not fully describe the role of H265, and WT activity is only observed when a general acid is present at that position.

Discussion

Site-directed mutants inconsistent with electrostatic mechanism

General acid/base chemistry is a common strategy for enzymes that catalyze hydrolytic reactions (see Chapter 1). In addition to a general acid and general base, hydrolytic reactions typically require residues to stabilize the developing negative charge in the transition state and tetrahedral intermediate (Figure 2.1). When one of the essential catalytic residues is a histidine, determining the relative importance of these functions can be difficult. Histidine must be protonated to serve as either a general acid or an electrostatic catalyst, so an ionization in the pH rate profile linked to that histidine does not define its role in catalysis. Therefore, better methods are needed for resolving a common mechanistic question in this family of enzymes.

In LpxC, determining the role of the essential active site histidine has been difficult. Two proposed mechanisms for LpxC catalysis are consistent with the published data, which differ in the role of His265 (Figure 2.1). In the electrostatic catalyst mechanism, His265 is essential because the positive charge on the N1 nitrogen helps to stabilize the oxanion intermediate. In the 2nd proposed mechanism, His265 also functions as a general acid by protonating the amine leaving group to form the glucosamine moiety. In the current study, site-directed mutants were employed in both the *E. coli* and *A. aeolicus* enzymes to probe the function of His265 (H253 in AaLpxC). In EcLpxC, mutation to alanine decreases activity by over 2000-fold (Table 2.2). However, mutation to glutamine, which facilitates hydrogen bonding but is not positively charged nor facilitates acid/base chemistry, is decreased by 600-fold. This suggests that the transition state, or possibly the protein structure, is modestly stabilized (~3.6-fold) by hydrogen bonding. Mutation to arginine further introduces a positive charge, but is less acidic than histidine, with a pK_a value of ~12. The H265R mutation decreases activity 170-fold compared to WT, which is ~11-fold higher than H265A. These results suggest that the LpxC transition state is stabilized by the presence of a positive charge at H265 by ~1.5 kcal/mol, but another 3 kcal/mol in $\Delta\Delta G$ is lost relative to WT without a group at position 265 that can donate a proton.

One possible explanation for the decreased activity of these mutants relative to WT could be diminished substrate affinity, as H265 has previously been shown to enhance product binding, and likely substrate binding as well (16). The H265A mutation destabilizes product binding by over 2 kcal/mol, suggesting a significant interaction. If H265R or H265Q were impaired in substrate binding, a decreased affinity for product

would be expected. However, as shown in Figure 2.4, H265Q and H265R bind product with affinities similar to WT (Figure 2.4), suggesting that restoring the ability to form a hydrogen bond at that position is sufficient to enhance product affinity. Mutations at residue 265 also have small effects on K_M . Therefore, there appears to be little correlation between catalytic activity and ligand affinity in these mutants.

Similarly, in AaLpxC the H265A mutation decreases the value of k_{cat}/K_M by 167-fold (8). Deacetylase activity measured in *E. coli* extracts containing AaLpxC mutated to R, E, Q, D, F, or N at H265 decreases the observed activity by greater than 500-fold. The decreases include both differences in LpxC concentration and activity, so these decreases in catalytic activity are likely comparable. Two possible conclusions can be drawn from these data: either LpxC requires a general acid at the essential histidine site, or the site-directed mutants are sterically altered relative to the His and thus the required positive charge is not properly oriented. Therefore, more careful perturbations at the catalytic histidine are required to resolve this question.

Positively charged analogues are not active; acidic analogues are efficient catalysts

To further evaluate the role of His265/253, histidine analogues with altered chemical properties were inserted into LpxC at this position by EPL (Figure 2.6). When the positively charged analogue 1-methyl-histidine is used, LpxC catalysis decreases by 110-fold relative to WT (k_{cat}/K_M), which is comparable to the 167-fold loss of activity observed for the H253A mutation in AaLpxC (Table 2.2). This suggests that even nearly isosteric residues cannot rescue LpxC catalysis by inclusion of a positive charge alone. When pyrazole was substituted at H265, the activity decreased > 60-fold; this value is limited by the detection limit of the assay at 30°C and available protein concentration,

and is likely decreased further. At pH 7.5, pyrazole is not expected to be significantly protonated, further suggesting that hydrogen-bonding at residue H265 is not sufficient to reconstitute WT activity even in a close imidazole analogue. In contrast, LpxC substituted with pyridyl alanine (pyrAla, $pK_a \sim 5.2$) efficiently catalyzes deacetylation, with k_{cat}/K_M values only 10% lower than the WT value at pH 7.5 (Table 2.3). Pyr-Ala is also capable of rotating to form a hydrogen bond with D246, which would be expected to form an inactive conformation. However, the high observed activity suggests a significant fraction of the enzyme is in an active conformation in which the pyridyl-nitrogen is rotated towards the substrate. Furthermore, when the pH dependence of LpxC-pyrAla was examined, it exhibits two ionizations similar to WT-LpxC, but the observed pK_{a2} is shifted to a value that is 1 pH unit lower than that of wild-type. Although both of the observed pK_{a2} values are higher than the pK_a s of these groups in solution (histidine is ~ 6 in solution and ~ 9 at H265; pyrAla is ~ 5.2 in solution and ~ 8 in the enzyme, Figure 2.7), the difference between the pK_a values is retained. In WT LpxC, the intrinsic pK_a of the imidazole side-chain is perturbed upward, perhaps by forming an ion pair with D246 (Figure 2.1). A similar perturbation of the pyridyl alanine is also expected and the pH dependence of this variant is consistent with this proposal. These results suggest that an acidic residue at position 265 is required to enhance catalysis in LpxC.

LpxC functions via a general acid/general base catalytic pair

Site-directed mutants of EcLpxC and AaLpxC demonstrate that replacing His265 with positively charged amino acids does not restore activity to WT levels (Table 2.2). Furthermore, EPL experiments show that positively charged histidine analogues at

residue 265 also do not facilitate catalysis, while acidic analogues restore wild type activity (Table 2.3). Taken together, these results provide insight into the question of the functional role played by the catalytic histidine. These data provide evidence that H265 in LpxC functions mainly as a general acid rather than an electrostatic catalyst to stabilize the transition state (Figure 2.1B). This mechanism is consistent with all the previously determined biochemical and structural data described in Chapter 1. Resolving this mechanism is important for a complete understanding of the essential interactions at the active site in LpxC, which also facilitates rational drug design for this antibiotic target. Development of EPL also has promise as a general method for studying the role of histidine side chains in enzyme mechanisms. Employing the approach used to solve the mechanistic question in LpxC may be an efficient way to answer similar questions in many other enzymes.

REFERENCES

- (1) White, R. J., Margolis, P. S., Trias, J., and Yuan, Z. Y. (2003) Targeting metalloenzymes: a strategy that works. *Current opinion in pharmacology* 3, 502-507.
- (2) Jackman, J. E., Fierke, C. A., Tumey, L. N., Pirrung, M., Uchiyama, T., Tahir, S. H., Hindsgaul, O., and Raetz, C. R. (2000) Antibacterial agents that target lipid A biosynthesis in gram-negative bacteria. Inhibition of diverse UDP-3-O-(r-3-hydroxymyristoyl)-n-acetylglucosamine deacetylases by substrate analogs containing zinc binding motifs. *J Biol Chem* 275, 11002-11009.
- (3) Clements, J. M., Coignard, F., Johnson, I., Chandler, S., Palan, S., Waller, A., Wijkmans, J., and Hunter, M. G. (2002) Antibacterial activities and characterization of novel inhibitors of LpxC. *Antimicrobial Agents and Chemotherapy* 46, 1793-1799.
- (4) McClerren, A. L., Endsley, S., Bowman, J. L., Andersen, N. H., Guan, Z., Rudolph, J., and Raetz, C. R. (2005) A slow, tight-binding inhibitor of the zinc-dependent deacetylase LpxC of lipid A biosynthesis with antibiotic activity comparable to ciprofloxacin. *Biochemistry* 44, 16574-16583.
- (5) Mdluli, K. E., Witte, P. R., Kline, T., Barb, A. W., Erwin, A. L., Mansfield, B. E., McClerren, A. L., Pirrung, M. C., Tumey, L. N., Warrenner, P., *et al.* (2006) Molecular validation of LpxC as an antibacterial drug target in *Pseudomonas aeruginosa*. *Antimicrobial Agents and Chemotherapy* 50, 2178-2184.
- (6) McClerren, A. L., Zhou, P., Guan, Z., Raetz, C. R., and Rudolph, J. (2005) Kinetic analysis of the zinc-dependent deacetylase in the lipid A biosynthetic pathway. *Biochemistry* 44, 1106-1113.
- (7) Hernick, M., and Fierke, C. A. (2005) Zinc hydrolases: the mechanisms of zinc-dependent deacetylases. *Arch Biochem Biophys* 433, 71-84.
- (8) Hernick, M., Gennadios, H. A., Whittington, D. A., Rusche, K. M., Christianson, D. W., and Fierke, C. A. (2005) UDP-3-O-((R)-3-hydroxymyristoyl)-N-acetylglucosamine deacetylase functions through a general acid-base catalyst pair mechanism. *J Biol Chem* 280, 16969-16978.
- (9) Lipton, A. S., Heck, R. W., Hernick, M., Fierke, C. A., and Ellis, P. D. (2008) Residue Ionization in LpxC Directly Observed by (^{67}Zn) NMR Spectroscopy. *J Am Chem Soc.*
- (10) Hedstrom, L. (2002) Serine protease mechanism and specificity. *Chemical Reviews* 102, 4501-4523.

- (11) Muir, T. W., Sondhi, D., and Cole, P. A. (1998) Expressed protein ligation: A general method for protein engineering. *Proc Natl Acad Sci U S A* 95, 6705-6710.
- (12) Muir, T. W. (2003) Semisynthesis of proteins by expressed protein ligation. *Annu Rev Biochem* 72, 249-289.
- (13) Hahn, M. E., and Muir, T. W. (2005) Manipulating proteins with chemistry: a cross-section of chemical biology. *Trends Biochem Sci* 30, 26-34.
- (14) Pellois, J. P., and Muir, T. W. (2006) Semisynthetic proteins in mechanistic studies: using chemistry to go where nature can't. *Current opinion in chemical biology* 10, 487-491.
- (15) Hernick, M., and Fierke, C. A. (2006) Molecular recognition by Escherichia coli UDP-3-O-(R-3-hydroxymyristoyl)-N-acetylglucosamine deacetylase is modulated by bound metal ions. *Biochemistry* 45, 14573-14581.
- (16) Hernick, M., and Fierke, C. A. (2006) Catalytic Mechanism and Molecular Recognition of E. coli UDP-3-O-(R-3-Hydroxymyristoyl)-N-acetylglucosamine Deacetylase Probed by Mutagenesis. *Biochemistry* 45, 15240-15248.
- (17) Jackman, J. E., Raetz, C. R., and Fierke, C. A. (1999) UDP-3-O-(R-3-hydroxymyristoyl)-N-acetylglucosamine deacetylase of Escherichia coli is a zinc metalloenzyme. *Biochemistry* 38, 1902-1911.
- (18) Whittington, D. A., Rusche, K. M., Shin, H., Fierke, C. A., and Christianson, D. W. (2003) Crystal structure of LpxC, a zinc-dependent deacetylase essential for endotoxin biosynthesis. *Proc Natl Acad Sci USA* 100, 8146-8150.
- (19) (2000) *Fmoc Solid Phase Peptide Synthesis: A Practical Approach*, Oxford University Press, New York.

CHAPTER 3.
ACTIVATION OF ESCHERICHIA COLI UDP-3-O-(R-3-
HYDROXYMYRISTOYL)-N-ACETYL GLUCOSAMINE DEACETYLASE BY
FE²⁺ YIELDS A MORE EFFICIENT ENZYME WITH ALTERED LIGAND
AFFINITY¹

Introduction

Treatment of infections caused by Gram-negative bacteria is often difficult, due in part to the antibiotic resistance associated with these organisms. Furthermore, Gram-negative organisms (*e.g. Yersinia pestis, Francisella tularensis*) have recently been identified as potential bioterror agents (1). For these reasons, new antibiotics that are effective in the treatment of Gram-negative bacterial infections are needed, including drugs that act on new targets. Possible targets in Gram-negative bacteria include the enzymes involved in the biosynthesis of lipopolysaccharides (LPS) that make up the outer membranes of these organisms (2-4). The lipid A portion of LPS is responsible for anchoring LPS to the cell surface; consequently, the lipid A biosynthetic pathway is a potential source of targets for antibiotic development (2). UDP-3-O-(R-3-hydroxymyristoyl)-N-acetylglucosamine deacetylase (LpxC) catalyzes the committed, and second overall, step in the biosynthesis of lipid A – the deacetylation of UDP-3-O-(R-3-hydroxymyristoyl)-N-acetylglucosamine to form UDP-3-O-(R-3-

¹ Reproduced in part from Hernick, M., Gattis, S.G., Penner-Hahn, J.E., and Fierke, C.A. (2010) *Biochemistry*, 2246-2255. The experiments described in Figure 3.2 and Table 3.1 were performed by S. Gattis; the experiments performed in Figures 3.3-3.7 and Table 3.1-3.4 were performed by M. Hernick. EXAFS analysis was contributed by J.E. Penner-Hahn. This chapter and the corresponding manuscript were written by S. Gattis.

hydroxymyristoyl)-glucosamine and acetate (Figure 3.1A) (5). Consequently, LpxC is an appealing target for antimicrobial development.

LpxC was originally classified as a “Zn²⁺-dependent” deacetylase based on the findings that LpxC activity is reversibly inhibited by incubation with metal chelators (*e.g.* ethylene diamine tetraacetic acid, EDTA; dipicolinic acid, DPA) and LpxC co-purifies with Zn²⁺ under aerobic conditions (6). However, these previous studies did not evaluate the ability of Fe²⁺ to activate LpxC. Recently, there have been several examples of “Zn²⁺-dependent” enzymes that have been reclassified as “Fe²⁺-dependent” enzymes, including peptide deformylase (PDF) (7-9), LuxS (10), and possibly histone deacetylase 8 (HDAC8) (11). The misidentification of the native metal cofactor as Zn²⁺ is attributed to the aerobic purification of these enzymes, with the oxidation of Fe²⁺ to Fe³⁺ and substitution of Zn²⁺ at the active site.

Herein, we demonstrate that replacement of the Zn²⁺ cofactor with Fe²⁺ in *E. coli* LpxC both enhances the catalytic activity and alters the affinity of this enzyme for ligands. In fact, Fe²⁺-LpxC functions as a mononuclear metal-dependent deacetylase with catalytic activity that is ~6-fold higher than Zn²⁺-LpxC. This enhancement in catalytic activity is due primarily to an increase in the value of the parameter k_{cat} , not K_{M} . X-ray absorption spectroscopy (XAS) experiments indicate that the metal ion in Fe²⁺-LpxC is 5 coordinate, suggesting that higher coordination numbers correlate with enhanced catalytic activity. In contrast to Zn²⁺-LpxC, the activity of the Fe²⁺-bound enzyme is sensitive to oxygen. Furthermore, the activity of native LpxC in crude *E. coli* cell lysates is aerobically sensitive, consistent with the presence of Fe²⁺-LpxC. These findings suggest that under normal growth conditions the native metal bound to LpxC in

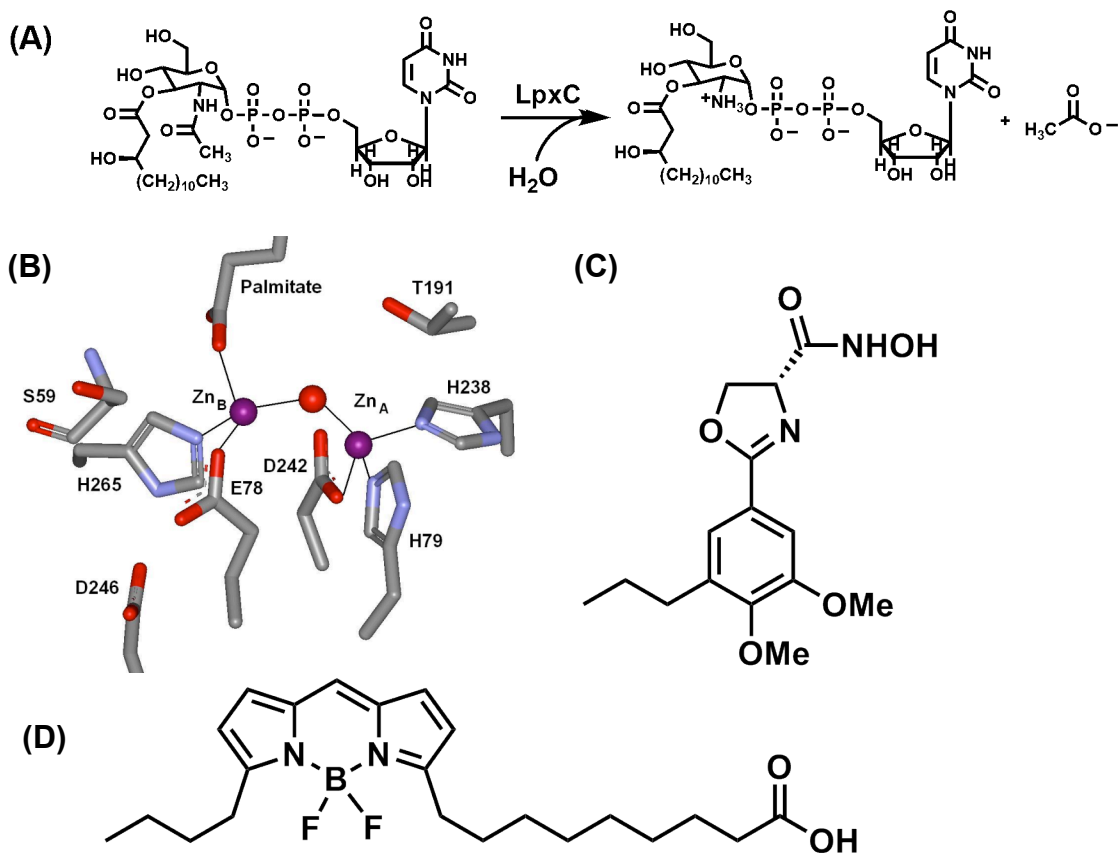


Figure 3.1: LpxC reaction and structures. (A) LpxC-catalyzed reaction. (B) Active site of LpxC from *A. aeolicus* containing two zinc ions: Zn_A (catalytic) and Zn_B (inhibitory). Figure was made from PDB 1P42. (C) Structure of L-161,240. (D) Structure of BODIPY-fatty acid.

E. coli is Fe²⁺. However, it is possible that the active site metal bound to LpxC *in vivo* could switch depending on the metal ion availability, thus allowing LpxC to function using different metal ion cofactors under different environmental conditions.

Material and Methods

General procedures

E. coli (WT and C63A variant) and *A. aeolicus* LpxC (AaLpxC) were over-expressed and purified according to published procedures using DEAE-sepharose and Reactive Red-120 affinity dye columns at 4° C and room temperature, respectively (5, 6, 12, 13). The apo- and single metal bound forms of LpxC were prepared by treatment with metal chelators (DPA/EDTA) followed by reconstitution with Zn²⁺ or Fe²⁺, as previously described (6, 14). All solutions (except for enzyme) were degassed with Ar prior to use. For Fe²⁺ experiments, a 400 mM FeCl₂ stock was prepared in 10 mM dithionite and diluted to 100 mM with 1X assay buffer prior to incubation with apo-LpxC. Similarly, a 100 mM ZnSO₄ solution was prepared in 25 mM bis-tris propane, 1.5 mM triscarboxyethylphosphine (TCEP) pH 7.5-8.7 and diluted to 100 mM with 1X assay buffer prior to incubation with apo-LpxC. The concentrations of metal stocks were verified by ICP-MS. To maintain anaerobic conditions, experiments were carried out either in an anaerobic chamber (Coy Laboratory Products, Grass Lake, MI) or using assay buffers containing 10 mM TCEP and were completed in < 2 hr to ensure that LpxC was maximally active during the course of the assays. All ICP-MS analysis was done at the University of Michigan, Department of Geology by Dr. Ted Huston.

LpxC deacetylase Assay

[¹⁴C]-UDP-3-*O*-(3-hydroxymyristoyl)-*N*-acetyl-glucosamine was prepared, and the deacetylase activity was measured as previously described (see Chapter 2), (6, 14, 15). To examine the metal ion stoichiometry of the Zn²⁺-LpxC-catalyzed reactions, apo-LpxC was incubated (5 μM WT or C63A in 20 mM bis-tris propane, pH 7.5) with 0-2 equivalents of ZnSO₄ for 1-2 hours at room temperature to form holoenzyme, and was then diluted to 100-200 nM in the assay buffer just prior to activity measurement. For Fe²⁺ stoichiometry measurements, apo-LpxC (10 μM WT or C63A in 20 mM bis-tris propane, 2-10 mM TCEP, pH 7.5) was incubated with FeCl₂ (1 to 500 μM) on ice for 5 to 60 minutes in an anaerobic chamber (if TCEP < 10 mM) and then diluted with assay buffer prior to measuring activity. Assay mixtures containing 20 mM bis-tris propane, pH 7.5, 10 mM TCEP (for Fe²⁺ measurements), bovine serum albumin (BSA, fatty acid free, 1 mg/mL), and [¹⁴C]-UDP-3-*O*-(3-hydroxymyristoyl)-*N*-acetyl-glucosamine (0.05 to 4 μM) were pre-equilibrated at 30 °C and the reactions were initiated by the addition of enzyme (0.5 to 5 nM). ICP-MS results indicate these samples contain ≤ 20 nM zinc, and the addition of BSA does not chelate metal from holo-LpxC. After incubation for various times, the reactions were quenched by the addition of sodium hydroxide, which also cleaves the myristate substituent from substrate and product for ease of separation. Substrate and product were separated on PEI-cellulose TLC plates (0.1 M guanidinium HCl), quantified by scintillation counting, and the initial rates of product formation (< 20% reaction) were determined from these data. To evaluate the steady-state kinetic parameters, activity was measured at seven to nine different concentrations of myrUDP-GlcNAc (50 nM to 4 μM). The steady-state parameters k_{cat} , K_M and k_{cat}/K_M were

obtained by fitting the Michaelis-Menten equation to the initial linear velocities measured at the various substrate concentrations using the curve-fitting program Kaleidagraph (Synergy Software), which also calculates the asymptotic standard errors. For pH studies of C63A LpxC, 20 mM bis-tris (pH 5.7 – 6.5) or bis-tris propane (pH 7 - 10) with 10 mM TCEP was used and pK_a values were obtained by fitting Eq. 3.1 to these data. Control experiments demonstrate that incubation of LpxC at various pH values for up to 30 min. does not lead to an irreversible decrease in activity.

For experiments with the hydroxamate inhibitor L-161,240 (13, 16, 17), a generous gift from Dr. Michael Pirrung, Zn^{2+} - or Fe^{2+} -LpxC (0.5 nM) was preincubated with inhibitor (0.5 to 500 nM, DMSO) or DMSO for 15 to 25 min at 30 °C in 20 mM bis-tris propane, 10 mM TCEP pH 7.5; 1 mg/mL BSA prior to initiation of the reaction by the addition of [^{14}C]-UDP-3-*O*-(3-hydroxymyristoyl)-*N*-acetyl-glucosamine (200 nM). Initial rates were processed as described above, and the IC_{50} values were obtained by fitting Eq. 3.2 to these data.

$$\text{Equation 3.1} \quad \frac{V}{K_{obs}} = \frac{k_1}{\left(1 + \frac{[H^+]}{K_{a1}} + \frac{(K_{a2})^2}{[H^+]^2}\right)}$$

$$\text{Equation 3.2} \quad \frac{v}{v_0} = \frac{IC_{50}}{([I] + IC_{50})}$$

Ultrafiltration Binding Assay

Dissociation constants (K_D) of [^{14}C]-UDP-3-*O*-(3-hydroxymyristoyl)-glucosamine from LpxC•product complexes were measured using ultrafiltration, as previously

described (18). Briefly, the concentration of product was held constant (50 - 60 nM) and the concentration of wild-type or C63A LpxC was varied (0 to 24 μ M). Enzyme and substrate were incubated at 30 °C for 15 – 30 min prior to the assay to allow for product formation and ligand equilibration. Assay mixtures were then transferred into ultrafiltration devices (Microcon MWCO 30K), and the free and bound products were separated by centrifuging the samples at 3000 rpm for 2.5 minutes. Equal volumes of the filtrate and retentate were removed, and the amounts of unbound (filtrate) and total product (retentate) were quantified using scintillation counting. The ratio of EP/ P_{total} was determined as a function of $[E]_{total}$ and the K_D values were obtained by fitting Eq. 3.3 to these data.

$$\text{Equation 3.3} \quad \frac{EP}{P_{total}} = \frac{\left(\frac{EP}{P_{total}} \right)_{Endpt}}{\left(1 + \frac{K_D}{E_{total}} \right)} + \left(\frac{EP}{P_{total}} \right)_{Background}$$

$K_D^{fatty\ acid}$ determination using fluorescence anisotropy measurements

The K_D value of 5-butyl-4,4-difluoro-4-bora-3a,4a-diaza-s-indacene-3-nonanoic acid (BODIPY[®] 500/510 C₄, C₉; Invitrogen) fatty acid for EcLpxC was determined using fluorescence anisotropy as previously described (18, 19). The concentration of BODIPY[®] fatty acid was held constant (0.1 mM; 25 mM HEPES, 10 mM TCEP pH 7.5, 100 μ M FeCl₂) and increasing concentrations of enzyme (0 to 100 μ M) were titrated into the solution at 30 °C. The fluorescence anisotropy (Ex 480 nm, Em 516 nm) was measured ~ 3 minutes after each addition of LpxC, and K_D values were determined by fitting Eq. 3.4 to these data.

$$\text{Equation 3.4 } \frac{E \cdot FA}{FA_{total}} = \frac{\left(\frac{E \cdot FA}{FA_{total}} \right)_{\text{Endpoint}}}{\left(1 + \frac{K_D}{E_{total}} \right)} + FL_{Bkgd}$$

X-ray Absorption Spectroscopy

XAS samples were prepared and analyzed as previously described (12). Briefly, a stoichiometric amount of apo-EcLpxC or apo-AaLpxC was added to a solution of 24 μM FeCl_2 (anaerobic chamber), or ZnSO_4 in 25 mM HEPES, 1.5 mM TCEP pH 7.5 and incubated on ice for 45 min (AaLpxC, room temperature for 25 min). The enzyme was concentrated using an Amicon Ultra-15 centrifugal filter unit (MWCO 10K) and unbound metal ions were removed by washing with buffer (25 mM HEPES, 1.5 mM TCEP pH 7.5) prior to concentration. Glycerol (20 μL) was mixed with the enzyme (60 μL) as a cryoprotectant, samples were transferred into Lucite cuvettes (3 x 2 x 25 mm) with 40 mm Kapton windows and frozen in $\text{N}_2(\text{l})$. The concentrations of Fe, Co and Zn were determined using ICP-MS, and all analyzed samples had a metal/enzyme stoichiometry of < 1 (range 0.14-0.63). XAS data were collected at the Stanford Synchrotron Radiation Laboratory (beam line 9-3) under dedicated conditions as fluorescence excitation spectra, using a solid-state Ge detector array equipped with a filter and Soller slits focused on the sample. All channels of each scan were examined for glitches, and the good channels were averaged for each sample (two independent samples for each protein) to give the final spectrum.

The program EXAFSPAK (20) was used to extract and analyze EXAFS data as previously described (12), using ab initio phase and amplitude parameters calculated using

FEFF 7.02 (21, 22). XANES data were normalized to tabulated absorption coefficients (23) using the program MBACK (24). The area of the 1s→3d transition in the XANES region was calculated by fitting the pre-edge region (7107-7118 eV) using the sum of a Gaussian and an arctan function; for comparison with previously published data, the fitted Gaussian area was normalized to the K-edge jump for Fe ($3.556 \times 10^2 \text{ cm}^2/\text{g}$).

Native LpxC deacetylase activity

LB media was inoculated with BL21(DE3) or BL21(DE3)pLysS cells and incubated in a shaker (250 rpm) overnight at 37 °C. The cells were harvested by centrifugation and the cell pellets resuspended in 20 mM bis-tris propane, 0 - 10 mM TCEP pH 7.5. The cells were washed with 5 mM CaCl₂ to remove divalent metal ions (1 x 2 mL) followed by buffer (2 x 2 mL), resuspended in buffer, and stored at -80 °C. Control experiments demonstrate that Ca²⁺ ($\leq 10 \text{ mM}$) has no significant effect on Zn²⁺-LpxC activity. Prior to assaying activity, cells were thawed, incubated with lysozyme (0.2 – 1.2 mg/mL) in assay buffer for 15 min at room temperature and the cell lysate was cleared by centrifugation (14,000 rpm, 15 min). A sample of the cleared lysate was analyzed for metal content by ICP-MS; the concentration of total Fe in these lysates is ~2-fold greater than Zn (Fe/Zn = 1.4 to 3.0). The cleared lysate was diluted 10-fold in assay buffer prior to measurement of activity as described above ([S] = 200 nM). To demonstrate that the observed activity was catalyzed by LpxC, the activity was also measured in the presence of the inhibitor L-161,240. *In vitro* control experiments indicate that exchange of Zn²⁺ for Fe²⁺ is facile *in vitro* but the opposite metal exchange is not readily observed and is likely thermodynamically unfavorable (25). Therefore, the

experiments in cell lysates should err on the side of underestimating the concentration of Fe^{2+} -LpxC.

Results

The activity of Fe^{2+} -LpxC is higher than Zn^{2+} -LpxC

Activation of apo-LpxC by various divalent metal ions was previously demonstrated with $\text{Co}^{2+} > \text{Zn}^{2+} > \text{Ni}^{2+} > \text{Mn}^{2+}$, while no increase in activity was observed following the addition of Mg^{2+} , Ca^{2+} , Cd^{2+} or Cu^{2+} to apo-LpxC (6). Stoichiometric addition of Zn^{2+} and Co^{2+} fully activate apo-LpxC, while excess concentration of Ni^{2+} (~3:1 Ni^{2+} :LpxC) is required suggesting that LpxC has weaker affinity for Ni^{2+} (6). Based on these findings, and the fact that aerobically purified LpxC contains 1-3 Zn^{2+} /enzyme, LpxC was characterized as a “zinc-dependent” deacetylase (6). Here we probe whether Fe^{2+} can also activate apo-LpxC.

Since Fe^{2+} is a redox-sensitive metal ion, activation of LpxC by Fe^{2+} was measured under anaerobic conditions (glove box or 10 mM TCEP). Under these conditions, addition of Fe^{2+} (1 – 3 equivalents) activates apo-LpxC. In fact, the initial velocity for deacetylation of myrUDP-GlcNAc (0.2 μM) under standard assay conditions (pH 7.5) is 6- to 9-fold higher with Fe^{2+} - compared to Zn^{2+} -LpxC, indicating that Fe^{2+} , like Co^{2+} , is better suited than Zn^{2+} for enhancing the catalytic activity of LpxC. Furthermore, comparable activity is observed for LpxC in the presence of both 1 and 3 Fe^{2+} equivalents, suggesting that the enzyme is saturated with Fe^{2+} in the pre-incubation conditions.

Metal ion stoichiometry

Crystal structures of AaLpxC reveal that the LpxC active site contains two metal ion binding sites (Figure 3.1B (26)): one catalytic site, Zn_A , and one inhibitory site, Zn_B . EcLpxC is activated by stoichiometric addition of either Zn^{2+} or Co^{2+} , while the addition of excess Zn^{2+} inhibits enzyme activity (6). Similarly, the activity of apo-EcLpxC is activated by the addition of Fe^{2+} . For WT LpxC, an initial increase in LpxC activity is observed as the concentration of metal is increased from 0 to 1 metal ions/enzyme for both Fe^{2+} and Zn^{2+} , followed by a decrease in enzyme activity as the concentration of metal ion is increased further (Figure 3.2), although the inhibition by zinc is significantly more severe. These results are consistent with metal ion binding tightly at the catalytic site to enhance catalytic activity, followed by binding of a weaker, second metal ion at the inhibitory site that decreases the observed catalytic activity. Comparison of the maximal activities achieved with Fe^{2+} and Zn^{2+} suggests that LpxC is 6-9-fold more active with bound Fe^{2+} than Zn^{2+} ; however, direct comparison of these activities in the WT enzyme is complicated by metal ion binding at the inhibitory site.

C63A mutation in LpxC decreases metal ion inhibition

To circumvent complications arising from metal ion inhibition, we proposed to preferentially decrease the metal affinity of the inhibitory site by selectively removing a ligand from this site. Structural data for AaLpxC indicate that the ligands for the inhibitory Zn^{2+} ion are the side chains of E78 and H265, a bound palmitate, and the catalytic water molecule (Figure 3.1B (26)), while EXAFS indicate that the inhibitory Zn^{2+} in EcLpxC has at least one S/Cl ligand (12). Sequence alignment of EcLpxC with AaLpxC and mapping of the Cys side chains onto the AaLpxC structure indicated that the side chain of Cys63 (equivalent to Ser59 in AaLpxC, Figure 3.1B) is the

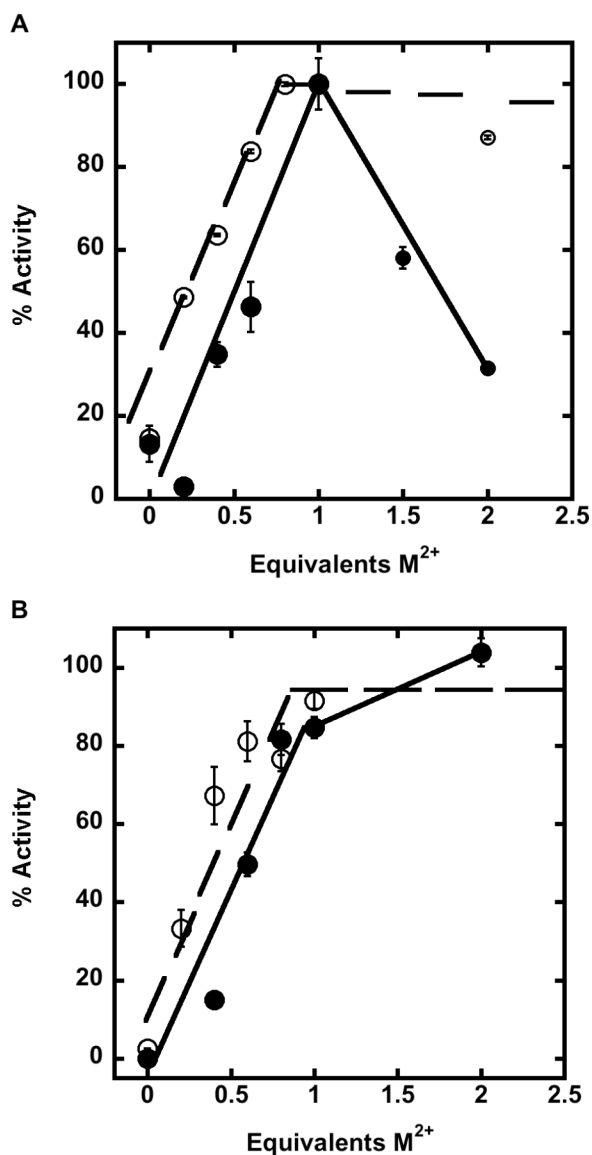


Figure 3.2: Activation of apo-LpxC by Zn²⁺ or Fe²⁺. Percentage of maximum deacetylase activity as a function of either Zn²⁺ (closed circles) or Fe²⁺ (open circles) metal ion stoichiometry was measured for WT LpxC (A) and C63A LpxC (B). C63A LpxC activity was assayed with up to 50-fold excess Fe²⁺ (not shown). The deacetylase activity for the substrate myr-UDPGlcNAc (0.2 μ M) was measured at 30 °C after incubation with varying equivalents of M²⁺, as described under “Materials and Methods”.

only S atom within 10 Å of the inhibitory Zn^{2+} ion, implying that Cys63 is the third protein ligand for the inhibitory metal ion site in EcLpxC (18, 19). Since the side chains of E78 and H265 play important roles in the catalytic mechanism of LpxC (14, 27), we chose to prepare the EcC63A mutant to further compare the properties of Zn^{2+} - and Fe^{2+} -LpxC.

Stoichiometric addition of either Fe^{2+} or Zn^{2+} to C63A LpxC increases the catalytic activity to $\geq 80\%$ of the maximal value observed at higher metal concentrations, indicating that C63A LpxC is activated by a single Fe^{2+} or Zn^{2+} ion. Furthermore, inhibition of C63A LpxC by metal ions is significantly reduced, consistent with the Cys63 side chain serving as a ligand for the inhibitory metal ion binding site. This decrease in metal ion inhibition facilitates a more accurate comparison of the maximal LpxC activity with the Fe^{2+} and Zn^{2+} cofactors.

Fe^{2+} activates steady-state turnover

Steady-state turnover was measured for LpxC (WT and C63A) reconstituted with stoichiometric Fe^{2+} or Zn^{2+} (Table 3.1) demonstrating that the value of k_{cat}/K_M for LpxC reconstituted with Fe^{2+} compared to Zn^{2+} is enhanced by 8-fold. The C63A mutation also increases the value of k_{cat}/K_M for LpxC reconstituted with Zn^{2+} and Fe^{2+} by 5-fold and 3.5-fold, respectively, relative to the wild-type enzyme, at least partly due to decreased metal inhibition. Since the data obtained for WT LpxC is complicated by differences in metal ion inhibition, we measured the relative effects of Zn^{2+} and Fe^{2+} on the steady-state parameters for the C63A mutant. These results (Table 3.1, Figure 3.3) show that switching the metal ion cofactor in C63A LpxC from Zn^{2+} to Fe^{2+} increases the values of both k_{cat} (4-fold) and k_{cat}/K_M (6-fold) with little effect on the value of K_M .

Table 3.1: Steady-state activity parameters for EcLpxC

Enzyme ^a	k_{cat} (min ⁻¹) ^b	K_M (μ M) ^b	k_{cat}/K_M (min ⁻¹ μ M ⁻¹) ^b	pKa ₁ ^c	pKa ₂ ^c	k_{cat}/K_M (min ⁻¹ μ M ⁻¹) at pH maximum ^c
Zn ²⁺ - LpxC ^d	ND	ND	34 ± 8 ^d	6.2 ± 0.2 ^e	9.2 ± 0.2 ^e	ND
Fe ²⁺ -LpxC	90 ± 3	0.32 ± 0.04	281 ± 24	ND	ND	ND
Zn ²⁺ -C63A	126 ± 12	0.7 ± 0.2	170 ± 34	6.6 ± 0.1	8.9 ± 0.1	260 ± 20
Fe ²⁺ -C63A	530 ± 30	0.5 ± 0.1	990 ± 130	6.8 ± 0.1	9.2 ± 0.1	760 ± 20

^a LpxC was reconstituted with stoichiometric (1:1) metal in a pre-incubation step, as described in the “Materials and Methods”. The measured values for k_{cat}/K_M catalyzed by apo-LpxC and apo-C63A LpxC are 15 and 11 min⁻¹ μ M⁻¹, respectively, likely due to metal contamination in the assay.

^b The initial rates of LpxC deacetylase activity were determined at 30 °C (20 mM bis-tris propane, 10 mM TCEP pH 7.5, 1 mg/mL BSA) with myrUDP-GlcNAc as the substrate as described in the “Materials and Methods”. The kinetic parameters were obtained by fitting the Michaelis-Menten equation to the initial velocities.

^c Deacetylation of myrUDPGlcNAc catalyzed by LpxC (Fe²⁺-WT and C63A) was determined at 30 °C as a function of pH using substrate concentrations below the K_M (< 0.2 μ M). The pKa values were obtained from the pH dependence of the values using Eq. 3.1 as described in the “Materials and Methods”.

^d k_{cat}/K_M for WT ZnLpxC is reported as mean and standard deviation of 5 replicates performed at a single subsaturating substrate concentration (200 nM) with LpxC incubated with stoichiometric Zn²⁺.

^e Taken from reference (14)

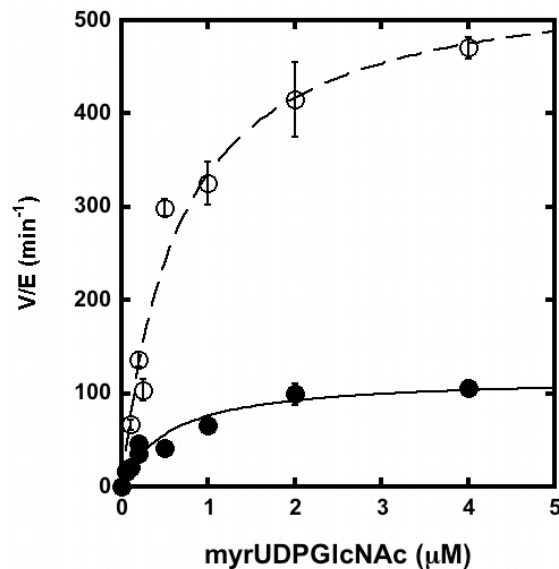


Figure 3.3: Steady-state turnover catalyzed by EcC63A. Zn^{2+} - (filled circle) or Fe^{2+} -C63A-LpxC (open circle) catalyzed initial rates of deacetylation of myr-UDPGlcNAc (0.05 – 4 μM) were measured at 30 °C in 20 mM bis-tris propane, 10 mM TCEP pH 7.5, as described under “Materials and Methods” using apo-enzyme reconstituted with stoichiometric metal ion. The parameters k_{cat} , K_{M} and $k_{\text{cat}}/K_{\text{M}}$ (Table 3.1) were obtained by fitting the Michaelis-Menten equation to these data.

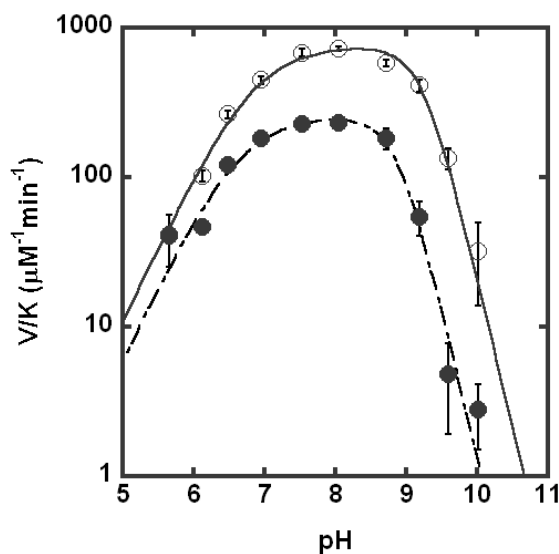


Figure 3.4: pH-dependence of LpxC. V/K values for Zn^{2+} - C63A (●) or Fe^{2+} - C63A (○) LpxC were measured at 30 °C using subsaturating concentrations of myr-UDPGlcNAc ($\leq 0.2 \mu\text{M}$) and enzyme reconstituted with stoichiometric metal ion, as described under “Materials and Methods”. The pK_{a} values (see Table 3.1) were determined by fitting Eq. 3.1 to the data.

The WT LpxC-catalyzed reaction exhibits a bell-shaped dependence on pH, wherein pK_{a1} and pK_{a2} are proposed to represent ionization of Glu78 and another group located near the metal ion, such as H265, respectively (14, 27). The pH-dependence of k_{cat}/K_M catalyzed by C63A LpxC activated by Zn^{2+} or Fe^{2+} (Figure 3.4) shows a bell-shaped pH profile, indicating that at least two ionizations are important for maximal activity, consistent with pH profiles previously measured for WT LpxC (14, 27). However, at high pH the decrease in activity for C63A LpxC has a squared dependence on the proton concentration (Figure 3.4), suggesting that two deprotonations affect the activity at high pH. Therefore, the C63A mutant is best described by three ionizations: one at low pH and two at high pH. These data are fit using an equation that assumes that the two high pH ionizations have comparable pK_a values. The reactions catalyzed by EcC63A LpxC reconstituted with either stoichiometric Zn^{2+} or Fe^{2+} have nearly identical pH-profiles, indicating that the Fe-enzyme has higher catalytic activity regardless of the pH. Furthermore, the fitted values for pK_{a1} and pK_{a2} for the C63A mutant are slightly higher and comparable to, respectively, the values determined for wild-type LpxC (Table 3.1), suggesting that the same ionizations are observed for both WT and the C63A mutant. The additional ionization at high pH observed for the C63A mutant could be due to several factors. For example, several ionizable LpxC residues not directly implicated in catalysis, such as H19 or K143 (18), could be perturbed in the C63A mutant and ionization of these residues could become observable in the steady-state kinetics. Alternatively, replacing the cysteine thiol with an alanine may lower the metal-water pK_a such that it is observable at high pH. Ionization of these groups could directly affect the stability of the transition state or could reversibly destabilize the active structure of LpxC.

XAS analysis of LpxC

The change in LpxC activity observed with Fe^{2+} and Zn^{2+} cofactors may correlate with an alteration in the preferred coordination numbers and/or geometries of the respective metal ions. For peptide deformylase (PDF), the higher coordination number of Fe^{2+} -PDF compared to Zn^{2+} -PDF is proposed to contribute to the higher activity that is observed with the Fe^{2+} cofactor (28). In biological zinc sites a coordination number of 4 (tetrahedral geometry) is observed most frequently, although 5 and 6 ligands are also observed, while Fe^{2+} prefers higher coordination numbers (5 or 6) (29-31). Previous XAS studies of AaLpxC and *Pseudomonas aeruginosa* LpxC (PaLpxC) with a single bound Zn^{2+} (12) demonstrated that the catalytic zinc ion has four N/O ligands. Similarly, crystal structures of the zinc-inhibited and the cacodylate complex of AaLpxC indicate that the catalytic zinc ion is tetrahedral (26, 32). The best fits to the EXAFS data for EcLpxC with Zn^{2+} bound to both the catalytic and inhibitory sites is 3 N/O and 1 S/Cl while the fit for EcLpxC with Co^{2+} at the catalytic site is 5 N/O. These previous data suggest that the increased activity of the Co^{2+} EcLpxC (17) correlates with the higher coordination number.

To probe determinants of the enhanced activity of Fe^{2+} -LpxC, we examined the coordination environments of EcLpxC and AaLpxC with stoichiometric Fe^{2+} bound at the catalytic site. The XANES and EXAFS data for these samples are shown in Figure 3.5. The XANES region of the XAS spectra ($1s \rightarrow 3d$ transitions) provides valuable information about metal ion coordination number and oxidation state. The $1s \rightarrow 3d$ transitions (pre-edge areas) observed for 4-, 5- and 6-coordinate Fe are $19.8 - 25 \times 10^{-2}$ eV, $12.4 - 18.8 \times 10^{-2}$ eV, and $3.1 - 9.9 \times 10^{-2}$ eV, respectively (33-35). The Fe pre-edge

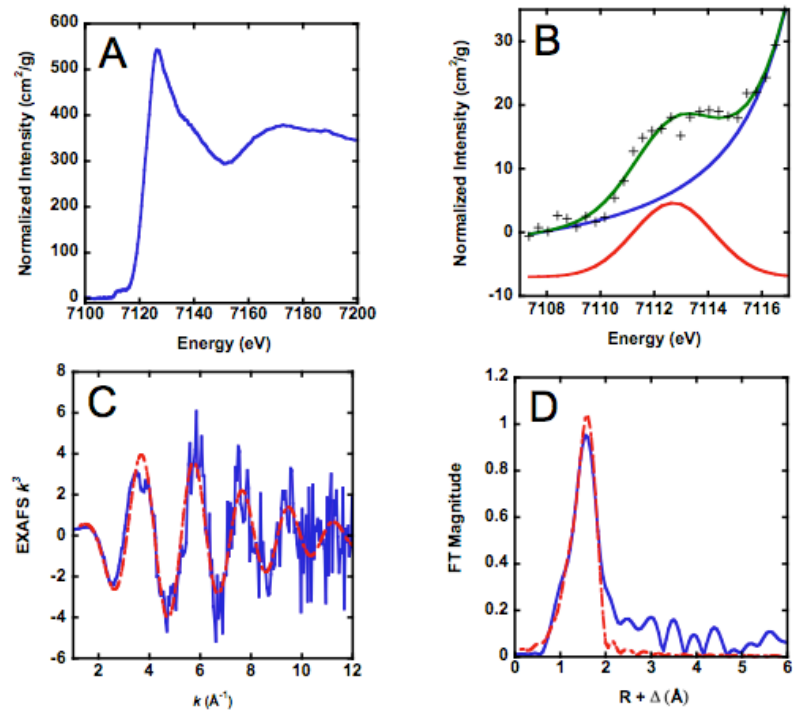


Figure 3.5: XAS of Fe^{2+} -EcLpxC. (A) XANES region. (B) Expansion of XANES showing $1s \rightarrow 3d$ transition with calculated background (blue) and best fit (green). Gaussian fit to $1s \rightarrow 3d$ transition is shown offset vertically for clarity. (C) k^3 weighted EXAFS data (blue) together with best fit using 5 oxygen ligands (red, dashed). (D) Fourier transform of EXAFS data: experimental (solid line) and fit (dashed line) to 5 N/O ligands.

Table 3.2. XANES pre-edge areas

Sample	1s->3d (sample 1)	1s->3d (sample 2)	1s->3d average
Fe ²⁺ -AaLpxC	11.2 x 10 ⁻² eV	14.9 x 10 ⁻² eV	13.1 x 10 ⁻² eV
Fe ²⁺ -EcLpxC	12.1 x 10 ⁻² eV	12.1 x 10 ⁻² eV	12.1 x 10 ⁻² eV

Table 3.3. Fitting results for Fe-LpxC

	N ^a	R (Å) ^b	s ² ×10 ³ (Å ² ×10 ³) ^c	F ^d	BVS ^e
Fe²⁺-AaLpxC					
Sample 1	4	2.100	5.7	0.66	1.5
	5	2.100	7.7	0.67	1.9
	6	2.100	9.7	0.70	2.2
Sample 2	4	2.100	6.0	0.40	1.5
	5	2.096	8.2	0.42	1.9
	6	2.097	10.5	0.44	2.3
Fe²⁺-EcLpxC					
Sample 1	4	2.100	6.4	0.30	1.5
	5	2.105	8.2	0.30	1.8
	6	2.106	10.1	0.32	2.2
Sample 2	4	2.090	6.8	0.33	1.5
	5	2.090	8.8	0.33	1.9
	6	2.090	10.9	0.35	2.3

^aEXAFS coordination number, fixed at integer values

^bFe-O bond length. Although the experimental accuracy is estimated at ±0.02 Å, values are reported to 0.001 Å in order to show the precision of the data

^cDebye-Waller factors

^dRoot-mean square deviation between data and fit

^eBond-valence sum

areas calculated for EcLpxC (12.1×10^{-2} eV) and AaLpxC ($11.2 - 14.9 \times 10^{-2}$ eV) are both consistent with a 5-coordinate Fe species (Table 3.2), and in particular, are significantly smaller than the values observed for tetrahedral Fe. This conclusion is supported by the EXAFS data for both WT Fe²⁺-EcLpxC and Fe²⁺-AaLpxC (Table 3.3, Figure 3.5). Consistent with our observations for Zn-AaLpxC and Zn-PaLpxC (12), the EXAFS data for Fe²⁺-EcLpxC and Fe²⁺-AaLpxC show significant disorder. Fits using 4, 5, or 6 low-Z ligands all give similar quality fits, with Debye-Waller factors that increase as the fitted coordination number increases (Table 3.3). Although it was possible in most cases to fit the data using a mixed ligation mode of 3-5 (O/N) + 1 S, in no case did these fits result in more than a modest (i.e., < 10%) improvement in fit quality, improvement that can be accounted for by the doubling in the number of adjustable parameters. Further evidence that the EXAFS data do not support the presence of mixed (N/O)+S ligation comes from the fact that in most cases the apparent Fe-S parameters are chemically unreasonable (e.g., apparent Fe-S distances < 2 Å, apparent Fe-S Debye-Waller factors $s^2 > 0.01 \text{ \AA}^2$). In all cases, both (N/O) only and (N/O)+S fits, the apparent Fe-(N/O) distance is ~2.1 Å, significantly longer than that found for the 4-coordinate Zn²⁺ that is observed in many XAS and crystallographic studies of AaLpxC, PaLpxC and EcLpxC (12), and consistent with the distances found for 5-coordinate Fe²⁺. This conclusion is supported by the fact that the 5-coordinate Fe-(N/O) fits consistently give the bond-valence sum values (36, 37) closest to 2.

Crystallographic analyses of AaLpxC and PaLpxC complexed with hydroxamate inhibitors or palmitate indicate that the catalytic zinc changes geometry upon ligand binding to square pyramidal (5 coordinate) (26, 38). These data indicate that the

geometry of the metal site is flexible, consistent with our finding that the Fe^{2+} site appears to adopt a 5-coordinate structure even in the absence of added inhibitors. Since the Fe-LpxC coordination sphere is best fit to 5 (N/O) ligands, the added ligand is most likely a water molecule as observed in other proteins where metal substitution leads to a higher coordination number, such as carbonic anhydrase (39) and peptide deformylase (28). These observations are consistent with the suggestion that the higher activity and ligand affinity of Fe^{2+} -EcLpxC correlates with the higher coordination number of Fe^{2+} .

Effect of Fe^{2+} on molecular recognition

The metal ion status of LpxC was previously shown to influence the binding affinity of LpxC for small molecules, which has important implications for the development of LpxC inhibitors as potential antibiotics (18, 19). Here, we examine whether substitution of EcLpxC with Fe^{2+} alters the affinity of small molecules for LpxC compared to Zn^{2+} by measuring the affinities of myrUDPGlcNAc (K_D^{Product}) and a fluorescent fatty acid ($K_D^{\text{fatty acid}}$) for LpxC (WT and C63A) using ultrafiltration and fluorescence anisotropy, respectively. The C63A mutation in LpxC causes a small enhancement in the binding affinity of these ligands, irrespective of the metal ion at the active site (Table 3.4); the value of K_D^{Product} and $K_D^{\text{fatty acid}}$ are lowered 3-4- and < 2-fold, respectively, compared to WT LpxC. The value of K_D^{Product} is not significantly altered when comparing Fe^{2+} - to Zn^{2+} -EcLpxC, in either WT or C63A, suggesting that product binding in these enzymes is similar and/or that there is not a direct metal ion-product interaction in these complexes. In contrast, a ~6-fold increase in $K_D^{\text{fatty acid}}$ is observed for LpxC (WT and C63A) substituted with Fe^{2+} compared to Zn^{2+} , indicating that changing the metal ion significantly alters recognition of this small molecule, consistent with the

Table 3.4. LpxC molecular recognition parameters

Enzyme ^a	K_D^{Product} (μM) ^b	$K_D^{\text{Fatty acid}}$ (μM) ^c	IC_{50} (nM) ^d
Apo-LpxC	1.5 ± 0.5	25 ± 1	ND
Zn ²⁺ -LpxC	1.6 ± 0.2^e	7 ± 0.6^f	ND
Fe ²⁺ -LpxC	1.9 ± 0.3	45 ± 3	ND
Apo-C63A	0.5 ± 0.1	17 ± 1	ND
Zn ²⁺ -C63A	0.40 ± 0.07	7 ± 1	4 ± 0.4
Fe ²⁺ -C63A	0.6 ± 0.1	44 ± 3	2 ± 0.2

^a Metal substituted LpxC was reconstituted with stoichiometric metal ion (1:1) as described in the “Materials and Methods”.

^b Product (myr-UDPGlcNH₂) binding to LpxC was measured at 30 °C (20 mM bis-tris propane, 10 mM TCEP pH 7.5) using ultrafiltration as described in the “Materials and Methods”. The K_D values were obtained by fitting Eq. 3.4 to the data.

^c BODIPY-fatty acid binding to LpxC was measured at 30 °C (20 mM bis-tris propane, 10 mM TCEP pH 7.5, 100 μM ZnSO₄ or FeCl₂) using fluorescence anisotropy as described in the “Materials and Methods”. The K_D values were obtained by fitting Eq. 3.5 to the data.

^d Hydroxamate L161, 240 inhibition of LpxC activity was measured at 30 °C (20 mM bis-tris propane, 10 mM TCEP pH 7.5, 1 mg/mL BSA) and 200 nM myrUDPGlcNAc as described in the “Materials and Methods”. The IC_{50} values were obtained by fitting Eq. 2 to the data.

^e Data are adapted from ref (18). ^f Data are adapted from ref (19).

direct metal ion-fatty acid interaction observed in crystal structures of the LpxC•palmitate complex (14, 32). Finally, a modest (2-fold) enhancement in inhibition (IC_{50} value) by the hydroxamate inhibitor L-161,240 is observed for LpxC with bound Fe^{2+} compared to Zn^{2+} (Table 3.4). This is comparable to the 2-fold decrease in K_i for inhibition of histone deacetylase 8 by suberoylanilide hydroxamic acid upon switching the active site metal ion from Zn^{2+} to Fe^{2+} (11).

Oxygen sensitivity of Fe^{2+} -EcLpxC activity

Since Fe^{2+} is a redox-sensitive metal ion, it is unstable in oxygen. The initial rate for deacetylation catalyzed by LpxC after reconstitution with stoichiometric Fe^{2+} is decreased ≥ 8 -fold when assayed under aerobic conditions compared to anaerobic conditions (glove box). Furthermore, similar decreases were observed when the deacetylase activity of Fe^{2+} -LpxC was measured in the presence of catalase (100 mg/mL), dithiothreitol (2 mM), dithionite (10 mM) or TCEP (≤ 2 mM) under aerobic conditions, suggesting these conditions are not sufficient for maintaining Fe in the reduced form. However, when higher concentrations of TCEP (10 mM) are added to the assay, comparable deacetylase activity is observed for Fe^{2+} -LpxC under both aerobic and anaerobic conditions over 2 hours (Figure 3.6). In contrast, there is no change in Zn^{2+} -LpxC activity when the concentration of TCEP is varied under these conditions (Figure 3.6A). Notably the activity of Fe^{2+} -EcLpxC does not go to zero, but to the level observed for Zn^{2+} -EcLpxC activity, suggesting that under these conditions the Fe^{2+} cofactor is oxidized to Fe^{3+} and replaced by nM concentrations of adventitious Zn^{2+} in the assay. *In vitro* control experiments demonstrate that Fe^{2+} -LpxC inactivated by exposure to oxygen

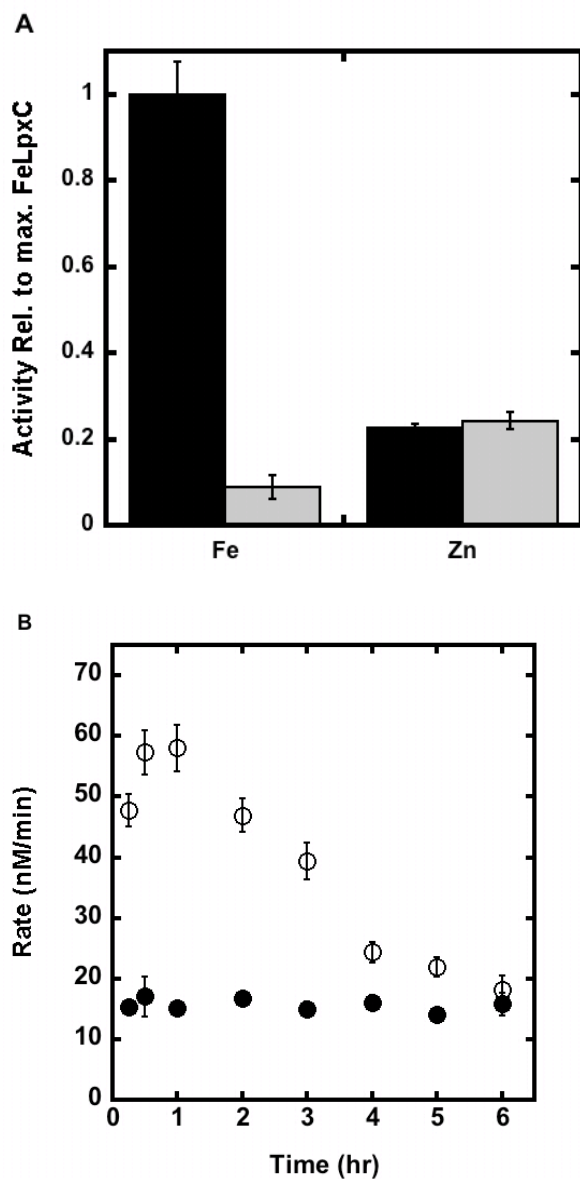


Figure 3.6: Dependence of LpxC activity on reducing agents. (A) The activity of Fe²⁺- and Zn²⁺-EcLpxC was measured at 30 °C in buffer containing either 10 mM (black bars) or 0.5 mM (gray bars) TCEP as described in the “Materials and Methods” section. (B) Apo-EcLpxC was reconstituted with either Fe²⁺ (open circle) or Zn²⁺ (filled circle) and the resulting activity was measured at 30 °C (20 mM bis-tris propane, 10 mM TCEP, pH 7.5) as a function of time.

can be reactivated by addition of divalent metal ions. These results demonstrate that the activity of Fe^{2+} -LpxC, and not Zn^{2+} -LpxC, is sensitive to exposure to oxygen.

Native LpxC activity

To analyze the metal ion cofactor bound to LpxC *in vivo*, we measured the oxygen sensitivity of natively expressed LpxC in *E. coli* cell lysates. *E. coli* cells (BL21(DE3) without the LpxC expression plasmid) were grown, lysed and the resulting LpxC activity was measured over time (15 min - 3 hr following lysis) in buffers containing either ≤ 1 mM or 10 mM TCEP. The total native EcLpxC activity in cell lysates is ~3-fold higher in assays containing 10 mM TCEP compared to 0.1 mM TCEP (Figure 3.7 – column A). Furthermore, over 3 hours the activity decreases ~5-fold (Figure 3.7, column B) to a residual activity that is stable in the cell lysate. If the residual activity measured in the presence of the LpxC hydroxamate inhibitor L-161,240 (Figure 3.7, column C), reflecting background deacetylation catalyzed by other enzymes, is subtracted from the oxygen sensitive activity, then the observed activity decreases 5- to 7-fold in the presence of oxygen. This decrease is consistent with the higher activity of Fe^{2+} -LpxC compared to Zn^{2+} -LpxC. These findings suggest that the majority of the native LpxC expressed in *E. coli* contains a bound Fe^{2+} cofactor.

Discussion

LpxC activity correlates with metal geometry

The kinetic experiments indicate that Fe^{2+} can serve as a cofactor for *E. coli* LpxC, a mononuclear metal-dependent deacetylase, and that the Fe^{2+} cofactor alters the functional properties of LpxC compared to Zn^{2+} . Specifically, LpxC substituted with a

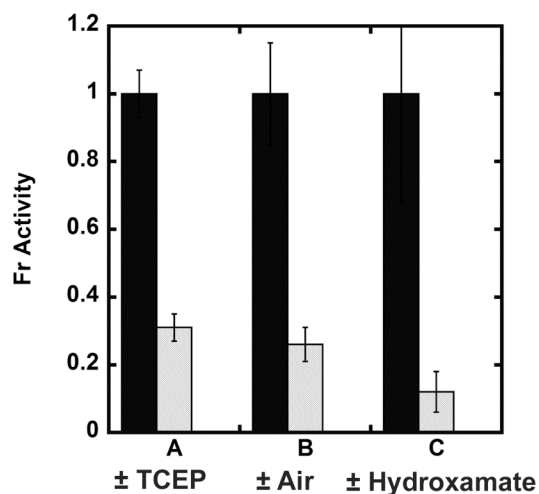


Figure 3.7: Native LpxC activity. The LpxC deacetylase activity of *E. coli* crude cell lysates was measured at 30 °C as described in “Materials and Methods” and normalized to fractional activity of the maximum for each experiment. (A) LpxC activity of *E. coli* cell lysate measured in 20 mM bis-tris propane pH 7.5 containing 10 mM (black bar) or 0.1 mM TCEP (gray bar). (B) *E. coli* cell lysate activity assayed in 10 mM TCEP immediately following lysis (black bar) or after incubation on ice for 3 hours under aerobic (benchtop) conditions post-lysis (gray bar). (C) The LpxC inhibitor L-161,240 inhibits 90% of the deacetylase activity in the *E. coli* cell lysate (20 mM bis-tris propane, 10 mM TCEP pH 7.5). The concentration of L-161,240 was 0 μ M (black bar) or (1 μ M) (gray bar).

single catalytic Fe^{2+} has 6- to 8-fold higher activity than Zn^{2+} -LpxC. Comparison of the steady-state kinetic parameters for the C63A mutant indicate that switching from Zn^{2+} to Fe^{2+} leads to a 6-fold increase in the value of $k_{\text{cat}}/K_{\text{M}}$, with a nearly comparable effect on the value of k_{cat} (4-fold). The single site mutation, C63A, eliminates much of the metal inhibition that complicates analysis of LpxC activity, likely by removing a ligand to the inhibitory metal.

Metal substitution in LpxC increases the value of both the steady-state parameters $k_{\text{cat}}/K_{\text{M}}$ and k_{cat} . The dependence of the value of $k_{\text{cat}}/K_{\text{M}}$ for LpxC on the active site metal ion and on mutations (Table 3.1; (14, 18)) argue that substrate association is not the rate-limiting step under these conditions even though the value of $k_{\text{cat}}/K_{\text{M}}$ ($\leq 1.6 \times 10^7 \text{ M}^{-1}\text{s}^{-1}$; Table 3.1) approaches that of diffusion-controlled rate constants measured for many enzymes ($10^7 - 10^8 \text{ M}^{-1}\text{s}^{-1}$) (40). Furthermore, the solvent kinetic isotope effect of 2 observed for $k_{\text{cat}}/K_{\text{M}}$ catalyzed by LpxC (18) suggests that the chemical step is a rate contributing step for this kinetic parameter. Additionally, under conditions of saturating substrate and high enzyme concentration, a burst of product formation is not observed, suggesting that the rate-limiting step in k_{cat} occurs at or before the chemical step (27). Therefore, it is reasonable to assume that the increases in $k_{\text{cat}}/K_{\text{M}}$ and k_{cat} upon substitution of Zn^{2+} with Fe^{2+} are attributable mainly to an enhancement in the chemical step.

The best fit of the models to the XAS data is 5 N/O ligands for both Fe^{2+} -substituted EcLpxC and AaLpxC compared to the 4 N/O ligands observed for WT Zn^{2+} -LpxC presumably due to an additional water ligand (12). These results are consistent with the hypothesis that the higher activity of the Fe^{2+} -substituted EcLpxC correlates with

the coordination number. Previously, the enhanced activity of Fe^{2+} -peptide deformylase (PDF) has been proposed to be due, at least in part, to the higher coordination number of Fe^{2+} -PDF compared to Zn^{2+} -PDF (8, 28, 41-43). The XAS and activity data for Fe^{2+} -EcLpxC, in concert with recent crystallography data demonstrating a square pyramidal zinc site in LpxC-complexed with hydroxamate inhibitors or palmitate (26, 38), suggest that the proposed mechanism for deacetylation should be modified to incorporate a 5-coordinate metal ion, in both the ground and transition states (Figure 3.8). In this mechanism, the metal ion serves both to lower the $\text{p}K_{\text{a}}$ of the metal-bound water and to coordinate the substrate (myrUDPGlcNAc). Coordination of the substrate to the metal ion can assist in polarization of the carbonyl group, enhancing the electrophilicity of the carbonyl carbon. However, enhancement of activity by the 5-coordinate Fe^{2+} cofactor could also be due to small differences in metal-ligand bond length and ligand geometry that optimize the positions of the metal-bound water, the substrate carbonyl carbon and active site side chains for catalyzing deacetylation. Following substrate binding, the side chain of E78 serves as a general base catalyst to activate the metal-water for attack on the carbonyl carbon of the substrate (14, 27); the resulting oxyanion intermediate is stabilized by the side chain of T191 and the metal ion (18). The mechanism that is most consistent with the crystallographic, theoretical studies and mutagenesis data (14, 18, 44) is that the side chain of protonated H265 (rather than protonated E78 as proposed for most metalloproteinases (45)) facilitates breakdown of the tetrahedral intermediate by protonation of the leaving group.

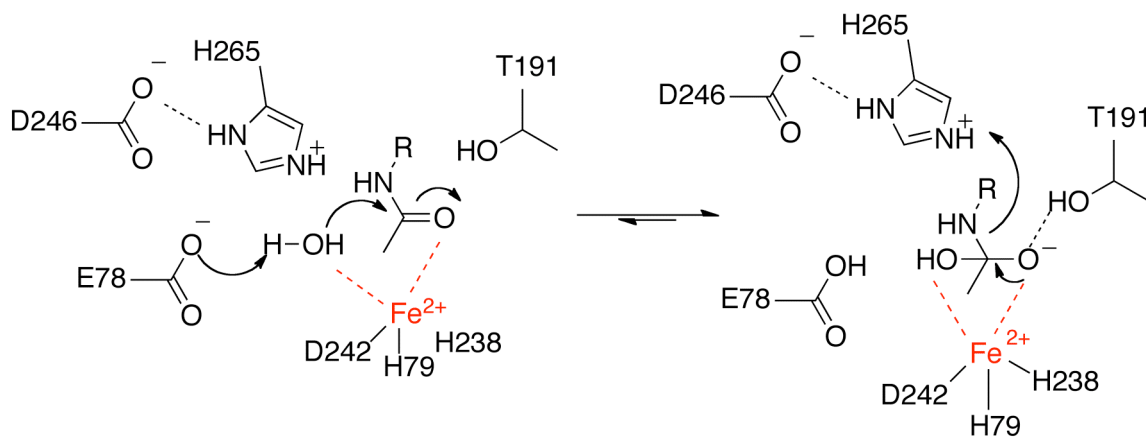


Figure 3.8: Proposed mechanism of FeLpxC.

Molecular recognition is affected by metal substitution.

Previously it has been demonstrated that apo-LpxC, LpxC with a single bound zinc, and the zinc-inhibited form of LpxC (Zn_2 -LpxC) bind ligands with different affinity (19); similarly, switching the catalytic metal from Zn^{2+} to Fe^{2+} alters molecular recognition as well. The affinity of Fe^{2+} -EcLpxC for a hydroxamate inhibitor increases by a small degree (~2-fold), consistent with crystal structures indicating that the metal geometry in LpxC-hydroxamate complexes is 5-coordinate (square pyramidal) (26, 38). A similar increase in hydroxamate inhibitor affinity has been observed upon switching the active site metal from Zn^{2+} to Fe^{2+} in histone deacetylase 8 (11). In addition, the affinity of Fe^{2+} -EcLpxC for the BODIPY fatty acid inhibitor is decreased by 6-fold compared to the Zn-bound enzyme. Both changes in affinity are likely due to alteration of the geometry of the metal-ligand coordination leading to alterations in interactions with other active site groups. Since the majority of LpxC inhibitors currently being developed as antibiotics interact with the active site metal ion, it is clear that the identity of this metal ion will affect the inhibitor efficacy.

Fe^{2+} -LpxC is redox-sensitive in vitro and present in E. coli

Differences in the *in vitro* behaviors of Fe^{2+} -LpxC and Zn^{2+} -LpxC may provide information that will enable identification of the metal ion cofactor used by LpxC *in vivo*. In particular, the higher activity and oxygen sensitivity of Fe^{2+} -LpxC compared to Zn^{2+} -LpxC provides a means to evaluate the metal cofactor bound to LpxC in *E. coli* lysates. A majority of the native LpxC activity in *E. coli* cell lysates is lost upon exposure to oxygen (Figure 3.7). This suggests that *E. coli* grown aerobically in rich media (LB) use Fe^{2+} as the main metal cofactor in LpxC and *not* Zn^{2+} . However, both Fe^{2+} and Zn^{2+} can

activate LpxC-catalyzed deacetylation and this metal-switching capability may allow the LpxC to function, and *E. coli* to grow, under different environmental conditions, including limiting iron concentrations. Thus, LpxC likely fits into the category of a “cambialistic” enzyme that can be activated by either Fe or Zn, like several other enzymes, including the cambialistic Mn or Fe superoxide dismutases (46), metallo-beta-lactamase L1 (47, 48), and the glyoxylases (49-51).

Given the effects of the active site metal bound to LpxC on turnover and molecular recognition, and the ongoing efforts to identify small-molecular inhibitors for this enzyme, most of which feature moieties that bind the catalytic metal ion, further experiments to determine the behavior and specificity of this enzyme *in vivo* are needed.

REFERENCES

- (1) Roth, L. D., Khan, A.S., Lillibridge, S.R., Ostroff, S.M., Hughes, J.M. (2002) Public health assessment of potential biological terrorism agents. *Emerging infectious diseases* 8, 225-230.
- (2) Raetz, C. R. H., and Whitfield, C. (2002) Lipopolysaccharide endotoxins. *Annual Review of Biochemistry* 71, 635-700.
- (3) Wyckoff, T. J. O., Raetz, C. R. H., and Jackman, J. E. (1998) Antibacterial and anti-inflammatory agents that target endotoxin. *Trends in Microbiology* 6, 154-159.
- (4) White, R. J., Margolis, P. S., Trias, J., and Yuan, Z. Y. (2003) Targeting metalloenzymes: a strategy that works. *Current Opinion in Pharmacology* 3, 502-507.
- (5) Young, K., Silver, L. L., Bramhill, D., Cameron, P., Eveland, S. S., Raetz, C. R. H., Hyland, S. A., and Anderson, M. S. (1995) The envA permeability cell division gene of Escherichia coli encodes the second enzyme of lipid A biosynthesis - UDP-3-O-(R- 3-hydroxymyristoyl)-N-acetylglucosamine deacetylase. *Journal of Biological Chemistry* 270, 30384-30391.
- (6) Jackman, J. E., Raetz, C. R. H., and Fierke, C. A. (1999) UDP-3-O-(R-3-hydroxymyristoyl)-N-acetylglucosamine deacetylase of Escherichia coli is a zinc metalloenzyme. *Biochemistry* 38, 1902-1911.
- (7) Groche, D., Becker, A., Schlichting, I., Kabsch, W., Schultz, S., and Wagner, A. F. V. (1998) Isolation and crystallization of functionally competent Escherichia coli peptide deformylase forms containing either iron or nickel in the active site. *Biochemical and Biophysical Research Communications* 246, 342-346.
- (8) Rajagopalan, P. T. R., Yu, X. C., and Pei, D. H. (1997) Peptide deformylase: A new type of mononuclear iron protein. *Journal of the American Chemical Society* 119, 12418-12419.
- (9) Becker, A., Schlichting, I., Kabsch, W., Groche, D., Schultz, S., and Wagner, A. F. V. (1998) Iron center, substrate recognition and mechanism of peptide deformylase. *Nature Structural Biology* 5, 1053-1058.
- (10) Zhu, J. G., Dizin, E., Hu, X. B., Wavreille, A. S., Park, J., and Pei, D. H. (2003) S-ribosylhomocysteinase (LuxS) is a mononuclear iron protein. *Biochemistry* 42, 4717-4726.

- (11) Gantt, S. L., Gattis, S. G., and Fierke, C. A. (2006) Catalytic activity and inhibition of human histone deacetylase 8 is dependent on the identity of the active site metal ion. *Biochemistry* 45, 6170-6178.
- (12) McClure, C. P., Rusche, K. M., Peariso, K., Jackman, J. E., Fierke, C. A., and Penner-Hahn, J. E. (2003) EXAFS studies of the zinc sites of UDP-(3-O-acyl)-N-acetylglucosamine deacetylase (LpxC). *Journal of Inorganic Biochemistry* 94, 78-85.
- (13) Jackman, J. E., Fierke, C. A., Tumey, L. N., Pirrung, M., Uchiyama, T., Tahir, S. H., Hindsgaul, O., and Raetz, C. R. H. (2000) Antibacterial agents that target lipid A biosynthesis in Gram- negative bacteria - Inhibition of diverse UDP-3-O-(R-3-hydroxymyristoyl)-N-acetylglucosamine deacetylases by substrate analogs containing zinc binding motifs. *Journal of Biological Chemistry* 275, 11002-11009.
- (14) Hernick, M., Gennadios, H. A., Whittington, D. A., Rusche, K. M., Christianson, D. W., and Fierke, C. A. (2005) UDP-3-O-((R)-3-hydroxymyristoyl)-N-acetylglucosamine deacetylase functions through a general acid-base catalyst pair mechanism. *Journal of Biological Chemistry* 280, 16969-16978.
- (15) Sorensen, P. G., Lutkenhaus, J., Young, K., Eveland, S. S., Anderson, M. S., and Raetz, C. R. H. (1996) Regulation of UDP-3-O- R-3-hydroxymyristoyl -N-acetylglucosamine deacetylase in Escherichia coli - The second enzymatic step of lipid a biosynthesis. *Journal of Biological Chemistry* 271, 25898-25905.
- (16) Onishi, H. R., Pelak, B. A., Gerckens, L. S., Silver, L. L., Kahan, F. M., Chen, M. H., Patchett, A. A., Galloway, S. M., Hyland, S. A., Anderson, M. S., *et al.* (1996) Antibacterial agents that inhibit lipid A biosynthesis. *Science* 274, 980-982.
- (17) Jackman, J. E., Raetz, C. R., and Fierke, C. A. (1999) UDP-3-O-(R-3-hydroxymyristoyl)-N-acetylglucosamine deacetylase of Escherichia coli is a zinc metalloenzyme. *Biochemistry* 38, 1902-1911.
- (18) Hernick, M., and Fierke, C. A. (2006) Catalytic Mechanism and Molecular Recognition of E. coli UDP-3-O-(R-3-Hydroxymyristoyl)-N-acetylglucosamine Deacetylase Probed by Mutagenesis. *Biochemistry* 45, 15240-15248.
- (19) Hernick, M., and Fierke, C. A. (2006) Molecular recognition by Escherichia coli UDP-3-O-(R-3-hydroxymyristoyl)-N-acetylglucosamine deacetylase is modulated by bound metal ions. *Biochemistry* 45, 14573-14581.
- (20) George, G. N. *see* <http://www-ssrl.slac.stanford.edu/exafspak.html>.
- (21) Ankudinov, A. L., and Rehr, J. J. (1997) Relativistic calculations of spin-dependent x-ray-absorption spectra. *Physical Review B* 56, R1712-R1715.

- (22) Ankudinov, A. L., Ravel, B., Rehr, J. J., and Conradson, S. D. (1998) Real-space multiple-scattering calculation and interpretation of x-ray-absorption near-edge structure. *Physical Review B* 58, 7565-7576.
- (23) McMaster, W. H., Del Grande, J.H., Mallet, N.K., Hubbell, J.H. (1969) *Compilation of X-Ray Cross Sections*, Lawrence Livermore National Laboratory Report UCRL-50174, Sec II, Rev. 1, NIST, US Department of Commerce.
- (24) Weng, T. C., Waldo, G. S., and Penner-Hahn, J. E. (2005) A method for normalization of X-ray absorption spectra. *Journal of Synchrotron Radiation* 12, 506-510.
- (25) Irving, H., and Williams, R. J. P. (1948) Order of Stability of Metal Complexes. *Nature* 162, 746-747.
- (26) Whittington, D. A., Rusche, K. M., Shin, H., Fierke, C. A., and Christianson, D. W. (2003) Crystal structure of LpxC, a zinc-dependent deacetylase essential for endotoxin biosynthesis. *Proc Natl Acad Sci USA* 100, 8146-8150.
- (27) McClerren, A. L., Zhou, P., Guan, Z., Raetz, C. R. H., and Rudolph, J. (2005) Kinetic Analysis of the Zinc-Dependent Deacetylase in the Lipid A Biosynthetic Pathway. *Biochemistry* 44, 1106-1113.
- (28) Jain, R. K., Hao, B., Liu, R. P., and Chan, M. K. (2005) Structures of E-coli peptide deformylase bound to formate: Insight into the preference for Fe²⁺ over Zn²⁺ as the active site metal. *Journal of the American Chemical Society* 127, 4558-4559.
- (29) Lippard, S. J., Berg, J.M. (1994) *Principles of Bioinorganic Chemistry*, University Science Books, Mill Valley, California.
- (30) Frausto da Silva, J. J. R., Williams, R.J.P. (2001) *The Biological Chemistry of the Elements*, Oxford University Press, New York.
- (31) Kaim, W., Schwederski (1994) *Bioinorganic Chemistry: Inorganic Elements in the Chemistry of Life*, John Wiley and Sons LTD, Chichester.
- (32) Gennadios, H. A., and Christianson, D. W. (2006) Binding of uridine 5'-diphosphate in the "basic patch" of the zinc deacetylase LpxC and implications for substrate binding. *Biochemistry* 45, 15216-15223.
- (33) Shu, L., Chiou, Y. M., Orville, A. M., Miller, M. A., Lipscomb, J. D., and Que, L., Jr. (1995) X-ray absorption spectroscopic studies of the Fe(II) active site of catechol 2,3-dioxygenase. Implications for the extradiol cleavage mechanism. *Biochemistry* 34, 6649-6659.

- (34) Westre, T. E., Kennepohl, P., DeWitt, J. G., Hedman, B., Hodgson, K. O., and Solomon, E. I. (1997) A multiplet analysis of Fe K-edge 1s->3d pre-edge features of iron complexes. *Journal of the American Chemical Society* 119, 6297-6314.
- (35) Roe, A. L., Schneider, D. J., Mayer, R. J., Pyrz, J. W., Widom, J., and Que, L. (1984) X-Ray Absorption-Spectroscopy of Iron-Tyrosinate Proteins. *Journal of the American Chemical Society* 106, 1676-1681.
- (36) Thorp, H. H. (1992) Bond Valence Sum Analysis of Metal-Ligand Bond Lengths in Metalloenzymes and Model Complexes. *Inorganic Chemistry* 31, 1585-1588.
- (37) Brown, I. D., and Altermatt, D. (1985) Bond-Valence Parameters Obtained from a Systematic Analysis of the Inorganic Crystal-Structure Database. *Acta Crystallographica Section B-Structural Science* 41, 244-247.
- (38) Mochalkin, I., Knafels, J. D., and Lightle, S. (2008) Crystal structure of LpxC from *Pseudomonas aeruginosa* complexed with the potent BB-78485 inhibitor. *Protein Sci* 17, 450-457.
- (39) Hakansson, K., Wehnert, A., and Liljas, A. (1994) X-Ray-Analysis of Metal-Substituted Human Carbonic-Anhydrase-Ii Derivatives. *Acta Crystallographica Section D-Biological Crystallography* 50, 93-100.
- (40) Fersht, A. R. (1999) *Structure and Mechanism in Protein Science: A Guide to Enzyme Catalysis and Protein Folding*, W. H. Freeman and Company, New York.
- (41) Rajagopalan, P. T., Datta, A., and Pei, D. (1997) Purification, characterization, and inhibition of peptide deformylase from *Escherichia coli*. *Biochemistry* 36, 13910-13918.
- (42) Rajagopalan, P. T., and Pei, D. (1998) Oxygen-mediated inactivation of peptide deformylase. *J Biol Chem* 273, 22305-22310.
- (43) Chan, M. K., Gong, W., Rajagopalan, P. T., Hao, B., Tsai, C. M., and Pei, D. (1997) Crystal structure of the *Escherichia coli* peptide deformylase. *Biochemistry* 36, 13904-13909.
- (44) Robinet, J. J., and Gauld, J. W. (2008) DFT investigation on the mechanism of the deacetylation reaction catalyzed by LpxC. *The journal of physical chemistry B* 112, 3462-3469.
- (45) Christianson, D. W., and Cox, J. D. (1999) Catalysis by metal-activated hydroxide in zinc and manganese metalloenzymes. *Annual Review of Biochemistry* 68, 33-57.
- (46) Martin, M. E., Byers, B. R., Olson, M. O. J., Salin, M. L., Arceneaux, J. E. L., and Tolbert, C. (1986) A *Streptococcus-Mutans* Superoxide-Dismutase That Is Active

with Either Manganese or Iron as a Cofactor. *Journal of Biological Chemistry* 261, 9361-9367.

- (47) Hu, Z., Spadafora, L. J., Hajdin, C. E., Bennett, B., and Crowder, M. W. (2009) Structure and Mechanism of Copper- and Nickel-Substituted Analogues of Metallo-beta-lactamase L1 (dagger). *Biochemistry*.
- (48) Hu, Z. X., Gunasekera, T. S., Spadafora, L., Bennett, B., and Crowder, M. W. (2008) Metal content of metallo-beta-lactamase L1 is determined by the bioavailability of metal ions. *Biochemistry* 47, 7947-7953.
- (49) Limphong, P., McKinney, R. M., Adams, N. E., Makaroff, C. A., Bennett, B., and Crowder, M. W. (2009) The metal ion requirements of *Arabidopsis thaliana* Glx2-2 for catalytic activity. *J Biol Inorg Chem*.
- (50) Limphong, P., Nimako, G., Thomas, P. W., Fast, W., Makaroff, C. A., and Crowder, M. W. (2009) *Arabidopsis thaliana* Mitochondrial Glyoxalase 2-1 Exhibits beta-Lactamase Activity. *Biochemistry* 48, 8491-8493.
- (51) Limphong, P., McKinney, R. M., Adams, N. E., Bennett, B., Makaroff, C. A., Gunasekera, T., and Crowder, M. W. (2009) Human Glyoxalase II Contains an Fe(II)Zn(II) Center but Is Active as a Mononuclear Zn(II) Enzyme. *Biochemistry* 48, 5426-5434.

CHAPTER 4.
THE ACTIVE SITE METAL ION IN UDP-3-*O*-(*R*-3-HYDROXYMYRISTOYL)-*N*-
ACETYLGLUCOSAMINE DEACETYLASE (LPXC) SWITCHES BETWEEN
FE²⁺ AND ZN²⁺ DEPENDING ON CELLULAR CONDITIONS

Introduction

Gram-negative bacteria are important targets in the continuing fight against antibiotic-resistant infections. The development of new antibiotics to treat infections caused by resistant organisms is critically needed, and will require novel targets. One potential source of targets in Gram negative bacteria is the Lipid A biosynthetic pathway (Figure 4.1) (1, 2), an essential building block of lipopolysaccharides (LPS) that makes up the outer leaflet surrounding the cell wall in Gram-negative bacteria (2-4). In addition to being essential for cell viability, LPS are also referred to as endotoxin (2, 4, 5) and are responsible for immunogenic stimulation in septic shock that can lead to a number of deleterious effects, including severe hypotension and multiple organ dysfunction (5). Consequently, inhibitors of lipid A biosynthesis have the potential to serve as both antibiotics and antiendotoxins. UDP-3-*O*-(*R*-3-hydroxymyristoyl)-*N*-acetylglucosamine deacetylase (LpxC) catalyzes the committed, and second overall, step in lipid A biosynthesis - the hydrolysis of UDP-3-*O*-myristoyl-*N*-acetylglucosamine to UDP-3-*O*-myristoyl-glucosamine and acetate (Figure 4.1) (6-8). Consequently, inhibitors of LpxC are an active area of drug development (9-12).

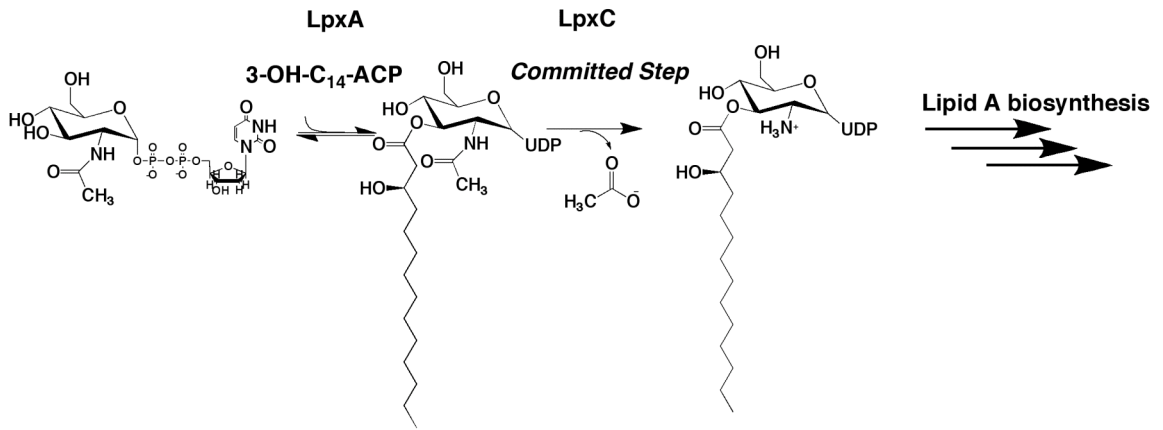


Figure 4.1: Role of LpxC in Lipid A biosynthesis.

LpxC was previously identified as a mononuclear Zn^{2+} metalloenzyme (13); however, recent evidence has shown that LpxC is more active with Fe^{2+} as its metal ion cofactor compared to Zn^{2+} (14) (see Chapter 3). Several enzymes previously described as Zn^{2+} -dependent enzymes have recently been reclassified as Fe^{2+} enzymes, including peptide deformylase (PDF), LuxS, and possibly histone deacetylase 8 (HDAC8) (15-19). Iron is a highly abundant transition metal ion in cells (20, 21); however, the Fe^{2+} redox state which activates LpxC catalysis is oxygen-sensitive, oxidizing to Fe^{3+} in air (14). Therefore, it is not yet clear which metal ion activates LpxC *in vivo*.

Both iron and zinc exist in high amounts in the cell, with total concentrations around 0.2 mM in *E. coli* (21). However, the concentrations of the readily exchangeable, or “free”, metal ions are vastly different. While estimates vary, the best data available for readily exchangeable Fe^{2+} and Zn^{2+} come from mammalian cells, where estimates indicate that $[Zn^{2+}_{free}]$ is picomolar (10 - 400 pM) (22, 23), and $[Fe^{2+}_{free}]$ is micromolar (0.2-6 μ M) (24-27). The combination of the higher concentration of readily exchangeable Fe^{2+} , and the enhanced reactivity of Fe^{2+} -bound LpxC (14) suggest that the native cofactor bound to LpxC in *E. coli* might be Fe^{2+} rather than Zn^{2+} . Therefore we developed rapid purification methods and activity assays to analyze the metal ion status of LpxC *in vivo*. Using these methods, we demonstrate that under normal growth conditions Fe-bound LpxC is the predominate form. However, the ratio of Fe/Zn bound to LpxC depends on the cellular metal content. Although LpxC binds Zn^{2+} with much higher affinity than Fe^{2+} , the higher cellular concentration of $[Fe^{2+}_{free}]$ contributes to the formation of Fe^{2+} -bound LpxC *in vivo*. Together these data indicate that Fe^{2+} is the biologically relevant cofactor for LpxC under common growth conditions although metal

switching occurs in response to metal availability. Furthermore, metal switching may be important for regulating the LpxC activity upon other changes in cellular conditions.

Materials and Methods

General Procedures, Protein Expression and Plasmid Construction

All solutions were prepared in “metal-free” plasticware, with reagents that did not contain extraneous metal ions and/or were treated with Chelex (Biorad). The metal content of solutions, reagents and proteins were measured by inductively coupled plasma emission mass spectrometry (ICP-MS; Dr. Ted Huston, Univ. of Michigan). LpxC and LpxC-fusion proteins were over-expressed in BL21(DE3) *E. coli* transformed with pET-derived expression plasmids and purified according to published procedures using DEAE-sepharose and Reactive Red-120 affinity dye columns (7, 13, 28). The apo- and single metal bound forms of LpxC were prepared by treatment with metal chelators followed by reconstitution with Zn^{2+} or Fe^{2+} as previously described (13, 14, 28).

The pEcC63ALpxC expression plasmid (14) was modified to encode a fusion between LpxC and an IgG-binding protein, termed a ZZ tag (29-31), with a TEV protease site in the linker region between the two proteins. An Nco I restriction site was introduced at the C-terminal stop codon of LpxC by using the QuikChange mutagenesis kit (Stratagene) with the primer 5'- CCT TCA GCT GTA CTG GCA CCA TGG GGA TCC GAA TTC GAG CTC CG -3' and its reverse complement. The ZZ-tag insert was amplified using PCR from the ZZ region of the commercial vector pEZZ (Amersham) with the introduction of Xho I and EcoR I restriction sites as well as a stop codon at the 3' end (forward primer 1: 5' - CGA TGA ACT CGA GGA CAA CAA ATT CAA CAA

AG – 3' and reverse primer 1: 5' – TAA AGA ATT CTC AGG TTT CTA GAT TCG CGT CTA CTT TCG G – 3'). The DNA fragment was extended using PCR amplification to add a TEV-protease cleavage site and an Nco I restriction site using the forward primer 2 5' – ATG ACT TGC AAC CCA TGG GAG AAC CTG TAC TTC CAG GGT CTC GAG GAC AAC – 3' and the reverse primer 1 (above). The PCR product and pLpxC plasmid containing the new Nco I restriction site were digested with Nco I and EcoRI, and ligated together, catalyzed by T4 DNA Ligase (New England Biolabs), to create the expression plasmid pEcC63ALpxC-ZZ. The plasmid sequence was verified by the University of Michigan DNA Sequencing Core. The presence of the ZZ-tag does not alter the LpxC activity or product affinity. However, the activity of the LpxC-ZZ fusion protein is more sensitive to freeze/thaw cycles than the untagged LpxC (data not shown).

IgG Pull-down experiments

E. coli BL21(DE3) cells transformed with pC63ALpxC-ZZ were grown in Chemically Defined Media (CDM) (32). Protein expression was induced when the cells reached an OD₆₂₀ of 0.6 by the addition of 1 mM isopropyl- β -D-thiogalactoside (IPTG) along with the addition of either no added metals, 5 - 20 μ M ZnSO₄, 5 - 20 μ M ferric ammonium citrate, or both metal supplements and the cells were incubated overnight at 30 °C. The cells were pelleted by centrifugation, washed once with 5 mM CaCl₂ and twice with 10 mM Mops pH 7. Control experiments demonstrate that 10 mM Ca²⁺ has no effect on the activity of Zn-LpxC or apo-LpxC. The washed cell pellets from 100 mL growth media were transferred to an anaerobic glove box, resuspended in 3 mL pulldown

buffer (40 mM Mops pH 8, 150 mM NaCl, 10 mM TCEP, 0.1% NP-40), and lysed by incubation with lysozyme (1 mg/mL) at room temperature for 15-30 minutes. The tubes were sealed with parafilm, removed from the glove box, and the cell lysate was cleared by centrifugation (12,000 rpm, 15-30 min.). The sealed tubes were transferred back into the glove box, a portion of cleared lysate (200 μ L) was set aside for ICP-MS analysis, and the remaining cleared lysate was incubated with 100 μ L IgG-sepharose beads (Sigma) for 30 minutes. The IgG-sepharose beads were washed with 3 x 1 mL pulldown buffer, resuspended in 297 μ L pulldown buffer, and EcC63A LpxC and metal ions were eluted from the IgG beads by either addition of 3 μ L AcTEV protease (Invitrogen, 10 U/ μ L) or 10 mM nitric acid and incubation at room temperature overnight. The metals in the eluate were analyzed by ICP-MS. The concentration of EcC63A LpxC in the eluate was determined using the Bradford Assay (Sigma) with purified LpxC as the standard. For control experiments, purified apo-LpxC-ZZ (100 μ M) was reconstituted with 1 equivalent of either ZnSO₄ or FeCl₂ in the anaerobic glove box. The holo-LpxC (9 μ M final) was then diluted into cell lysate prepared from BL21(DE3) cells transformed with the pEcC63A plasmid, encoding LpxC without a ZZ-tag, and incubated for 30 minutes at room temperature. The lysate was then applied to IgG-agarose beads, washed as described above, and the bound LpxC-ZZ was removed by incubation in 10 mM nitric acid overnight followed by ICP-MS analysis of metal ions in the eluate.

Native LpxC deacetylase activity

Chemically Defined Media (CDM) (32) (unsupplemented or supplemented with 20 μ M ZnSO₄ and/or 20 μ M ferric ammonium citrate) was inoculated with BL21(DE3)

cells and grown in a shaker (250 rpm) overnight at 37 °C. The cells were harvested by centrifugation, and the cell pellets resuspended in 20 mM bis-tris propane, 10 mM TCEP pH 7.5. The cells were washed, lysed and clarified as described for the pull-down assays above. Metal ion concentrations in the cleared lysate were determined by ICP-MS analysis. The cleared lysate was diluted 10-fold in assay buffer prior to measurement of activity (see below) using 200 nM substrate. The assays on the cleared lysates were performed either: immediately in the glove box, after a 15 min incubation in air, and after 2.5 hours incubation in air. The ratio of LpxC with Fe and Zn bound was calculated from these data using equations 4.1 – 4.3 where: A_0 is the activity measured anaerobically, A_{Fe} and A_{Zn} are the specific activity of Fe- and Zn-LpxC and E_{Fe}/E_{tot} and E_{Zn}/E_{tot} are the fraction of the total LpxC that contains bound Fe and Zn, respectively. The specific activity of Zn-LpxC is estimated from the activity measured after 2.5 hr incubation in air since under these conditions Zn replaces the active site Fe (14) (see Chapter 3). The specific activity of Fe-LpxC (A_{Fe}) has previously been shown to be 6-fold higher than that of Zn-LpxC (A_{Zn}) (14). To demonstrate that the native activity observed was specifically due to LpxC activity, control assays were performed with the LpxC-specific hydroxamate inhibitor L-161,240 (14).

Equation 4.1

$$A_0 = A_{Fe} E_{Fe} / E_{Tot} + A_{Zn} E_{Zn} / E_{Tot} = 6A_{Zn} E_{Fe} / E_{Tot} + A_{Zn} (1 - E_{Fe} / E_{Tot})$$

Equation 4.2

$$E_{Fe} / E_{Tot} = \frac{A_0 - A_{Zn}}{5A_{Zn}}$$

Equation 4.3
$$\frac{E_{Fe}}{E_{Zn}} = \frac{E_{Fe}}{1 - E_{Fe}}$$

LpxC Assay

LpxC activity was measured as previously described (28, 33, 34). For native activity measurement, assays were performed in 20 mM bis-tris propane, 10 mM TCEP, pH 7.5, bovine serum albumin (BSA, fatty acid free, 1 mg/mL), and [¹⁴C]-UDP-3-*O*-(3-hydroxymyristoyl)-*N*-acetyl-glucosamine (200 nM). Mixtures were pre-equilibrated at 30 °C, and the reactions were initiated by the addition of cell lysate. LpxC assays were also carried out in Fe²⁺ buffers for affinity determinations, as described below. After incubation for various times, the reactions were quenched by the addition of sodium hydroxide, which also cleaves the myristate substituent for ease of separation. Substrate and product were separated on PEI-cellulose TLC plates (0.1 M guanidinium HCl) and quantified by scintillation counting. Initial rates of product formation (< 20% reaction) were determined from these data.

In vitro Metal Ion Affinity and Exchange

To remove contaminating metal ions, ultrafiltration devices (Microcon MWCO 30K) were incubated with 10 mM Hepes pH 7.5, 500 μM EDTA, 100 mM dipicolinic acid (DPA) for 30 minutes (500 μL), followed by 3 x 500 μL washes with ultrapure water. To examine metal exchange *in vitro*, 10 μM LpxC C63A with either bound Zn²⁺ or Fe²⁺ was incubated in an anaerobic chamber with various concentrations of ZnSO₄ or FeCl₂ (0 – 300 μM) for ≥15 minutes in 20 mM bis-tris propane, pH 7.5, 10 mM TCEP.

The free and bound metal ions were separated by centrifugation (3000 x g, 4 min) in an ultrafiltration device and then the metals in an equal volume of filtrate and retentate were analyzed by ICP-MS.

For Zn^{2+} affinity measurements, apo-LpxC C63A (1-200 μ M) was incubated in a metal ion and pH buffer containing 1 mM nitriloacetic acid (NTA), 5 mM Mops pH 7, 2.5 μ M DPA, and 0 – 0.5 mM Zn_{tot} (0 – 3.3 nM Zn_{free}) at 30° C for 30 minutes in an anaerobic chamber (35, 36). Free and bound metal were separated by ultrafiltration, described above, and metal ions measured by ICP-MS. The concentration of Zn_{free} in the metal buffers was calculated using the program MINEQL+ (Environmental Research Software). The value of K_D^{Zn} was obtained by fitting a binding isotherm to these data.

The affinity of LpxC for Fe^{2+} was measured by assaying catalytic activity in the presence of varying free Fe^{2+} concentrations in an anaerobic glove box in 1 mM NTA, 5 mM Mops pH 7 serving as both a pH and metal buffer. The assays contained 0 – 950 μ M total Fe (Fe_{free}^{2+} 0-2.6 μ M), as calculated by MINEQL+ (Environmental Research Software), and 10 nM LpxC, in the presence of 1 mg/mL BSA. The Fe^{2+} affinity of LpxC was unchanged by pre-equilibrating the BSA with a buffered Fe^{2+} solution. The assay mixtures, containing all components except substrate, were incubated for 4 hours on ice followed by 30 minutes at 30°C in the anaerobic glove box. Assays were initiated by the addition of substrate (200 nM final), and processed as described above.

Metal dissociation rates

The first order rate constant for M^{2+} dissociation from LpxC was measured by the time-dependent loss of activity upon incubation with EDTA. C63A LpxC reconstituted

with stoichiometric Zn^{2+} - or Fe^{2+} was diluted into assay buffer containing 1 mM EDTA. At various times (0 – 30 min) an aliquot was diluted 100-fold into assay buffer (2 nM LpxC, 200 nM substrate). The reactions were quenched by the addition of sodium hydroxide and analyzed as described above. The observed rates are not dependent on the concentration of EDTA. To measure the effect of fatty acids on metal dissociation kinetics, 100 μ M palmitate was incubated with Me^{2+} -C63A LpxC for 1 hour on ice prior to dilution into EDTA.

Results

LpxC purified from E. coli contains mainly bound Fe^{2+}

LpxC purified from *E. coli* was previously shown to contain bound Zn^{2+} ; however, this protein was purified under aerobic conditions with 2 mM dithiothreitol as the reducing agent (13), which is not sufficient to prevent oxidation of bound Fe^{2+} (14). To clarify the identity of the biologically relevant metal ion cofactor, we purified LpxC under anaerobic conditions to re-examine the identity of the native metal cofactor. For all of these experiments we used an LpxC variant, EcC63A (14), that has reduced affinity for metal ions at the inhibitory site, fused to a cleaveable C-terminal ZZ tag (29-31) (EcLpxCC63A-Tev-ZZ, or LpxC-ZZ) to facilitate rapid purification of LpxC from crude cell lysates. LpxC-ZZ was induced in BL21(DE3) cells grown in minimal media containing varied metal supplements and rapidly isolated by incubation with IgG beads followed by elution with either nitric acid or TEV protease. The metals and protein in the column eluate were determined by ICP-MS and Bradford assays, respectively. This method minimizes contamination of LpxC by adventitious metal ions. Control

experiments using cells containing LpxC without the ZZ tag demonstrate that little or no ($< 1 \mu\text{M}$) protein or metal ions are observed in the eluate. In general, LpxC-ZZ co-purifies with mainly Fe^{2+} and some Zn^{2+} , while no other divalent metal ions (e.g. Co, Ni, Cu) are observed at greater than trace levels ($< 3 - 5\%$). A sub-stoichiometric metal ratio is also observed under all conditions, suggesting that LpxC-ZZ is not normally saturated with metals under physiological conditions, as further examined in control experiments described below. Calculations (see discussion) rationalize the substoichiometric metal content observed. LpxC-ZZ purified from cells grown in minimal (CDM) media with or without iron supplementation contains mainly bound Fe (Table 4.1); however, supplementation of the media with zinc increases the Zn/Fe ratio bound to LpxC-ZZ. Furthermore, the Fe/Zn ratio bound to LpxC-ZZ varies with the $(\text{Fe}/\text{Zn})_{\text{total}}$ ratio in the cell lysate in a roughly linear fashion (Figure 4.2), suggesting that LpxC co-purifies with the most abundant metal ion in the cells. The same trend is observed when expression is lowered by adding 10-fold less IPTG (Figure 4.2), indicating that the metal content is not an artifact of high overexpression.

One possible explanation of the correlation between the metals bound to LpxC-ZZ and the metal content of the cell lysate is that the metals bound to LpxC equilibrate with the cell lysate after cell lysis. To examine this, we incubated LpxC-ZZ reconstituted with either stoichiometric Zn^{2+} or Fe^{2+} with cell lysates followed by purification using IgG beads and measurement of the metal content. These experiments demonstrate that the metal ion bound to LpxC-ZZ does not dissociate or equilibrate with metals in the cell lysate during the pulldown procedure (Table 4.3). Consequently, the pull-down experiments measure the bound metal content of LpxC-ZZ expressed in *E. coli* at cell

Table 4.1: Metal stoichiometry of EcC63A LpxC-ZZ purified from *E. coli*.^a

Growth Media	Lysate Fe/Zn Ratio	Fe/LpxC ^b	Zn/LpxC ^b
CDM ^c	3.2	0.41 ± 0.11	0.08 ± 0.01
+ Fe ^c	22.3	0.59 ± 0.14	0.04 ± 0.00
+ Zn ^c	0.34	0.10 ± 0.07	0.25 ± 0.07
+ Fe and Zn ^c	2.9	0.42 ± 0.10	0.10 ± 0.06

^aEcC63A LpxC-ZZ was purified as described in Materials and Methods. The metal concentration was determined by ICP-MS and the protein concentration measured using a Bradford assay.

^bData represent the average and standard deviation from 2 replicate experiments. Data at additional media conditions are shown in Figure 4.2. ICP-MS data have standard error of ± 5%.

^cChemically defined media supplemented with nothing, 20 μM Fe, 20 μM Zn or both.

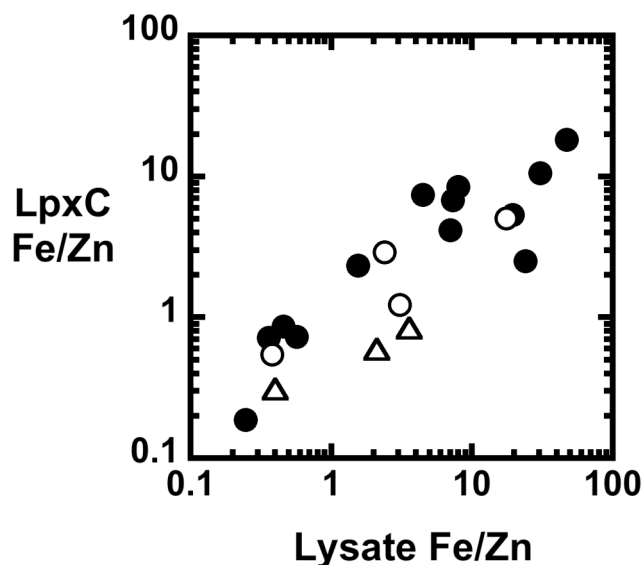


Figure 4.2: Metal content of EcC63A LpxC-ZZ isolated from *E. coli*. EcC63A LpxC ZZ was expressed in BL21(DE3)pEcC63ALpxC-ZZ grown in minimal media with and without Fe or Zn supplementation (5 – 20 μM) and induced by addition of either 1 mM IPTG (closed circles) or 0.1 mM IPTG (open circles). The protein was purified using the IgG pulldown under anaerobic conditions (see Materials and Methods). The Fe/Zn ratio of metal bound to LpxC and in the cleared lysate was analyzed by ICP-MS. The LpxC Fe/Zn ratio in natively expressed LpxC was determined by activity (triangles), as described in the legend of Figure 4.3, and these data are consistent with the pulldown data.

lysis and indicate that LpxC incorporates the most available metal ions in a manner reflective of the cellular Fe/Zn ratio.

Native activity is oxygen-sensitive and dependent on Fe/Zn_{total}

We have previously shown that LpxC activity in crude cell lysates from cells grown in LB media is redox-sensitive, consistent with the presence of Fe^{2+} -LpxC (14). To further examine the dependence of the metal content of LpxC in *E. coli* on metal availability we measured the native LpxC activity of *E. coli* cell lysates (no recombinant LpxC) prepared from BL21(DE3) grown in minimal media supplemented with Fe or Zn (Figure 4.3). The cells were lysed in an anaerobic chamber, and the LpxC activity was assayed immediately after lysis anaerobically (reflecting Zn-LpxC and Fe-LpxC) as well as after sufficient incubation in air (2.5 hr) to allow the Fe^{2+} -LpxC to oxidize and bind Zn^{2+} (14). The ratio of Fe^{2+} -LpxC to Zn^{2+} -LpxC determined from the native activity in cell lysates (see Methods) depends on the $(Fe/Zn)_{total}$ metal ratio in the cell lysate, comparable to the pull-down experiments reported above (Figure 4.2). Notably, the LpxC activity of cells grown in media without metal supplementation is comparable to the activity of Fe-supplemented cells (Figure 4.3), further suggesting that native LpxC contains a bound Fe^{2+} cofactor in minimal media. Furthermore, these data confirm that the correlation between the identity of the metal cofactor of native LpxC with the metal availability is not due to overexpression of LpxC-ZZ.

Table 4.2. Kinetic and thermodynamic parameters of LpxC-C63A

Enzyme	$K_D^{\text{Metal Ion}}$	k_{cat}^b (min^{-1})	K_M^b (μM^{-1})	k_{cat}/K_M^b ($\text{min}^{-1}\mu\text{M}^{-1}$)
Zn ²⁺ -C63A	60 ± 20 pM ^a	126 ± 12	0.7 ± 0.2	170 ± 34
Fe ²⁺ -C63A	112 ± 43 nM ^a	530 ± 30	0.5 ± 0.1	990 ± 130

^aThe affinity of LpxC-C63A for Zn²⁺ and Fe²⁺ was determined using ultrafiltration or activity measurements in buffered metal solutions at 30°C, pH 7, as described in Materials and Methods.

^bAdapted from reference (14)

Table 4.3. Metal content of holo-LpxC-ZZ after incubation with *E. coli* lysates.^a

Growth Media	Holo-E	Fe/LpxC	Zn/LpxC
CDM	Fe	1.02	0.04
CDM	Zn	0.12	2.20 ^b
+ 20 μM Fe	Zn	0.15	1.17 ^b
+ 20 μM Zn	Fe	0.69	0.13

^aApo-LpxC-ZZ was reconstituted with stoichiometric Fe or Zn, as indicated, and then incubated with cell lysates of *E. coli* that do not express LpxC-ZZ grown in the indicated media. LpxC-ZZ was purified using an IgG pulldown (see materials and methods) and the metal content was analyzed by ICP-MS (standard error is ± 5%).

^bIn some cases, LpxC-ZZ bound more than one Zn/subunit. Additional zinc binding sites in LpxC have been visualized by X-ray crystallography (37).

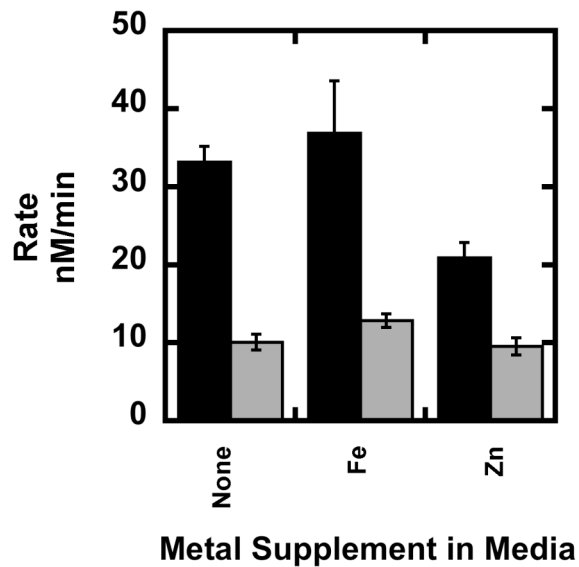


Figure 4.3: Native LpxC activity varies with metal supplementation. *E. coli* BL21(DE3) cells (without overexpressed LpxC) were grown in minimal media with and without 20 μ M metal supplementation, lysed, and assayed for deacetylase activity as described in Methods and Methods either anaerobically (black bars) or after exposure to room oxygen for 2 hours (gray bars).

LpxC binds Zn more tightly than Fe

To further clarify the metal ion selectivity of LpxC, we determined the affinities of the enzyme for Fe^{2+} and Zn^{2+} maintaining the metal concentration with metal ion buffers. Determination of the zinc affinity using ultrafiltration and ICP-MS analysis reveals a K_D of 60 ± 20 pM (Figure 4.4, Table 4.2). This value is comparable to the proposed cellular free Zn^{2+} concentrations (22, 23). The dissociation constant of LpxC for Fe^{2+} , determined from enhancement of catalytic activity, is 110 ± 40 nM (Figure 4.4, Table 4.2). This value is lower than the estimated cellular free Fe^{2+} concentration (24, 38). These results predict that, despite the ~2000-fold higher affinity for Zn^{2+} , Fe^{2+} -LpxC is the thermodynamically favored form under biological conditions due to the significantly higher concentration of cellular Fe^{2+} , which is consistent with the pulldown results.

To probe the lability of bound metal cofactors, LpxC was reconstituted with either Fe^{2+} or Zn^{2+} , incubated with excess concentrations of the competing metal ion for 15 min and then the identity of the bound metal ions were determined. These experiments demonstrate that the Fe^{2+} cofactor bound to LpxC readily exchanges with excess Zn^{2+} (Figure 4.5A), while little exchange is observed when Zn^{2+} -LpxC is incubated with excess Fe^{2+} . These data are consistent with the higher affinity of LpxC for Zn compared to Fe and the data can be modeled by a competitive binding equation (Eq. 4.4 and 4.5) with the measured metal affinities. These calculations confirm that at the concentrations used for the exchange experiments, ZnLpxC should dominate at equilibrium.

$$\text{Equation 4.4-5 } \frac{E \cdot Fe}{E_{Tot}} = \frac{1}{1 + \frac{K_D^{Fe}}{Fe_{free}} \left(1 + \frac{Zn_{free}}{K_D^{Zn}} \right)} \quad \frac{E \cdot Zn}{E_{Tot}} = \frac{1}{1 + \frac{K_D^{Zn}}{Zn_{free}} \left(1 + \frac{Fe_{free}}{K_D^{Fe}} \right)}$$

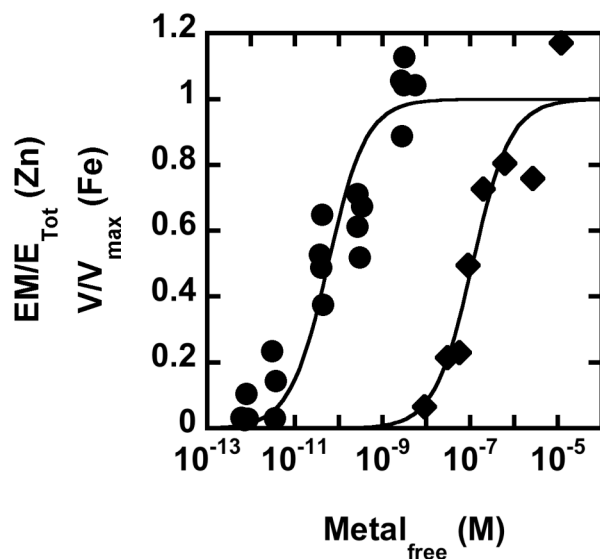


Figure 4.4: Affinity of C63A-LpxC for Fe^{2+} and Zn^{2+} . ApoLpxC was equilibrated with buffered metal solutions. Bound zinc (circles) was analyzed by ultrafiltration and ICP-MS (K_D^{Zn}); bound iron (diamonds) was analyzed by enhancement of LpxC activity (K_D^{Fe}), as described in Materials and Methods.

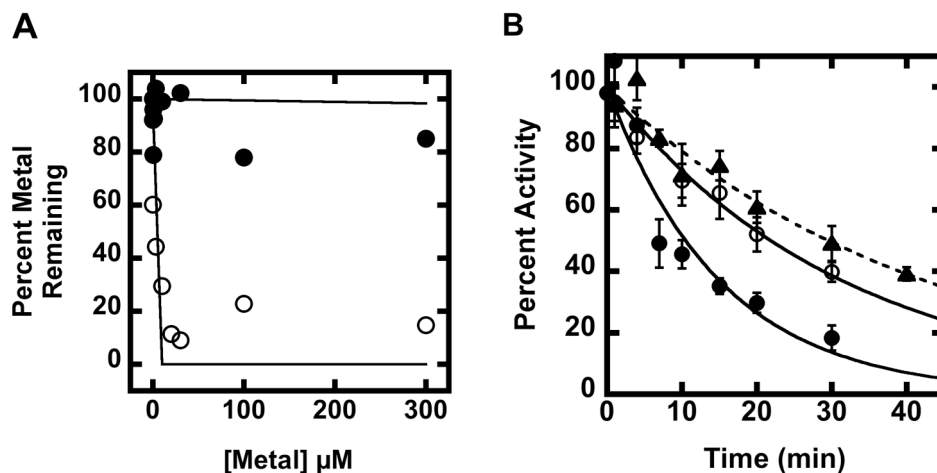


Figure 4.5. LpxC metal ion dissociation *in vitro*. (A) 10 μM Zn-LpxC (closed circles) or Fe-LpxC (open circles) was incubated at varying concentrations of competing metal ion, and the percentage of original metal remaining was determined by ultrafiltration followed by ICP-MS analysis, as described in Materials and Methods. Lines show calculated data from Eq. 4 and 5. (B) 200 nM ZnLpxC (open circles), ZnLpxC + 100 μM palmitate (triangles), or FeLpxC (closed circles) were incubated 1 mM EDTA for various times and then at those times the activity was determined by dilution (100-fold) into an assay, as described in Materials and Methods.

The rate constants for dissociation of metals from LpxC were determined by the time-dependent decrease in activity upon dilution of the enzyme into EDTA. These measurements reveal that the rate constant for dissociation (k_{off}) of Zn^{2+} and Fe^{2+} from LpxC are 0.032 ± 0.003 and $0.067 \pm 0.004 \text{ min}^{-1}$, respectively (Figure 4.5B). The similarity in the dissociation rate constants for Fe^{2+} and Zn^{2+} is unexpected given the significantly higher affinity of LpxC for Zn^{2+} . Therefore, the discrimination between the two metal ions is observed mainly in the apparent association rate constants which are estimated from the values of K_D and k_{off} as $\sim 9 \times 10^6$ (Zn) and $1 \times 10^4 \text{ M}^{-1}\text{s}^{-1}$ (Fe). Addition of palmitate to Zn-LpxC slows the dissociation rate constant by ~ 1.3 -fold to a half-time of 30 min at 25°C suggesting that metal exchange in cell lysates could be inhibited by ligand binding. These data demonstrate that LpxC can equilibrate *in vitro* and presumably in the cell, disfavoring the possibility that the *in vivo* metal selectivity is determined by a kinetic trap.

Discussion

LpxC co-purifies with the “most abundant” metal ion

Early experiments demonstrate that LpxC purified under aerobic conditions contains bound Zn^{2+} (13). However, recent results demonstrate that Fe^{2+} -LpxC is 6-8 – fold more active than Zn^{2+} -LpxC (Table 4.2), (14). Furthermore, in the presence of oxygen, the Fe^{2+} cofactor bound to LpxC is oxidized to Fe(III) which dissociates and is replaced by Zn^{2+} (14). Therefore, to examine the *in vivo* metal content of LpxC, we developed a rapid pull-down experiment using an IgG-binding ZZ-tag that could be carried out under anaerobic conditions. These experiments demonstrate that although Fe

is the major metal bound to LpxC purified from cells grown in minimal media, the enzyme also contains bound Zn. Furthermore, the Fe/Zn ratio of metals bound to LpxC-ZZ is linearly dependent on the Fe/Zn ratio in the cell lysate (Figure 4.2). Control experiments demonstrate that the metal ions bound to LpxC do not dissociate or re-equilibrate during this purification procedure (Table 4.3). Therefore, the measured LpxC metal content reflects the metals bound to LpxC *in vivo* when the cells are lysed. The demonstration that the Fe/Zn ratio varies with the metal content of the media suggests that *in vivo* LpxC binds and is activated by the “most available” metal ion. These results predict that LpxC normally functions using Fe^{2+} as the co-factor; however, it can switch to Zn^{2+} when cellular conditions favor metal switching.

Native LpxC activity suggests Fe^{2+} co-factor

One caveat of the pulldown experiments is that the metal content of overexpressed LpxC is measured and overexpression could disrupt cellular metal homeostasis. Therefore, the metal content of native LpxC in *E. coli* grown in media containing varying metal concentrations was estimated, distinguishing Fe-LpxC and Zn-LpxC by the redox sensitivity of the catalytic activity (14). The native LpxC activity is highest in cell lysates prepared from cells grown in minimal media with or without iron supplementation and this activity is redox sensitive (Figure 4.3). In contrast, the LpxC activity in cell lysates from cells grown in Zn-supplemented media is lower and less sensitive to exposure to oxygen. Furthermore, the Fe/Zn content of native LpxC calculated from these activity measurements varies with the Fe/Zn ratio of the total cell lysates, in agreement with the results obtained from the pulldown assays (Figure 4.2), demonstrating that the observed metal variation in LpxC is not an artifact of

overexpression. In summary, these data indicate that while LpxC is activated by Fe^{2+} *in vivo* under most growth conditions, this enzyme is uniquely suited to switch to binding a Zn^{2+} cofactor as a means to regulate activity and/or adapt to environmental conditions.

Metal selectivity is determined by association kinetics and thermodynamics

To explore the basis for LpxC metal ion selectivity, we measured the thermodynamics and kinetics for binding Fe^{2+} or Zn^{2+} to LpxC *in vitro*. LpxC binds Fe^{2+} 1000-fold weaker than Zn^{2+} ($K_D \sim 100$ nM and 60 pM, respectively) (Figure 4.4). This differential affinity is consistent with the increased Lewis acidity and greater ligand stabilization energy predicted by the Irving-Williams series of metal stability constants (39, 40).

Unexpectedly, the rate constants for dissociating Zn^{2+} and Fe^{2+} from the LpxC•metal complex are comparable (0.03 and 0.067 s^{-1} , respectively (Figure 4.5B) despite the large differential in binding affinity. This result indicates that the metal selectivity occurs in the apparent association rate constant, estimated as 10^7 $\text{M}^{-1}\text{s}^{-1}$ and 10^4 $\text{M}^{-1}\text{s}^{-1}$ for Zn^{2+} and Fe^{2+} , respectively, and implies that association of Fe^{2+} is not a diffusion-controlled step. Similar metal association kinetics have previously been observed for human carbonic anhydrase II (CAII) where differential association rate constants for Zn^{2+} and Cu^{2+} ($10^4 - 10^5$ and 10^9 $\text{M}^{-1}\text{s}^{-1}$, respectively) have been observed (41, 42). Analysis of the zinc binding kinetics of CAII mutants suggest a two-step mechanism: diffusion-controlled zinc association to form a complex with two protein ligands followed by a second, slower step that includes coordination of the third protein ligand (43). A similar two-step mechanism could explain the kinetics for Fe^{2+} binding to LpxC.

Given the relatively facile dissociation of the active site metal under *in vitro* conditions ($t_{1/2} = 10 - 25$ min), retention of the *in vivo* metal ion during purification of LpxC could have been difficult. However, little metal exchange or dissociation was observed in cell lysates (Table 4.3). This result suggests that metal exchange/dissociation from LpxC is inhibited in lysates. One possible mechanism for this inhibition could be the formation of a ternary LpxC•metal•ligand complex that decreases the metal dissociation rate constant, allowing purification of the *in vivo* metal under the necessary time-scale (~60 min). Fatty acids, such as palmitate, are a possible candidate for inhibition of metal dissociation since they co-purify with LpxC expressed in *E. coli* and interact with active site metal ions when bound to LpxC (14, 33, 37). In fact, palmitate modestly decreases dissociation of zinc (~1.3-fold, Figure 4.5B), suggesting that in the cellular milieu, small molecules including palmitate may contribute to inhibiting the metal exchange/dissociation of LpxC. Alternatively, cell lysis in an anaerobic environment, where cysteine ligands remains reduced, may not result in a significant increase in free metal concentrations. This, combined with the dilution factor from the cytosol into the cell lysis buffer, may result in concentrations of metal ions low enough to prevent exchange during the timecourse of the experiment. Additionally, metal dissociation may be slower at ~0°C (on ice) than measured at 30°C.

Equilibrium-based metal selection mechanism can explain LpxC metal content in vivo

Although LpxC binds Zn^{2+} with 1000-fold higher affinity than Fe^{2+} , the predominant metal bound to LpxC in *E. coli* is Fe^{2+} (Figures 4.2 and 4.3, Table 4.1). The mechanisms for determination of the *in vivo* Fe/Zn metal selectivity of proteins are currently unclear. Selectivity has previously been suggested to depend on metal

availability and/or regulated by metallochaperones (44). Here we examine whether the observed *in vivo* metal content of LpxC can be rationalized solely by metal affinity and concentration. While the total cellular Fe and Zn concentrations are comparable at ~0.2 mM in most systems (21), the best estimates for the “free” or “readily exchangeable” cellular concentrations of Fe^{2+} and Zn^{2+} are vastly different. The best measurements, carried out mainly in mammalian cells, indicate that $\text{Zn}^{2+}_{\text{free}}$ is between 10-400 pM while $\text{Fe}^{2+}_{\text{free}}$ is 0.2-6 μM or higher (22-27). Therefore, for LpxC the readily exchangeable Fe^{2+} concentration is likely above the K_D , while the readily exchangeable Zn is near or below the K_D , rationalizing the predominance of $\text{LpxC}\cdot\text{Fe}^{2+}$ *in vivo*. Furthermore, perturbations in the cellular metal ion pool could influence the metal content of LpxC, as observed in response to alterations in the metal content of the media.

From purely thermodynamic considerations, the percentage of Fe- and Zn-bound LpxC can be calculated from the metal affinities and concentrations using a competitive model for LpxC metal binding (Equations 4.4 and 4.5), as shown in Figure 4.6. These calculations reveal that if LpxC is under thermodynamic control, the balance of Fe- and Zn-LpxC is readily altered by changes in the free metal concentrations (Figure 4.6). For example, at the highest Fe_{free} and lowest Zn_{free} concentrations reported, 6 μM and 10 pM, respectively, LpxC would be expected to be 98% Fe and 0.3 % Zn. At the opposite extreme, 0.2 μM Fe_{free} and 400 pM Zn_{free} , LpxC would be expected bind 19% Fe and 70% Zn. These calculations indicate that the observed metal content and variability of LpxC, including the sub-stoichiometric metal content, can be explained solely using a thermodynamic model. These calculations also demonstrate how the metal affinities, combined with the *in vivo* concentrations of “free” metal ions, make LpxC well-suited

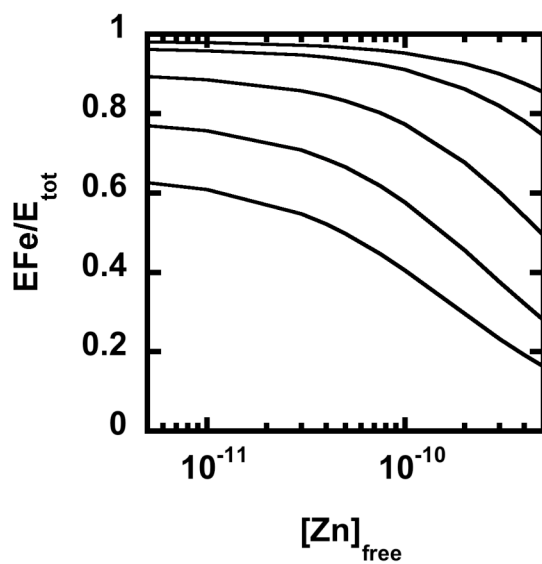


Figure 4.6. Calculated $Fe\bullet LpxC$ fraction as a function of $[Fe]_{free}$ and $[Zn]_{free}$. $E\bullet Fe/E_{Tot}$ was calculated as a function of $[Zn]_{free}$ at 0.2, 0.4, 1, 3, or 6 μM $[Fe]_{free}$ using Eq. 4.4.

for metal switching *in vivo*. Importantly, this model for LpxC metal ion specificity depends only on thermodynamics; no chaperones or other regulatory elements are required to explain the observed behavior of LpxC *in vivo*. However, this correlation does not rule out the involvement of chaperones or other regulatory elements in determination of the *in vivo* metal selectivity of LpxC.

Since it is proposed that the concentration of free or readily exchangeable $\text{Fe} > \text{Zn}$ *in vivo*, these results would predict that LpxC normally functions using Fe^{2+} as the co-factor; however, it can switch to Zn^{2+} when cellular conditions favor metal switching. This switching may be a method to adapt to changing conditions that a bacterial cell may encounter during varied growth conditions or under conditions of oxidative stress, such as those encountered in a human macrophage (45). Metal switching may also be a novel regulatory mechanism, whereby the activity of LpxC can be finely tuned by changes in intracellular metal ion concentrations.

LpxC may now be considered the latest member of a growing class of non-heme Fe^{2+} hydrolases that were previously thought to be zinc enzymes, such as peptide deformylase, LuxS, and possibly HDAC8 (15-19, 46-48). However, LpxC should not be considered a specific Fe^{2+} -protein, but rather an M^{2+} -enzyme that is most often Fe^{2+} and is subject to switching in altered cellular conditions. Consequently, various environments, such as infection in a host or conditions of oxidative stress, may also result in perturbation of cellular metal ion conditions and therefore change the active-site metal ion bound to LpxC. The results from these studies suggest that metal switching may be used by LpxC as a way to regulate activity and/or as a way to adapt to changing environmental conditions. This new potential mechanism has important implications for

understanding metalloenzyme homeostasis, as well as future drug design for this antibiotic target.

REFERENCES

- (1) Jackman, J. E., Fierke, C. A., Tumey, L. N., Pirrung, M., Uchiyama, T., Tahir, S. H., Hindsgaul, O., and Raetz, C. R. (2000) Antibacterial agents that target lipid A biosynthesis in gram-negative bacteria. Inhibition of diverse UDP-3-O-(r-3-hydroxymyristoyl)-n-acetylglucosamine deacetylases by substrate analogs containing zinc binding motifs. *J Biol Chem* 275, 11002-11009.
- (2) Wyckoff, T. J. O., Raetz, C. R. H., and Jackman, J. E. (1998) Antibacterial and anti-inflammatory agents that target endotoxin. *Trends in Microbiology* 6, 154-159.
- (3) Reeves, P. R., Hobbs, M., Valvano, M. A., Skurnik, M., Whitfield, C., Coplin, D., Kido, N., Klena, J., Maskell, D., Raetz, C. R. H., *et al.* (1996) Bacterial polysaccharide synthesis and gene nomenclature. *Trends in Microbiology* 4, 495-503.
- (4) Raetz, C. R., and Whitfield, C. (2002) Lipopolysaccharide endotoxins. *Annu Rev Biochem* 71, 635-700.
- (5) Opal, S. M. (2007) The host response to endotoxin, antilipopolysaccharide strategies, and the management of severe sepsis. *Int J Med Microbiol* 297, 365-377.
- (6) Young, K., Silver, L. L., Bramhill, D., Caceres, C. A., Stachula, S. A., Shelly, S. E., Raetz, C. R. H., and Anderson, M. S. (1993) The 2nd-Step of Lipid a Biosynthesis, Udp-3-Q-Acyl-GlcnaC Deacetylase Is Encoded by the Pleiotropic Permeability/Cell Division Gene EnvA of Escherichia-Coli. *Faseb Journal* 7, A1268-A1268.
- (7) Young, K., Silver, L. L., Bramhill, D., Cameron, P., Eveland, S. S., Raetz, C. R., Hyland, S. A., and Anderson, M. S. (1995) The envA permeability/cell division gene of Escherichia coli encodes the second enzyme of lipid A biosynthesis. UDP-3-O-(R-3-hydroxymyristoyl)-N-acetylglucosamine deacetylase. *J Biol Chem* 270, 30384-30391.
- (8) Hernick, M., and Fierke, C. A. (2005) Zinc hydrolases: the mechanisms of zinc-dependent deacetylases. *Arch Biochem Biophys* 433, 71-84.
- (9) McClerren, A. L., Endsley, S., Bowman, J. L., Andersen, N. H., Guan, Z., Rudolph, J., and Raetz, C. R. (2005) A slow, tight-binding inhibitor of the zinc-dependent deacetylase LpxC of lipid A biosynthesis with antibiotic activity comparable to ciprofloxacin. *Biochemistry* 44, 16574-16583.
- (10) Mdluli, K. E., Witte, P. R., Kline, T., Barb, A. W., Erwin, A. L., Mansfield, B. E., McClerren, A. L., Pirrung, M. C., Tumey, L. N., Warren, P., *et al.* (2006)

Molecular validation of LpxC as an antibacterial drug target in *Pseudomonas aeruginosa*. *Antimicrobial Agents and Chemotherapy* 50, 2178-2184.

- (11) Barb, A. W., McClerren, A. L., Snehelatha, K., Reynolds, C. M., Zhou, P., and Raetz, C. R. H. (2007) Inhibition of lipid A biosynthesis as the primary mechanism of CHIR-090 antibiotic activity in *Escherichia coli*. *Biochemistry* 46, 3793-3802.
- (12) White, R. J., Margolis, P. S., Trias, J., and Yuan, Z. Y. (2003) Targeting metalloenzymes: a strategy that works. *Current opinion in pharmacology* 3, 502-507.
- (13) Jackman, J. E., Raetz, C. R., and Fierke, C. A. (1999) UDP-3-O-(R-3-hydroxymyristoyl)-N-acetylglucosamine deacetylase of *Escherichia coli* is a zinc metalloenzyme. *Biochemistry* 38, 1902-1911.
- (14) Hernick, M., Gattis, S. G., Penner-Hahn, J. E., and Fierke, C. A. (2010) Activation of *E. coli* UDP-3-O-(R-3-hydroxymyristoyl)-N-acetylglucosamine deacetylase by Fe²⁺ yields a more efficient enzyme with altered ligand affinity. *Biochemistry* 49, 2246-2255.
- (15) Becker, A., Schlichting, I., Kabsch, W., Groche, D., Schultz, S., and Wagner, A. F. V. (1998) Iron center, substrate recognition and mechanism of peptide deformylase. *Nature Structural Biology* 5, 1053-1058.
- (16) Rajagopalan, P. T., and Pei, D. (1998) Oxygen-mediated inactivation of peptide deformylase. *J Biol Chem* 273, 22305-22310.
- (17) Rajagopalan, P. T. R., Yu, X. C., and Pei, D. H. (1997) Peptide deformylase: A new type of mononuclear iron protein. *Journal of the American Chemical Society* 119, 12418-12419.
- (18) Groche, D., Becker, A., Schlichting, I., Kabsch, W., Schultz, S., and Wagner, A. F. V. (1998) Isolation and crystallization of functionally competent *Escherichia coli* peptide deformylase forms containing either iron or nickel in the active site. *Biochemical and Biophysical Research Communications* 246, 342-346.
- (19) Gantt, S. L., Gattis, S. G., and Fierke, C. A. (2006) Catalytic activity and inhibition of human histone deacetylase 8 is dependent on the identity of the active site metal ion. *Biochemistry* 45, 6170-6178.
- (20) Finney, L. A., and O'Halloran, T. V. (2003) Transition metal speciation in the cell: Insights from the chemistry of metal ion receptors. *Science* 300, 931-936.
- (21) Outten, C. E., and O'Halloran, T. V. (2001) Femtomolar sensitivity of metalloregulatory proteins controlling zinc homeostasis. *Science* 292, 2488-2492.

- (22) Bozym, R. A., Thompson, R. B., Stoddard, A. K., and Fierke, C. A. (2006) Measuring picomolar intracellular exchangeable zinc in PC-12 cells using a ratiometric fluorescence biosensor. *ACS Chem Biol* 1, 103-111.
- (23) Vinkenborg, J. L., Nicolson, T. J., Bellomo, E. A., Koay, M. S., Rutter, G. A., and Merkx, M. (2009) Genetically encoded FRET sensors to monitor intracellular Zn²⁺ homeostasis. *Nature Methods* 6, 737-U710.
- (24) Petrat, F., de Groot, H., and Rauen, U. (2001) Subcellular distribution of chelatable iron: a laser scanning microscopic study in isolated hepatocytes and liver endothelial cells. *Biochem J* 356, 61-69.
- (25) Espósito, B. P., Epsztejn, S., Breuer, W., and Cabantchik, Z. I. (2002) A review of fluorescence methods for assessing labile iron in cells and biological fluids. *Anal Biochem* 304, 1-18.
- (26) Meguro, R., Asano, Y., Odagiri, S., Li, C., Iwatsuki, H., and Shoumura, K. (2007) Nonheme-iron histochemistry for light and electron microscopy: a historical, theoretical and technical review. *Arch Histol Cytol* 70, 1-19.
- (27) MacKenzie, E. L., Iwasaki, K., and Tsuji, Y. (2008) Intracellular iron transport and storage: from molecular mechanisms to health implications. *Antioxid Redox Signal* 10, 997-1030.
- (28) Hernick, M., Gennadios, H. A., Whittington, D. A., Rusche, K. M., Christianson, D. W., and Fierke, C. A. (2005) UDP-3-O-((R)-3-hydroxymyristoyl)-N-acetylglucosamine deacetylase functions through a general acid-base catalyst pair mechanism. *J Biol Chem* 280, 16969-16978.
- (29) Nilsson, B., Forsberg, G., and Hartmanis, M. (1991) Expression and Purification of Recombinant Insulin-Like Growth-Factors from Escherichia-Coli. *Methods in Enzymology* 198, 3-17.
- (30) Nilsson, B., Moks, T., Jansson, B., Abrahmsen, L., Elmblad, A., Holmgren, E., Henrichson, C., Jones, T. A., and Uhlen, M. (1987) A Synthetic Igg-Binding Domain Based on Staphylococcal Protein-A. *Protein Engineering* 1, 107-113.
- (31) Lowenadler, B., Jansson, B., Paleus, S., Holmgren, E., Nilsson, B., Moks, T., Palm, G., Josephson, S., Philipson, L., and Uhlen, M. (1987) A Gene Fusion System for Generating Antibodies against Short Peptides. *Gene* 58, 87-97.
- (32) Outten, F. W., Outten, C. E., Hale, J., and O'Halloran, T. V. (2000) Transcriptional activation of an Escherichia coli copper efflux regulon by the chromosomal MerR homologue, CueR. *Journal of Biological Chemistry* 275, 31024-31029.

- (33) Hernick, M., and Fierke, C. A. (2006) Molecular recognition by Escherichia coli UDP-3-O-(R-3-hydroxymyristoyl)-N-acetylglucosamine deacetylase is modulated by bound metal ions. *Biochemistry* 45, 14573-14581.
- (34) Hernick, M., and Fierke, C. A. (2006) Catalytic Mechanism and Molecular Recognition of E. coli UDP-3-O-(R-3-Hydroxymyristoyl)-N-acetylglucosamine Deacetylase Probed by Mutagenesis. *Biochemistry* 45, 15240-15248.
- (35) McCall, K. A., and Fierke, C. A. (2000) Colorimetric and fluorimetric assays to quantitate micromolar concentrations of transition metals. *Analytical Biochemistry* 284, 307-315.
- (36) McCall, K. A., and Fierke, C. A. (2004) Probing determinants of the metal ion selectivity in carbonic anhydrase using mutagenesis. *Biochemistry* 43, 3979-3986.
- (37) Whittington, D. A., Rusche, K. M., Shin, H., Fierke, C. A., and Christianson, D. W. (2003) Crystal structure of LpxC, a zinc-dependent deacetylase essential for endotoxin biosynthesis. *Proc Natl Acad Sci USA* 100, 8146-8150.
- (38) Epsztejn, S., Kakhlon, O., Glickstein, H., Breuer, W., and Cabantchik, Z. I. (1997) Fluorescence analysis of the labile iron pool of mammalian cells. *Analytical Biochemistry* 248, 31-40.
- (39) Lippard, S. J., Berg, J.M. (1994) *Principles of Bioinorganic Chemistry*, University Science Books, Mill Valley, California.
- (40) Irving, H., and Williams, R. J. P. (1948) Order of Stability of Metal Complexes. *Nature* 162, 746-747.
- (41) Hunt, J. A., Ahmed, M., and Fierke, C. A. (1999) Metal binding specificity in carbonic anhydrase is influenced by conserved hydrophobic core residues. *Biochemistry* 38, 9054-9062.
- (42) Romans, A. Y., Graichen, M. E., Lochmuller, C. H., and Henkens, R. W. (1978) Kinetics and Mechanism of Dissociation of Zinc Ion from Carbonic-Anhydrase. *Bioinorganic Chemistry* 9, 217-229.
- (43) Kiefer, L. L., and Fierke, C. A. (1994) Functional-Characterization of Human Carbonic-Anhydrase-Ii Variants with Altered Zinc-Binding Sites. *Biochemistry* 33, 15233-15240.
- (44) Waldron, K. J., Rutherford, J. C., Ford, D., and Robinson, N. J. (2009) Metalloproteins and metal sensing. *Nature* 460, 823-830.
- (45) MacMicking, J., Xie, Q. W., and Nathan, C. (1997) Nitric oxide and macrophage function. *Annu Rev Immunol* 15, 323-350.

- (46) Chan, M. K., Gong, W., Rajagopalan, P. T., Hao, B., Tsai, C. M., and Pei, D. (1997) Crystal structure of the Escherichia coli peptide deformylase. *Biochemistry* 36, 13904-13909.
- (47) Jain, R. K., Hao, B., Liu, R. P., and Chan, M. K. (2005) Structures of E-coli peptide deformylase bound to formate: Insight into the preference for Fe²⁺ over Zn²⁺ as the active site metal. *Journal of the American Chemical Society* 127, 4558-4559.
- (48) Zhu, J. G., Dizin, E., Hu, X. B., Wavreille, A. S., Park, J., and Pei, D. H. (2003) S-ribosylhomocysteinase (LuxS) is a mononuclear iron protein. *Biochemistry* 42, 4717-4726.

CHAPTER 5. **Fe²⁺-DEPENDENT ACTIVITY OF HDAC8**

Introduction

Histone deacetylases (HDACs) are one class out of many enzymes that catalyze post-translational modification of histone proteins (1-3). In addition, numerous non-histone proteins have emerged in recent years as HDAC substrates, indicating that HDACs have a prominent role in regulating protein function in the cell (4-6). Not surprisingly, HDACs have attracted attention as a target for drug development to treat a wide variety of diseases (5, 7-9), and thus far one HDAC inhibitor (SAHA, Zolinza) has been approved for the treatment of cutaneous T-cell lymphoma (10).

HDACs catalyze the deacetylation of ϵ -acetyl lysines in proteins, and are divided into 4 classes based on mechanism and sequence similarity (see Chapter 1 for a full discussion) (11, 12). The metal-dependent HDACs (class 1, 2 and 4) are mononuclear metalloproteins, and have been typically described as Zn²⁺-enzymes. However, several pieces of evidence suggest a more careful analysis of the metal dependence is warranted, including the recent reclassification of several enzymes from Zn²⁺- to Fe²⁺-dependent (see Chapters 3 and 4), higher activity of Fe²⁺-HDAC8 than Zn²⁺-HDAC8, and the sensitivity of HDAC activity in cell lysates to oxygen (13).

Materials and Methods

General procedures and plasmid preparation

All experiments were performed in metal-free plastic ware and using reagents that do not contain extraneous metal ions, as verified by ICP-MS (Ted Huston, University of Michigan). Reagents were of the highest quality available from Sigma-Aldrich, unless otherwise noted. Recombinant His₆-tagged HDAC8 for *in vitro* assays was expressed and purified as described by Ni-IMAC chromatography (13). A ZZ-tagged version of HDAC8 (HDAC8-ZZ) was created for *in vivo* experiments, where the ZZ-tag represents an IgG-affinity tag (14-16). HDAC8-ZZ was expressed by modification of pHD2-TEV-His. An EcoR1 restriction site was introduced into the HDAC8 gene between the His-tag sequence and the TEV cleavage site using the QuikChange mutagenesis kit (Stratagene) with the primer 5'-CC ACC ACC ACC ACC ACT GAA TTC CGG CTG CTA ACA AAG CCC G-3' and its reverse complement. The sequence encoding the His-tag was then removed from the plasmid by digestion with EcoR1 and Xho1 and the linearized vector was purified on an agarose gel. The ZZ-tag sequence was prepared by PCR amplification of the ZZ region of the commercial vector pEZZ (Amersham) with the introduction of Xho1 and EcoR1 restriction sites at the 5'- and 3'- ends, as well as a stop codon (primer 1: 5' - CGA TGA ACT CGA GGA CAA CAA ATT CAA CAA AG - 3' and primer 2: 5' - TAA AGA ATT CTC AGG TTT CTA GAT TCG CGT CTA CTT TCG G - 3'). The PCR fragment was digested with Xho1 and EcoR1 and ligated into the Xho1/EcoR1 digested HDAC8 vector with T4 DNA Ligase (New England Biolabs), to create the expression plasmid pHD2-TEV-ZZ. The plasmid sequence was verified by the University of Michigan DNA Sequencing Core.

The mammalian HDAC-ZZ expression vector was constructed similarly. A Kpn1 restriction site was introduced just upstream of the start codon in pHD2-TEV-ZZ by site-directed mutagenesis using the primer 5'-CTT TAA GAA GGA GGT ACC CAT ATG GAA GAA CCG GAA GAA CCG GCC G-3' and its reverse complement. The modified vector was cleaved by incubation with Kpn1 and EcoR1 and the HDAC-TEV-ZZ DNA fragment was purified by electrophoresis. The mammalian expression vector pCDNA4/TO (Invitrogen) was then digested by the same enzymes and gel-purified. The HDAC-TEV-ZZ DNA was ligated into the digested vector by T4 DNA ligase (NEB) to create the new vector pHDAC/TO and confirmed by sequencing at the University of Michigan DNA sequencing core.

HDAC8-ZZ anaerobic purification

E. coli BL21(DE3) cells transformed with pHD2-TEV-ZZ were grown in Chemically Defined Media (CDM) (17), and protein expression was induced when the cells reached an OD₆₂₀ of 0.6 by the addition of 1 mM IPTG. At this time cells were supplemented with metal ion (20 μM ZnSO₄, 20 μM ferric ammonium citrate, or both 20 μM ZnSO₄ and 20 μM ferric ammonium citrate) or incubated without supplementation overnight at 30 °C. The cells were pelleted by centrifugation, washed once with 5 mM CaCl₂ and twice with 10 mM Mops, pH 7. Control experiments demonstrate that Ca²⁺ has no effect on HDAC8 activity. The washed cell pellets from each 100 mL culture were transferred to an anaerobic glovebox, resuspended in 3 mL pulldown buffer (40 mM Mops pH 8, 150 mM NaCl, 10 mM TCEP, 0.1% NP-40), and lysed by incubation with lysozyme (1 mg/mL) at room temperature for 30 minutes. The tubes were sealed with parafilm, removed from the glove box, and the cell lysate was cleared by centrifugation at

12,000 rpm for 30 minutes. The sealed tubes were transferred back into the glovebox, a portion of cleared lysate (200 μ L) was set aside for ICP-MS analysis, and the remaining cleared lysate was incubated with 100 μ L IgG-sepharose beads for 30 minutes. The IgG-sepharose beads were washed with 3 x 1 mL pulldown buffer, resuspended in 297 μ L pulldown buffer, and incubated with 3 μ L AcTEV protease (Invitrogen) at room temperature overnight to cleave HDAC8 from the IgG beads. The supernatant containing purified HDAC8 (200 μ L) was submitted for ICP-MS analysis. The concentration of HDAC8 was determined by the Bradford Assay (Sigma) using purified HDAC8 as the standard.

The pHDAC/TO plasmid was transfected into HeLa cells using the Effectene reagent (Qiagen) under standard growth conditions (37° C, 5% CO₂ incubator) in DMEM + 10% FBS media. 10 x 10 cm plates of HeLa cells were transfected according to kit instructions. Briefly, $\sim 10^6$ cells were plated the day before transfection, then on the day of transfection 2 μ g of DNA and 16 μ L enhancer solution in 300 μ L kit buffer EC were incubated for 5 min, followed by addition of 60 μ L Effectene. The entire solution was incubated for 15 min then added to the cells in freshly changed media. Cells were grown for 48 hours, then washed once with 5 mL metal-free phosphate buffered saline (PBS) with 5 mM CaCl₂ and once with PBS alone. Cells were harvested by a cell scraper, then transferred to the anaerobic chamber. Cells were resuspended in 1 mL pulldown buffer without lysozyme (osmotic lysis) for 30 min on ice, then pelleted at 14,000 rpm for 10 min. A sample of cell lysate was reserved for ICP analysis and the remainder was incubated with IgG-beads as described above.

Oxygen sensitivity in cell lysates

10 plates of HeLa cells were grown, washed, and lysed as described above without plasmid transfection. The HDAC activity in the lysate was assayed in the anaerobic chamber and after 3 hours in room air on ice in a standard enzyme assay (13) using the Fluor de Lys fluorescent peptide substrate (BIOMOL), with 1 – 10 μ L undiluted cell lysate in place of enzyme and analyzed as described.

Immunoprecipitation assays

10 plates of untransfected HeLa cells were harvested and lysed in the anaerobic chamber as described above. 10 μ L of HDAC8 antibody (Sigma) was added to the lysate for 2 hours, followed by addition of 50 μ L protein-G sepharose beads for an additional 2 hours. Beads were washed with pulldown buffer 3 x 500 μ L, then resuspended in 100 μ L pulldown buffer. The immunoprecipitated HDAC8 was then assayed by transferring 2 – 8 μ L bead slurry to a standard assay (13) in the glovebox or after 3 hours in room air.

Inhibition by SAHA

The dependence of the active site metal on inhibition by the clinically approved HDAC inhibitor, suberoylanalide hydroxamic acid (SAHA, Zolinza) was measured for Zn²⁺-, Fe²⁺-, and Co²⁺-HDAC8. SAHA was synthesized as previously described (18). Briefly, the commercially available suberic acid monomethyl ester was reacted with aniline by *N,N'*-dicyclohexylcarbodiimide and hydroxybenzotriazole in dimethylformamide and stirred at room temperature for 1.5 hours. The reaction was quenched by addition of water which precipitates the suberanilic acid monomethyl ester, which was dissolved in 1:1 petroleum ether:ethyl acetate and filtered through a silica column. Hydroxylamine was freshly prepared by mixing hydroxylamine HCl with KOH

in methanol and filtering out the precipitated KCl. The hydroxylamine and suberanilide monomethyl ester were combined in methanol and reacted at room temperature for one hour, and then SAHA was precipitated by addition of water and neutralization with acetic acid.

The SAHA inhibition constant (K_i) for metal-substituted HDAC8 was determined by globally fitting eq 5.1 using Prism 4.0 (GraphPad Software, Inc.) to the initial velocity for enzyme activity, varying the concentrations of both enzyme (E_{tot} , 0.2-0.8 μ M) and SAHA (I_{tot} , 0-3 μ M) at 50 μ M substrate. At $[S] \ll K_M$, the K_{app} value is nearly equal to the inhibition constant K_i .

Equation 5.1:
$$\frac{v}{v_0} = \frac{E_{tot} - I_{tot} - K_{app} + \sqrt{(E_{tot} - I_{tot} - K_{app})^2 + 4E_{tot}K_{app}}}{2E_{tot}}$$

K_D^{Zn} and K_D^{Fe} measurements

The affinity of HDAC8 for Zn^{2+} and Fe^{2+} was measured in an anaerobic glove box from an increase in activity in the presence of increasing concentrations of free Zn^{2+} or Fe^{2+} maintained using a metal ion buffer. The standard assay buffer (13) was replaced with 1 mM nitrilotriacetic acid (NTA), 147 mM NaCl, 2.7 mM KCl, 5 mM Mops, pH 7 buffer (19, 20) with $[Fe]_{total} = 0-950 \mu$ M ($[Fe^{2+}]_{free} = 0-2.6 \mu$ M) or $[Zn^{2+}]_{total} = 0-200 \mu$ M ($[Zn^{2+}]_{free} = 0-532$ pM) and 0.4 μ M HDAC8. The concentration of bound versus free metal ion was calculated using the program MINEQL+ (Environmental Research Software). The assay mixtures, containing all components except substrate, were incubated for 4 hours on ice in the anaerobic glove box. Assays were incubated at 30°C for 30 min, initiated by the addition of substrate (50 μ M final), and the products analyzed as described above. The activity is dependent on the concentration of $[Me^{2+}]_{free}$ and not the total concentration of the metal ion and buffer as determined by varying the concentration

of the buffer. The metal dissociation constant (K_{Me}) was determined from fitting a binding isotherm (Eq. 1) to the activity versus $[Me^{2+}]_{free}$ data using the program Kaleidagraph (Synergy Software) where A is the activity at saturating metal ion.

Equation 5.2:
$$\frac{v}{v_{max}} = \frac{A}{1 + \frac{K_D}{M_{free}}}$$

Results

HDAC8 expressed in E. coli is mostly Fe-bound

Recombinantly expressed HDAC8-ZZ was purified anaerobically from *E. coli* cells by IgG-affinity as described in Materials and Methods. When the purified protein was analyzed by ICP-MS, the fraction bound with iron was 0.68, while the fraction bound with zinc was 0.18 (Table 5.1) ($\pm 5\%$ standard error). When the media was supplemented with iron or zinc, there was little change in the metal content, with the fraction of Fe-bound found to be 0.42, 0.52, and 0.60 for zinc, iron, or both supplemented, respectively (Table 5.1). This suggests that in *E. coli* cells, HDAC8 binds both Zn^{2+} and Fe^{2+} , with a preponderance of bound iron regardless of growth conditions tested. However, since HDAC8 is a human protein, the metal cofactor bound in *E. coli* may be of limited relevance.

HDAC activity in HeLa cells is oxygen sensitive

HeLa cell lysate was assayed for deacetylase activity using the HDAC8 fluorescent peptide substrate (BIOMOL). Multiple HDAC isoforms can catalyze deacetylation of this substrate (21); therefore the deacetylation activity of the lysate

Table 5.1: Metal content of recombinant HDAC8-ZZ purified from *E. coli*. HDAC8 was purified anaerobically and analyzed as described in Materials and Methods. ICP-MS measurements are $\pm 5\%$ standard error.

Media	Fe-bound	Zn-bound
Minimal	0.57	0.18
+ 20 μM Fe	0.52	0.08
+ 20 μM Zn	0.42	0.17
+ 20 μM Fe + Zn	0.60	0.16

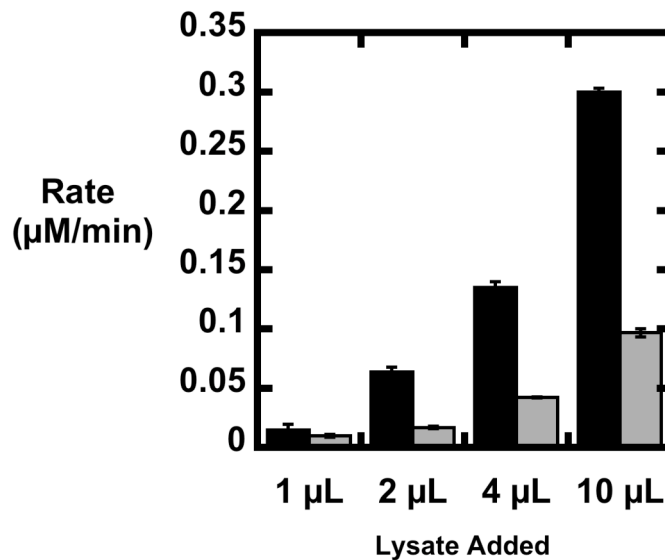


Figure 5.1: HeLa cell lysate is oxygen sensitive 1-10 μL HeLa cell lysate was assayed 3 hours after lysis anaerobically (black bars) or after exposure to room oxygen (gray bars) as described in Materials and Methods.

reflects a variety of HDAC isozymes. The lysate activity decreases significantly (1.5- to 3.8-fold, Fig 5.1) after exposure to oxygen, which is not consistent with a ZnHDAC but predicted in FeHDACs. The oxygen-dependence of the deacetylase activity suggests that HDAC isoforms, presumably including HDAC8, have some Fe-content in human cells.

Endogenously expressed HDAC8 was isolated from HeLa cells by immunoprecipitation assays to measure the activity of this isozyme. When beads that contained immunoprecipitated HDAC8 were assayed, deacetylase activity also decreased upon exposure to oxygen (~2-fold, Fig 5.2). Unexpectedly, the activity did not increase linearly with the volume of beads added to the assay. This may be due to complications arising from attempting to measure deacetylation of a soluble substrate by a bead-immobilized enzyme, in which the accessible surface of the beads may not scale linearly with the volume added. Nonetheless, the observed oxygen-sensitive activity further suggests that HDAC8 is partially Fe-bound in human cells.

Inhibition by SAHA is dependent on the active-site metal ion

Inhibition of class 1 HDACs by metal-chelating compounds is a popular strategy for developing new drugs. Because HDAC8 is activated by both Fe^{2+} and Zn^{2+} *in vitro* and, most likely, *in vivo*, we sought to determine if the identity of the active-site metal impacts the affinity of inhibitors that directly interact with the metal ion. In fact, inhibition of HDAC8 by the hydroxamic acid inhibitor SAHA is dependent on the identity of the active site metal ion. The IC_{50} constant for SAHA was determined as a function of both the enzyme and inhibitor concentrations using eq 5.1, since HDAC8 is unstable at protein concentrations lower than 0.2 μM . The measured IC_{50} values follow the same metal-dependent trend as that of the $k_{\text{cat}}/K_{\text{M}}$ values (13), with Co^{2+} -HDAC

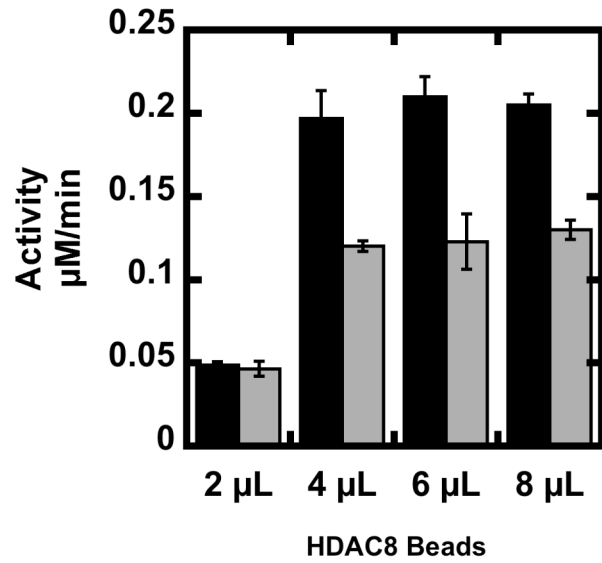


Figure 5.2: Immunoprecipitated HDAC8 is oxygen-sensitive. HDAC8 bound to sepharose beads by immunoprecipitation was added to a standard assay as described in Materials and Methods anaerobically (black bars) or after exposure to room oxygen (gray bars).

binding SAHA with the highest affinity (44 ± 15 nM), followed by Fe^{2+} -HDAC8 (130 ± 40 nM) and Zn^{2+} -HDAC8 (250 ± 25 nM) (Table 5.2; Figure 5.3). The decreased affinity of Zn^{2+} -HDAC8 for SAHA suggests an alteration in the active site environment upon metal substitution. Fe^{2+} and Co^{2+} typically more readily adopt higher coordination complexes than Zn^{2+} (22, 23), providing one possible explanation for the observed trend.

Metal affinities suggest sensitivity to cellular conditions

Of the transition metals that activate HDAC8, Fe and Zn exist in high amounts in the cell, with total concentrations around 0.1 - 0.2 mM in eukaryotic cells and *E. coli* (24-26), and are therefore the most likely native cofactors. Although highly active, cobalt is not abundant in the cell (26) and is not observed in purified protein. The affinity of HDAC8 for Zn^{2+} and Fe^{2+} was measured from the metal-dependent activation of catalytic activity with the free metal concentration maintained using a metal buffer (Figure 5.4). HDAC8 has significantly higher affinity for Zn^{2+} (K_D of 9 ± 1 pM) than Fe^{2+} (K_D of 1.1 ± 0.3 μM), consistent with the higher Lewis acidity of Zn^{2+} (23, 27). At first glance, this disparity suggests that HDAC8 should be a Zn-dependent enzyme in cells. However, previous measurements in eukaryotic cells indicate that the concentration of readily exchangeable Zn ($[\text{Zn}^{2+}]_{\text{free}} \sim 10 - 400$ pM (28, 29) is also orders of magnitude lower than the concentration of readily exchangeable Fe^{2+} , where $[\text{Fe}^{2+}]_{\text{free}} \sim 0.2-6$ μM (30-32). The similarities between the metal affinities of HDAC8 and the readily exchangeable metal concentrations in cells suggest that HDAC8 is thermodynamically poised to be activated by both Zn^{2+} or Fe^{2+} *in vivo*. The metal content of HDAC8 affects both the catalytic activity (13) and the inhibitor affinity *in vitro* (Table 5.2). Therefore, altering the metal

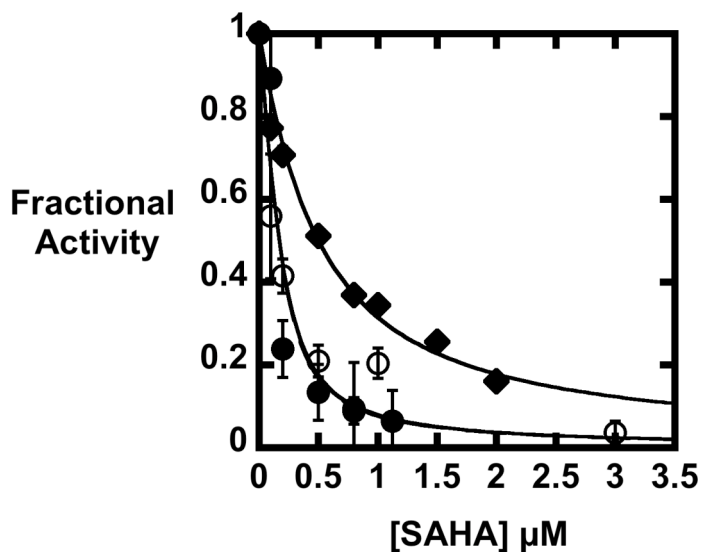


Figure 5.3: Inhibition by SAHA is dependent on the active site metal. HDAC8 substituted with Zn²⁺ (black diamonds), Fe²⁺ (open circles), or Co²⁺ (closed circles) was assayed at 0-3 μM inhibitor and 0.2-0.8 μM enzyme and fit to Equation 5.1 as described in Materials and methods. Data at 0.2 μM HDAC8 is shown; similar values were obtained at higher [E].

Table 5.2: SAHA inhibition constants.

	SAHA K_i (nM)	k_{cat}^a (s ⁻¹)	K_M^a (μM)	k_{cat}/K_M^a (M ⁻¹ s ⁻¹)
Zn ²⁺ -HDAC8	250 ± 25	0.90 ± 0.03	1100 ± 50	800 ± 50
Fe ²⁺ -HDAC8	130 ± 40	0.48 ± 0.01	210 ± 20	2300 ± 160
Co ²⁺ -HDAC8	44 ± 15	1.2 ± 0.2	160 ± 6	7500 ± 300

^a Steady-state parameters are adapted from reference (13)

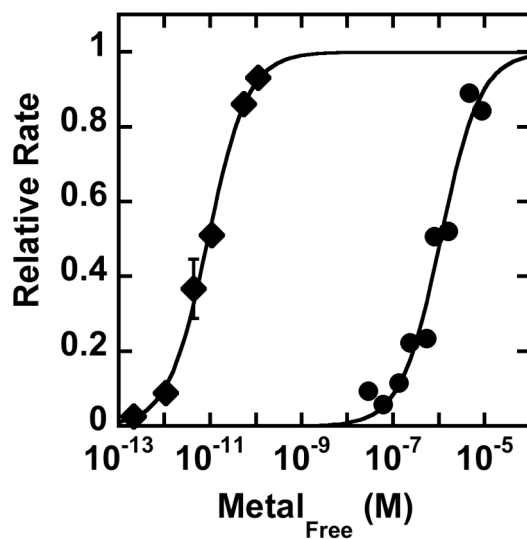


Figure 5.4: HDAC8 metal affinity. HDAC8 was assayed with increasing concentrations of free Zn²⁺(diamonds) or Fe²⁺(circles) as described in Materials and Methods. Equation 5.2 was fit to the activity as a function of $[M_{\text{free}}]$ to calculate $K_D^{M^{2+}}$. The Y-axis depicts normalized k_{cat}/K_M values.

cofactor *in vivo* will affect the catalytic efficiency and, possibly, the affinity and selectivity of acetylated substrates.

Preliminary cell culture pulldowns contain Fe- and Zn-HDAC8

HDAC8-ZZ was purified anaerobically from HeLa cells using a pulldown method and the purified protein was analyzed by ICP-MS as described in Materials and Methods. One issue with these preliminary data is that the metal/protein stoichiometry is >1 , suggesting metal contamination. In general, proteins and other biomolecules have a higher affinity and slower dissociation rate constant for Zn^{2+} than Fe^{2+} (i.e. HDAC8 and LpxC), therefore contamination by zinc is more likely than iron and any equilibration with metals in the lysate is likely to replace most of bound Fe^{2+} with Zn^{2+} . Therefore, the observation of $\sim 3:2$ Zn:Fe by ICP suggests that some or all of HDAC8 in HeLa cells contains some bound iron. However, additional work is needed to more precisely define the stoichiometry and conditions influencing HDAC8 metal binding *in vivo*.

Discussion

HDAC8 is Fe-bound in E. coli

Initial experiments to determine whether HDAC8 binds Fe^{2+} or Zn^{2+} *in vivo* were conducted in *E. coli*. Recombinant HDAC8-ZZ, when purified anaerobically, is mostly Fe-bound. In contrast to the behavior of the similarly studied deacetylase LpxC (see Chapter 4), the metal content of HDAC8 was not found to be dependent on the concentrations of iron or zinc in the growth media. One possible conclusion from these results is that HDAC8 is mostly Fe-bound under diverse cellular conditions. In LpxC, the most likely hypothesis to explain metal switching is that metal content is under thermodynamic control, where increases in available metal ions lead to an increase in the

content of the corresponding metal in the protein. It is possible that HDAC8 does switch metals *in vivo*, but is facilitated by a more complex mechanism that requires additional regulatory elements to properly control its metal ions, which are missing in *E. coli*. An alternative possibility is that small molecule metal chelators that catalyze exchange, such as those that have been proposed for copper enzymes (33), are required for efficient response to changes in intracellular metal ion levels. When the human protein HDAC8 is expressed in *E. coli*, such exchange factors may not properly interact with HDAC8, leading to improper metal ion content. The iron content in recombinant HDAC8 is intriguing, but further experiments are needed to determine whether or not these results are relevant in human cells.

Oxygen sensitivity suggests Fe-HDACs in HeLa cells

One of the principle differences between Fe^{2+} and Zn^{2+} is that Fe^{2+} rapidly oxidizes to Fe^{3+} , while Zn^{2+} is redox-insensitive. Therefore, it is expected that FeHDAC8 activity will be unstable under aerobic conditions, while ZnHDAC8 will not. This behavior was exploited to look for FeHDAC8 in cells, and the observed lysate deacetylase activity was oxygen-sensitive. Multiple HDAC isoforms exist in human cells and contribute the total deacetylase activity in cell extracts; therefore a significant fraction of the HDAC activity across multiple isoforms may contain Fe^{2+} . This oxygen sensitivity was also exploited in specific assays by immunoprecipitating HDAC8, in which the HDAC8-IP activity also decreased after exposure to oxygen. This method gives strong indirect evidence that HDAC8 contains some bound iron in cells, and that the HDAC family may behave similarly.

Inhibitor binding is dependent on active-site metal

In addition to the FDA-approved HDAC inhibitor Zolinza (SAHA), many other compounds are in development as HDAC inhibitors using a metal-chelation strategy. In light of the present questions regarding the *in vivo* metal ion, we sought to evaluate whether changing the metal ion affects the affinity of the inhibitor. A modest decrease of ~2- to 6-fold in K_i was observed when Zn^{2+} was substituted with Fe^{2+} or Co^{2+} , respectively. Although catalytic Zn^{2+} sites have been observed with four to six ligands with a variety of geometries (34), the ligand field stabilization energy of Co^{2+} and Fe^{2+} promotes an energetic preference for higher coordination numbers (35), which may enable Co^{2+} and Fe^{2+} to more readily stabilize a 5-coordinate complex. A similar preference for Fe^{2+} over Zn^{2+} by the hydroxamate inhibitor L-161,240 was observed in LpxC (see Chapter 3). The crystal structure of SAHA bound to HDAC8 shows that the inhibitor hydroxamate binds to the catalytic metal ion in a bidentate manner (36), forming a 5-coordinate Zn center. The lower K_M values observed for Co^{2+} - and Fe^{2+} -HDAC8s relative to that for Zn^{2+} -HDAC8 (13) (Table 5.2) are consistent with a stronger interaction of the substrate carbonyl with Co^{2+} or Fe^{2+} than with Zn^{2+} . Additionally, a crystal structure with bound Fe^{2+} has recently been solved (Dowling, Gattis, Fierke, and Christianson, in preparation). This structure, with the bound hydroxamate inhibitor M344, shows that the metal ligands in FeHDAC8 are identically positioned compared to ZnHDAC8, where both metal-substituted enzymes show identical square pyramidal (5-coordinate) geometry (Figure 5.5). Like SAHA, M344 binds Fe- and Co- substituted HDAC8 more tightly than ZnHDAC8 (Dowling et al, in preparation). Furthermore, the only significant difference in the metal coordination sphere is the orientation of the bound

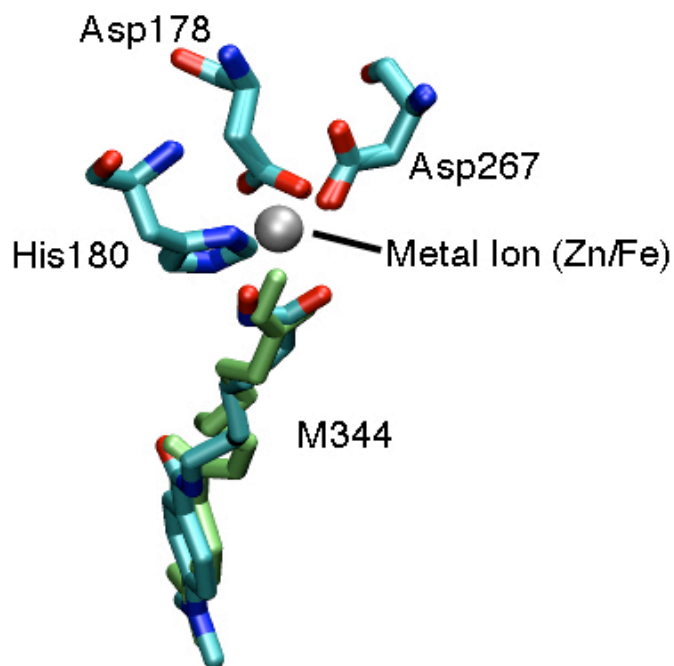


Figure 5.5. Fe- and Zn-substituted HDAC8 structures are nearly indistinguishable. D101L Fe²⁺- and Zn²⁺-HDAC8 structures were aligned in VMD and STAMP and colored by atom type. M344 (4-dimethylamino-N-(7-hydroxyamino)-7-oxoheptyl-benzamide) colored by atom (ZnHDAC8) or in green (FeHDAC8). ZnHDAC8-D101L derived from PDB file 3EW8; the FeHDAC8-D101L structure will be deposited in the PDB upon manuscript submission. FeHDAC8-D101L coordinates were solved by D. Dowling, Univ. of Pennsylvania, and are shown with permission.

inhibitor (Figure 5.5), consistent with the hypothesis that interactions with substrate may be the primary mechanism of rate acceleration of Fe^{2+} relative to Zn^{2+} in HDAC8.

M²⁺ Affinities Suggest Mixed Metal Content in vivo

The affinity of HDAC8 for Zn^{2+} is $\sim 10^5$ -fold tighter than the Fe^{2+} affinity (Figure 5.4), which explains the prevailing belief that HDAC8, and all other metal-dependent HDACs, are exclusively zinc-enzymes. One possibility is that any bound iron is oxidized during purification, and is replaced by the high-affinity zinc ion. A preference for binding Zn^{2+} is predicted by the increased Lewis acidity of Zn^{2+} compared to Fe^{2+} and is also in accordance with the Irving-Williams series of stability constants (23, 27). Nonetheless, it is still possible that HDAC8 could bind either Fe^{2+} or Zn^{2+} *in vivo* since the current data indicate that the intracellular concentration of readily exchangeable Zn^{2+} in cells is orders of magnitude lower than the readily exchangeable Fe^{2+} (5-400 pM vs. 0.2-6 μM) (28-32). Assuming that metal selectivity is determined mainly based on thermodynamics, a competitive binding equation (Equation 5.3) can be used to predict the fractional bound Zn^{2+} and Fe^{2+} at a given concentration of free Zn and Fe. These calculations demonstrate that in the expected physiological range of metal ion concentrations (10 – 400 pM and 0.2 – 6 μM for Zn^{2+} and Fe^{2+} , respectively), HDAC8 could vary from mainly Zn^{2+} -bound (97% Zn / 0.4% Fe) or Fe^{2+} -bound (8% Zn / 77% Fe). Therefore, HDAC8 could be activated by either metal ion *in vivo* and, possibly, the metal ion could vary depending on the cellular conditions. However, the determinant of $\text{Fe}^{2+}/\text{Zn}^{2+}$ selectivity in eukaryotic cells is currently unclear and could be facilitated by metallochaperones, or be under kinetic rather than thermodynamic control (37).

Therefore, direct measurement of metal-bound HDAC8 *in vivo* will be required to definitively identify the native cofactor and determine whether the metal content varies.

Equation 5.3:
$$\frac{E \cdot Fe}{E_{tot}} = \frac{1}{1 + \frac{K_{Fe}}{[Fe]_{free}} \left(1 + \frac{[Zn]_{free}}{K_{Zn}} \right)}$$

Intracellular metal ion homeostasis has previously been shown to control the metal ion bound to the eukaryotic Mn-dependent superoxide dismutase (SOD2) located in the mitochondria of *S. cerevisiae*. Deletion of the mitochondrial Mn transporter, *mtm1*, resulted in elevated mitochondrial iron concentrations and the formation of inactive SOD2 where Fe is substituted for Mn (38). It is likely that the metal cofactor bound to other proteins, such as HDAC8, is also sensitive to intracellular metal homeostasis (reviewed in (37)). Interestingly, the metal K_{DS} predict that HDAC8 is more sensitive to changes in intracellular metal ion concentrations than LpxC (see Chapter 4), as affinities for both metal ions are closer to the expected readily exchangeable concentration. To determine how metal switching may control protein function, further exploration of metal ion affinity, occupancy, and cellular availability *in vivo* is warranted.

Preliminary results consistent with a mixed metal content

The finding that HDAC8 purifies from bacteria predominantly iron-bound is interesting but not necessarily relevant to the metal content in eukaryotic cells. There may be regulatory proteins or metal-exchange factors present in the human cell that are missing or orthogonal in bacteria. Therefore, initial anaerobic purification experiments to determine the *in vivo* metal in HeLa cells were performed. Thus far, the total Zn-content exceeds the protein concentration, and some zinc is purified from cells containing no tagged HDAC8, indicating that zinc contamination is still a problem. However, iron is

also observed bound to the purified HDAC8-ZZ when expressed in HeLa cells, and the greater affinity of zinc versus iron likely leads to overestimation of the zinc content. Therefore, it is reasonable to suggest that HDAC8 purified from human cells contains some bound iron, consistent with our previous experiments. More work is needed to more carefully assess the Fe/Zn ratio, and to evaluate the factors that contribute to metal ion binding and/or switching in the cell. Such factors could include growth conditions and intracellular metal concentrations, as seen in LpxC (Chapter 4), or stress factors such as oxidative stress, which has been shown to alter the levels of metal ions in cells (39).

All of the above data strongly suggest that HDAC8 can function as an Fe-protein *in vivo*. This is important for several reasons, including the interest in HDACs as drug targets for the treatment of cancer, neurodegenerative diseases, and inflammation (5, 7-9). The majority of compounds in development are metal-chelators; as shown in Figure 5.3 and 5.5, altering the active site metal affects the interaction between an inhibitor and the protein. This means that future drug design would benefit from knowing whether a Zn-specific, Fe-specific, or more general chelator moiety is appropriate. In addition, understanding HDAC8 metal ion specificity may provide clues to understanding metal ion homeostasis more generally. Given that both HDAC8 and LpxC, a bacterial protein, seem to behave in a similar manner, it may be the case that Fe/Zn-proteins are much more common than currently thought.

REFERENCES

- (1) Kornberg, R. D., and Lorch, Y. (1999) Twenty-five years of the nucleosome, fundamental particle of the eukaryote chromosome. *Cell* 98, 285-294.
- (2) Jenuwein, T., and Allis, C. D. (2001) Translating the histone code. *Science* 293, 1074-1080.
- (3) Strahl, B. D., and Allis, C. D. (2000) The language of covalent histone modifications. *Nature* 403, 41-45.
- (4) Glozak, M. A., Sengupta, N., Zhang, X., and Seto, E. (2005) Acetylation and deacetylation of non-histone proteins. *Gene* 363, 15-23.
- (5) Drummond, D. C., Noble, C. O., Kirpotin, D. B., Guo, Z., Scott, G. K., and Benz, C. C. (2004) Clinical Development of Histone Deacetylase Inhibitors As Anticancer Agents. *Annu Rev Pharmacol Toxicol*.
- (6) Yang, X. J., and Seto, E. (2007) HATs and HDACs: from structure, function and regulation to novel strategies for therapy and prevention. *Oncogene* 26, 5310-5318.
- (7) Saha, R. N., and Pahan, K. (2005) HATs and HDACs in neurodegeneration: a tale of disconcerted acetylation homeostasis. *Cell Death Differ*.
- (8) Herman, D., Jentsch, K., Burnett, R., Soragni, E., Perlman, S. L., and Gottesfeld, J. M. (2006) Histone deacetylase inhibitors reverse gene silencing in Friedreich's ataxia. *Nat Chem Biol* 2, 551-558.
- (9) Grabiec, A. M., Tak, P. P., and Reedquist, K. A. (2008) Targeting histone deacetylase activity in rheumatoid arthritis and asthma as prototypes of inflammatory disease: should we keep our HATs on? *Arthritis Res Ther* 10, 226.
- (10) Mann, B. S., Johnson, J. R., He, K., Sridhara, R., Abraham, S., Booth, B. P., Verbois, L., Morse, D. E., Jee, J. M., Pope, S., *et al.* (2007) Vorinostat for treatment of cutaneous manifestations of advanced primary cutaneous T-cell lymphoma. *Clin Cancer Res* 13, 2318-2322.
- (11) de Ruijter, A. J., van Gennip, A. H., Caron, H. N., Kemp, S., and van Kuilenburg, A. B. (2003) Histone deacetylases (HDACs): characterization of the classical HDAC family. *Biochem J* 370, 737-749.
- (12) Yang, X. J., and Seto, E. (2008) The Rpd3/Hda1 family of lysine deacetylases: from bacteria and yeast to mice and men. *Nat Rev Mol Cell Biol* 9, 206-218.

- (13) Gantt, S. L., Gattis, S. G., and Fierke, C. A. (2006) Catalytic activity and inhibition of human histone deacetylase 8 is dependent on the identity of the active site metal ion. *Biochemistry* 45, 6170-6178.
- (14) Lowenadler, B., Jansson, B., Paleus, S., Holmgren, E., Nilsson, B., Moks, T., Palm, G., Josephson, S., Philipson, L., and Uhlen, M. (1987) A Gene Fusion System for Generating Antibodies against Short Peptides. *Gene* 58, 87-97.
- (15) Nilsson, B., Moks, T., Jansson, B., Abrahmsen, L., Elmblad, A., Holmgren, E., Henrichson, C., Jones, T. A., and Uhlen, M. (1987) A Synthetic Igg-Binding Domain Based on Staphylococcal Protein-A. *Protein Engineering* 1, 107-113.
- (16) Nilsson, B., Forsberg, G., and Hartmanis, M. (1991) Expression and Purification of Recombinant Insulin-Like Growth-Factors from Escherichia-Coli. *Methods in Enzymology* 198, 3-17.
- (17) Outten, F. W., Outten, C. E., Hale, J., and O'Halloran, T. V. (2000) Transcriptional activation of an Escherichia coli copper efflux regulon by the chromosomal MerR homologue, CueR. *Journal of Biological Chemistry* 275, 31024-31029.
- (18) Gediya, L. K., Chopra, P., Purushottamachar, P., Maheshwari, N., and Njar, V. C. O. (2005) A new simple and high-yield synthesis of suberoylanilide hydroxamic acid and its inhibitory effect alone or in combination with retinoids on proliferation of human prostate cancer cells. *Journal of Medicinal Chemistry* 48, 5047-5051.
- (19) McCall, K. A., and Fierke, C. A. (2000) Colorimetric and fluorimetric assays to quantitate micromolar concentrations of transition metals. *Analytical Biochemistry* 284, 307-315.
- (20) McCall, K. A., and Fierke, C. A. (2004) Probing determinants of the metal ion selectivity in carbonic anhydrase using mutagenesis. *Biochemistry* 43, 3979-3986.
- (21) Riestler, D., Hildmann, C., Grünwald, S., Beckers, T., and Schwienhorst, A. (2007) Factors affecting the substrate specificity of histone deacetylases. *Biochem Biophys Res Commun* 357, 439-445.
- (22) Frausto da Silva, J. J. R., Williams, R.J.P. (2001) *The Biological Chemistry of the Elements*, Oxford University Press, New York.
- (23) Lippard, S. J., Berg, J.M. (1994) *Principles of Bioinorganic Chemistry*, University Science Books, Mill Valley, California.
- (24) Vallee, B. L., and Falchuk, K. H. (1993) The biochemical basis of zinc physiology. *Physiol Rev* 73, 79-118.

- (25) Espósito, B. P., Epsztejn, S., Breuer, W., and Cabantchik, Z. I. (2002) A review of fluorescence methods for assessing labile iron in cells and biological fluids. *Anal Biochem* 304, 1-18.
- (26) Outten, C. E., and O'Halloran, T. V. (2001) Femtomolar sensitivity of metalloregulatory proteins controlling zinc homeostasis. *Science* 292, 2488-2492.
- (27) Irving, H., and Williams, R. J. P. (1948) Order of Stability of Metal Complexes. *Nature* 162, 746-747.
- (28) Bozym, R. A., Thompson, R. B., Stoddard, A. K., and Fierke, C. A. (2006) Measuring picomolar intracellular exchangeable zinc in PC-12 cells using a ratiometric fluorescence biosensor. *ACS Chem Biol* 1, 103-111.
- (29) Vinkenborg, J. L., Nicolson, T. J., Bellomo, E. A., Koay, M. S., Rutter, G. A., and Merckx, M. (2009) Genetically encoded FRET sensors to monitor intracellular Zn²⁺ homeostasis. *Nature Methods* 6, 737-U710.
- (30) Epsztejn, S., Kakhlon, O., Glickstein, H., Breuer, W., and Cabantchik, Z. I. (1997) Fluorescence analysis of the labile iron pool of mammalian cells. *Analytical Biochemistry* 248, 31-40.
- (31) Petrat, F., de Groot, H., and Rauen, U. (2001) Subcellular distribution of chelatable iron: a laser scanning microscopic study in isolated hepatocytes and liver endothelial cells. *Biochem J* 356, 61-69.
- (32) MacKenzie, E. L., Iwasaki, K., and Tsuji, Y. (2008) Intracellular iron transport and storage: from molecular mechanisms to health implications. *Antioxid Redox Signal* 10, 997-1030.
- (33) Kim, B. E., Nevitt, T., and Thiele, D. J. (2008) Mechanisms for copper acquisition, distribution and regulation. *Nat Chem Biol* 4, 176-185.
- (34) Hernick, M., and Fierke, C. A. (2005) Zinc hydrolases: The mechanisms of zinc-dependent deacetylases. *Archives of Biochemistry and Biophysics* 433, 71-84.
- (35) Berg, J. M., and Merkle, D. L. (1989) On the Metal-Ion Specificity of Zinc Finger Proteins. *Journal of the American Chemical Society* 111, 3759-3761.
- (36) Somoza, J. R., Skene, R. J., Katz, B. A., Mol, C., Ho, J. D., Jennings, A. J., Luong, C., Arvai, A., Buggy, J. J., Chi, E., *et al.* (2004) Structural snapshots of human HDAC8 provide insights into the class I histone deacetylases. *Structure* 12, 1325-1334.
- (37) Waldron, K. J., Rutherford, J. C., Ford, D., and Robinson, N. J. (2009) Metalloproteins and metal sensing. *Nature* 460, 823-830.

- (38) Yang, M., Cobine, P. A., Molik, S., Naranuntarat, A., Lill, R., Winge, D. R., and Culotta, V. C. (2006) The effects of mitochondrial iron homeostasis on cofactor specificity of superoxide dismutase 2. *Embo Journal* 25, 1775-1783.
- (39) Kroncke, K. D., and Klotz, L. O. (2009) Zinc Fingers as Biologic Redox Switches? *Antioxidants & Redox Signaling* 11, 1015-1027.

CHAPTER 6. SUMMARY, CONCLUSIONS, AND FUTURE DIRECTIONS

Summary and Conclusions

The preceding chapters describe studies on two metallohydrolases, UDP-3-*O*-(*R*-3-hydroxymyristoyl)-*N*-acetylglucosamine deacetylase (LpxC) and histone deacetylase 8 (HDAC8). These studies answer important questions about the chemical mechanism, as well as raise the possibility that iron may replace zinc as the catalytic metal ion, depending on cellular conditions.

Mechanism of LpxC

Zinc hydrolases typically function via a catalytic general acid/base mechanism (1). In LpxC, previously published data suggests that a conserved glutamate, E78 in *E. coli*, functions as the general base, deprotonating the nucleophilic water as it attacks the carbonyl substrate (2, 3). However, determining the identity of the general acid has been more difficult. This is frequently the case in zinc hydrolases that contain active site histidines, which can function as either a general acid or as an electrostatic catalyst (1, 4). In LpxC, H265 is proposed to function either as an electrostatic catalyst, by stabilizing the oxyanion tetrahedral intermediate, or as a general acid, by protonating the amine leaving group (Figure 6.1).

To determine the precise role of H265, a combination of mutagenesis and expressed protein ligation (EPL) was used. When H265 was mutated to alanine, a

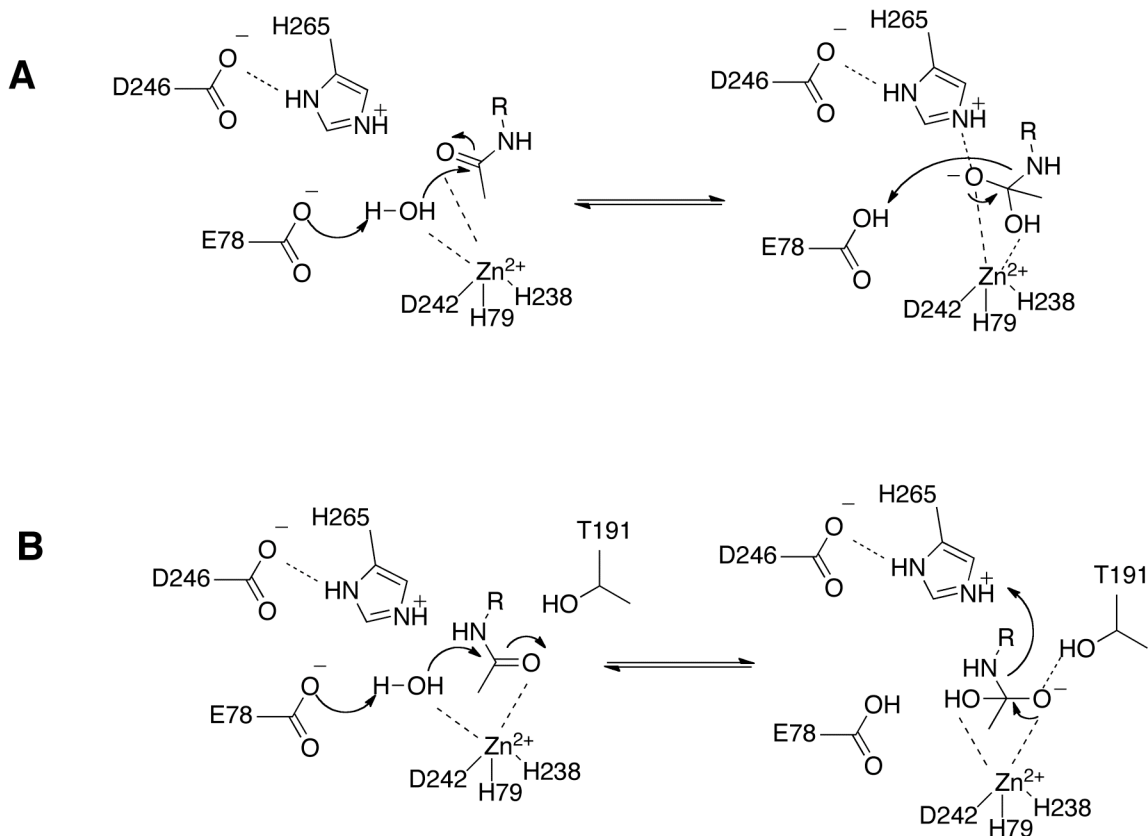


Figure 6.1: Possible LpxC chemical mechanisms. (A) E78 as a single general acid/base, (B) E78 as the general base, H265 as the general acid.

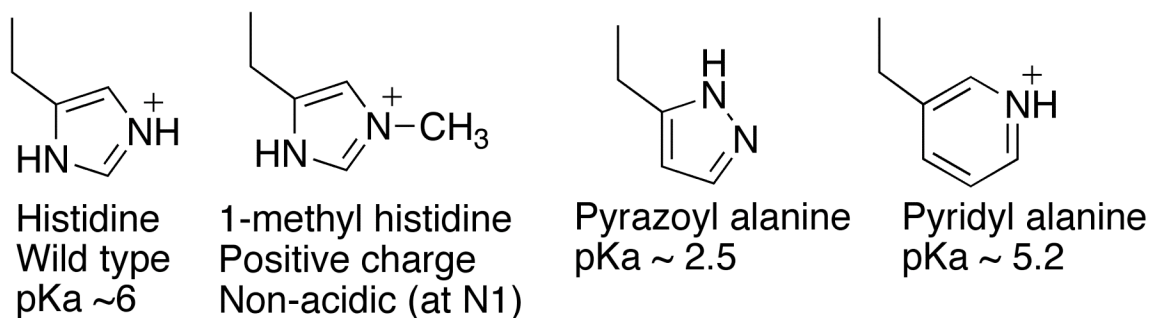


Figure 6.2: Analogues used in EPL studies.

>2000-fold loss in activity was observed in *E. coli*. Mutation to glutamine or arginine, which separately test the ability to rescue catalysis by introducing hydrogen bonding and positive charge, restore k_{cat}/K_M to within 600- and 170-fold of WT, respectively. This 3 – 10-fold increase relative to the alanine mutant suggests that a positive charge is important at H265, but that activity remains > 100-fold lower than that of the wild-type enzyme. However, mutagenesis using the 20 naturally occurring amino acids is limited, and an alternative explanation is that positively charged amino acid side-chains cannot achieve the proper orientation in the active site relative to histidine for efficient catalysis. Therefore, the more precise technique of expressed protein ligation (EPL) (5-8) was used. As described in Chapter 1, EPL allows incorporation of any chemical group accessible by synthetic chemistry, and perturbs the protein only by introducing a cysteine at a ligation site on the N-terminal side of the site of interest. To use this method to analyze the role of H265 in *A. aeolicus* LpxC (AaLpxC), residues 1-246 were ligated with a 25 amino acid peptide corresponding to residues 247-271, leading to a semisynthetic protein with a Y247C mutation and the last 11 amino acids deleted. The last 11 amino acids were left off the synthetic peptide for ease of synthesis and to match the construct previously used in crystallography experiments (see future directions below).

To examine the function of H265, four functional groups were incorporated at that position in the semisynthetic LpxC by EPL (Figure 6.2). In addition to the histidine control, they included a non-acidic positive charge at N1 (methyl-histidine), and two acidic histidine analogues with perturbed pK_a s: pyrazole ($pK_a \sim 2.5$), and pyridyl-alanine ($pK_a \sim 5.2$). Methyl-histidine (MeHis) was not able to rescue activity, suggesting that even a positively charged residue with close structural similarity to histidine is not

sufficient to restore WT-like activity. With a pK_a value of 2.5, pyrazole is not expected to be protonated at the pH tested, and LpxC with this modification was inactive. However, LpxC containing pyridyl-alanine (pyrAla) at this position was active, and catalyzed deacetylation within 1.2-fold of WT at pH 7.5. In addition, pH profiles demonstrated that pK_{a2} for LpxC-pyrAla is shifted ~ 1 unit lower, as expected when comparing the pK_a s of histidine and pyrAla.

These data disfavor the single catalytic acid/base mechanism, and provide the first direct evidence that LpxC functions via a general acid/base pair mechanism. This is a significant finding, as previous kinetic, mutagenesis, pH profiles, NMR, and crystallographic studies were consistent with the acid/base pair mechanism but do not definitively distinguish between the two mechanisms. A detailed understanding of the catalytic mechanism of LpxC is important for the development of inhibitors for this antibiotic target, as well as understanding the diversity and evolution of the zinc hydrolase family.

Fe/Zn metal switching

Although described as ‘zinc hydrolases’, many such enzymes are active with a variety of divalent metal ions (1). LpxC had previously been demonstrated to be active with several divalent species, including Co^{2+} , Ni^{2+} , Mn^{2+} , Cd^{2+} , and Zn^{2+} (9). However, Fe^{2+} had not been examined until recently, when it was found that Fe^{2+} -LpxC has activity 6-8 fold greater than with the presumed *in vivo* metal ion, Zn^{2+} (see Chapter 3-4 and (10)). Iron is highly abundant in the cell, and is thought to have a higher readily exchangeable or ‘free’ metal ion concentration (11-14), leading to the proposal that LpxC could actually be an iron enzyme like the previously mis-classified Fe-enzymes peptide

deformylase, LuxS, and others (15, 16). Subsequent studies of FeLpxC demonstrated that substitution with Fe^{2+} primarily enhances k_{cat} and $k_{\text{cat}}/K_{\text{M}}$ with a minimal effect on K_{M} . Switching from zinc to iron also alters affinity for small molecules 2 – 6-fold. X-ray absorption spectroscopy suggests that FeLpxC is 5-coordinate compared to the previously studied 4-coordinate ZnLpxC (17), suggesting one possible basis for the observed rate acceleration. Significantly, FeLpxC is oxygen-sensitive, in contrast to ZnLpxC, which is stable in oxygen. When affinity-tagged LpxC was rapidly purified anaerobically, it was found to contain a mixture of Fe and Zn, and the ratio of Fe/Zn was found to vary as a function of the cellular Fe/Zn. Cell lysates containing only endogenous LpxC activity similarly exhibited oxygen-sensitive deacetylase activity that varied with growth-conditions. Although the affinity of LpxC for Zn^{2+} is much tighter than the affinity for Fe^{2+} , the K_{D} values for each are comparable to the expected free metal ion concentrations *in vivo*, leading to a model in which LpxC metal ion switching can be explained by equilibria.

These findings lead to several important conclusions. First, they call into question the prevailing assumption that LpxC is a zinc metalloenzyme. Previous researchers likely missed Fe-activity due to its lability in room oxygen, and future work should be informed by the knowledge that LpxC can use Fe^{2+} both *in vitro* and *in vivo*. Second, from a purely practical level, LpxC is an antibiotic target where chelating the metal ion is the principle strategy; knowing which metal ion is bound under what cellular conditions will assist these efforts.

Finally, these findings raise a broader question about metal specificity in general. It has been known for many years that *in vitro*, numerous metalloenzymes can function

with multiple metal ions (1). However, the idea that a protein *in vivo* could use different metal ions under different cellular conditions has been less well appreciated (18). In Chapter 5, the idea that metal switching could be a more wide spread phenomenon was explored by examining the metal specificity of the mammalian protein HDAC8. Like LpxC, HDAC8 is a member of a large “zinc” hydrolase family, and was previously shown to be active with a variety of divalent metals, including Zn^{2+} and Fe^{2+} (19). Despite its characterization as a zinc protein, several interesting pieces of evidence point to HDAC8 being able to use iron *in vivo*, including oxygen-sensitive activity in cell lysates and immunoprecipitation assays. Determination of the dissociation constants revealed that like LpxC, the metal content of HDAC8 would be expected to be sensitive to intracellular metal ion concentrations. It is likely that HDAC8 is or can be an Fe^{2+} -enzyme under certain cellular conditions, and it remains to be seen whether the metal ion content is regulated by stimuli such as growth conditions, oxidative stress, and the like, and whether this is an important novel method for regulating the activity of metalloenzymes.

Future directions

Mechanism of LpxC

The sensitivity of the LpxC activity to the structure of the amino acid at position 265 argues strongly for a general acid/general base pair mechanism. However, spectroscopic or structural evaluation of LpxC containing the histidine analogue pyrAla would further examine the role of this site as the catalytic general acid. When constructing the semisynthetic LpxC via EPL, the C-terminal 11 amino acids were deleted so that the semisynthetic protein would mirror the construct that yielded optimal

crystals for solving the AaLpxC structure (20). In the near future, we intend to obtain sufficient material to crystallize and solve the structure of AaLpxC-pyrAla, in collaboration with Prof. David Christianson, Univ. of Pennsylvania. These experiments will be useful in showing the orientation of the H265 analogue, as well as the residue that forms a hydrogen bonds with H265, D246. We would expect to see the pyrAla overlay well with the native histidine structure, and if the structure was solved with the tetrahedral mimic cacodylate, the aromatic ring should be rotated around its axis such that the acidic nitrogen is positioned closest to the $-CH_3$, in analogy to its role in protonating the leaving group amine (2). Additionally, these analogues should be tested in the context of the D246A mutation to determine its role in positioning the unnatural amino acid. If D246 does hold the methyl-histidine in the wild-type conformation, as discussed in Chapter 2, it is possible that the D246A enzyme would allow the imidazole to rotate and facilitate N3 to act as a general acid, leading to an increase in activity.

NMR would also be a useful tool for measuring the pK_a of the pyrAla moiety in LpxC to test the general acid/base pair mechanism. The pyrAla has a single nitrogen, and would be expected to have a well defined ^{15}N resonance (by natural abundance) in relation to the other histidines in LpxC. Correlating the observed differences in activity between histidine and pyrAla with the chemical shifts observed by NMR as a function of pH would provide strong evidence that the pK_a observed by activity reflects the ionization of the pyridyl nitrogen, as hypothesized. We hope to conduct these experiments in collaboration with Prof. Hashim Al-Hashimi, Univ. of Michigan Dept. of Chemistry.

The development of EPL as a tool also has more general applications. In LpxC, it could be used at other positions for more targeted studies, including probing the role of specific residues in the hydrophobic tunnel or the UDP binding site to provide additional molecular recognition information that could be used to improve upon lead compounds in drug development. These experiments also validate EPL as a method for determining the role of a catalytic histidine in any enzyme, which has not been possible to date. The M^{2+} -deacetylase HDAC8 shares many mechanistic similarities with LpxC, and has been proposed on the basis of crystallography to function via a general acid/base pair mechanism (21). Recent evidence from kinetic studies, mutagenesis, and pH profiles have called this into question ((22, 23), Gantt and Fierke, unpublished). EPL experiments such as those described herein would be very useful in the study of HDAC8.

An alternative method that may be more generally applicable would be to use a fully expressed protein with the unnatural amino acids generated via an orthogonal tRNA/tRNA synthetase, such as those developed by Schultz and coworkers (24, 25). This method has significant advantages, as the entire protein is synthesized *in vivo* by the cell, eliminating complications arising from peptide synthesis and ligation, as well as the potential for insoluble protein fusions, as observed in the LpxC EPL experiments (Chapter 2). Assuming that the protein expresses reasonably well, it can be purified by whatever standard methods exist for the WT protein it is to be compared to. However, this method is limited by the orthogonal tRNA/tRNA synthetases that must be created, usually by directed evolution methods, for each unnatural amino acid. Currently, incorporation of unnatural amino acids such as methyl histidine have been reported (25), and in principle, other analogues like those described above could be used pending

successful rounds of tRNA/tRNA synthetase optimization as previously described (24, 25).

Fe/Zn Metal switching

The results with LpxC and HDAC8 demonstrating metal switching open up a host of novel ideas that can be tested. In LpxC, it is clear that changes in growth conditions alter the metal ion status of the protein, but several questions remain about how that process might occur. The experiments to date on LpxC have not addressed the time-dependence of LpxC metal switching *in vivo*, or whether individual proteins can switch back and forth between zinc and iron metal cofactors as conditions are altered. To address these questions, pulse-chase experiments would be valuable, in which cultures expressing LpxC in certain metal conditions are switched to media with different metals and the metals bound to LpxC are measured as a function of time using the described anaerobic pulldown procedure (Chapter 4). By monitoring both the cellular metal ratio and the bound metal ratio, it should be possible to determine how rapidly cells respond to changes in metals in the growth media, and how rapidly metalloproteins, like LpxC, re-equilibrate. These experiments could be done with and without protein synthesis inhibitors, to determine whether switching occurs via an equilibrium process, as suggested from the current data, or whether switching is achieved only when older protein is degraded and newly synthesized protein folds around the newly favored metal ion.

A further avenue of research would be to determine what, if any, evolutionary advantage is gained by the ability to use both iron and zinc. One method by which eukaryotes fight infection is by chelating circulating iron to levels too low to support

bacterial growth (26-28). It may be interesting to examine the relationship between iron-limited growth rates and LpxC expression and/or metal ion content. Additionally, the determinants of Fe/Zn specificity in proteins is not yet well understood. One difference between the metal sites of zinc-specific proteins (such as carbonic anhydrase II) and LpxC and HDAC8, is the absence of “second-shell” hydrogen bonding groups between the protein and the metal ligands (29, 30). This may be a hallmark of proteins that switch between Fe and Zn metals and should be explored further. If mutants are discovered that alter the Zn/Fe selectivity, then these mutants can also be used to explore the evolutionary advantages of Zn/Fe switching. Analysis of the growth rates and cell viability of *E. coli* with these LpxC mutants in variable media would begin to address this question.

In HDAC8, many more questions about the *in vivo* metal remain to be answered. Anaerobic purification from mammalian cells still requires careful optimization to definitively analyze the metals bound to HDAC8 and to explore the possibility of metal switching. The current evidence strongly suggests that there is some FeHDAC8 *in vivo*, so determining how much, and under what conditions FeHDAC8 or ZnHDAC8 is favored will be the most crucial experiments going forward. If HDAC8 does vary its metal depending on intracellular metal ion concentrations, that will suggest that many members of this metallohydrolase superfamily should be studied more carefully for equilibrium-based metal switching. If instead, the metal bound to HDAC8 does not correlate with metal content in the media, it will be important to see what other stimuli might be responsible for determining the identity of the active site metal. In eukaryotic cells, it may be the case that extracellular metal ion concentrations are not variable

enough to induce switching, but that other changes, such as oxidative stress (31, 32), do. In this model, enzyme-bound Fe^{2+} is oxidized, forming Fe^{3+} , which dissociates from the enzyme and is replaced by Zn^{2+} . Determination as to whether growth conditions, oxidative stress, or any other stimuli regulate metal switching in HDAC8 will be an important avenue of future research.

Concluding remarks

This work has revealed novel features of two medically important metallohydrolases, LpxC, which is an antibiotic target, and HDAC8, which has potential for treatments of cancer, neurodegenerative diseases, and inflammation. Determining the chemical mechanism by EPL is an important step in understanding LpxC in detail, but also is a step forward in using chemical biology tools to study the mechanism of metallohydrolases, which hopefully can be extended to explore the role of histidines in other enzymes, as described above. In both LpxC and HDAC8, the concept of catalytic metal switching between iron and zinc contradicts the prevailing assumption in the literature that a metalloenzyme exclusively uses one metal ion at all times. Although they are members of the same broad class of metallohydrolases, LpxC and HDAC8 are essentially unrelated proteins, making it unlikely they are unique in this ability to use multiple metal ions *in vivo*. The more probable assumption is that metal switching is a common phenomenon, affecting the activity and regulation of numerous proteins, and deserves further study.

REFERENCES

- (1) Hernick, M., and Fierke, C. A. (2005) Zinc hydrolases: The mechanisms of zinc-dependent deacetylases. *Archives of Biochemistry and Biophysics* 433, 71-84.
- (2) Hernick, M., Gennadios, H. A., Whittington, D. A., Rusche, K. M., Christianson, D. W., and Fierke, C. A. (2005) UDP-3-O-((R)-3-hydroxymyristoyl)-N-acetylglucosamine deacetylase functions through a general acid-base catalyst pair mechanism. *J Biol Chem* 280, 16969-16978.
- (3) McClerren, A. L., Zhou, P., Guan, Z., Raetz, C. R., and Rudolph, J. (2005) Kinetic analysis of the zinc-dependent deacetylase in the lipid A biosynthetic pathway. *Biochemistry* 44, 1106-1113.
- (4) Christianson, D. W., and Lipscomb, W. N. (1989) Carboxypeptidase-A. *Accounts of Chemical Research* 22, 62-69.
- (5) Pellois, J. P., and Muir, T. W. (2006) Semisynthetic proteins in mechanistic studies: using chemistry to go where nature can't. *Current opinion in chemical biology* 10, 487-491.
- (6) Hahn, M. E., and Muir, T. W. (2005) Manipulating proteins with chemistry: a cross-section of chemical biology. *Trends Biochem Sci* 30, 26-34.
- (7) Muir, T. W. (2003) Semisynthesis of proteins by expressed protein ligation. *Annu Rev Biochem* 72, 249-289.
- (8) Muir, T. W., Sondhi, D., and Cole, P. A. (1998) Expressed protein ligation: A general method for protein engineering. *Proc Natl Acad Sci U S A* 95, 6705-6710.
- (9) Jackman, J. E., Raetz, C. R., and Fierke, C. A. (1999) UDP-3-O-(R-3-hydroxymyristoyl)-N-acetylglucosamine deacetylase of *Escherichia coli* is a zinc metalloenzyme. *Biochemistry* 38, 1902-1911.
- (10) Hernick, M., Gattis, S. G., Penner-Hahn, J. E., and Fierke, C. A. (2010) Activation of *E. coli* UDP-3-O-(R-3-hydroxymyristoyl)-N-acetylglucosamine deacetylase by Fe²⁺ yields a more efficient enzyme with altered ligand affinity. *Biochemistry* 49, 2246-2255.
- (11) Bozym, R. A., Thompson, R. B., Stoddard, A. K., and Fierke, C. A. (2006) Measuring picomolar intracellular exchangeable zinc in PC-12 cells using a ratiometric fluorescence biosensor. *ACS Chem Biol* 1, 103-111.
- (12) Vinkenborg, J. L., Nicolson, T. J., Bellomo, E. A., Koay, M. S., Rutter, G. A., and Merckx, M. (2009) Genetically encoded FRET sensors to monitor intracellular Zn²⁺ homeostasis. *Nature Methods* 6, 737-U710.

- (13) Epsztejn, S., Kakhlon, O., Glickstein, H., Breuer, W., and Cabantchik, Z. I. (1997) Fluorescence analysis of the labile iron pool of mammalian cells. *Analytical Biochemistry* 248, 31-40.
- (14) Petrat, F., de Groot, H., and Rauen, U. (2001) Subcellular distribution of chelatable iron: a laser scanning microscopic study in isolated hepatocytes and liver endothelial cells. *Biochem J* 356, 61-69.
- (15) Rajagopalan, P. T. R., Yu, X. C., and Pei, D. H. (1997) Peptide deformylase: A new type of mononuclear iron protein. *Journal of the American Chemical Society* 119, 12418-12419.
- (16) Zhu, J. G., Dizin, E., Hu, X. B., Wavreille, A. S., Park, J., and Pei, D. H. (2003) S-ribosylhomocysteinase (LuxS) is a mononuclear iron protein. *Biochemistry* 42, 4717-4726.
- (17) McClure, C. P., Rusche, K. M., Peariso, K., Jackman, J. E., Fierke, C. A., and Penner-Hahn, J. E. (2003) EXAFS studies of the zinc sites of UDP-(3-O-acyl)-N-acetylglucosamine deacetylase (LpxC). *Journal of Inorganic Biochemistry* 94, 78-85.
- (18) Waldron, K. J., Rutherford, J. C., Ford, D., and Robinson, N. J. (2009) Metalloproteins and metal sensing. *Nature* 460, 823-830.
- (19) Gantt, S. L., Gattis, S. G., and Fierke, C. A. (2006) Catalytic activity and inhibition of human histone deacetylase 8 is dependent on the identity of the active site metal ion. *Biochemistry* 45, 6170-6178.
- (20) Whittington, D. A., Rusche, K. M., Shin, H., Fierke, C. A., and Christianson, D. W. (2003) Crystal structure of LpxC, a zinc-dependent deacetylase essential for endotoxin biosynthesis. *Proc Natl Acad Sci USA* 100, 8146-8150.
- (21) Finnin, M. S., Donigian, J. R., Cohen, A., Richon, V. M., Rifkind, R. A., Marks, P. A., Breslow, R., and Pavletich, N. P. (1999) Structures of a histone deacetylase homologue bound to the TSA and SAHA inhibitors. *Nature* 401, 188-193.
- (22) Gantt, S. L., Joseph, C. G., and Fierke, C. A. (2009) Activation and inhibition of histone deacetylase 8 by monovalent cations. *J Biol Chem*.
- (23) Dowling, D. P., Gantt, S. L., Gattis, S. G., Fierke, C. A., and Christianson, D. W. (2008) Structural Studies of Human Histone Deacetylase 8 and Its Site-Specific Variants Complexed with Substrate and Inhibitors (dagger) (,) (double dagger). *Biochemistry* 47, 13554-13563.
- (24) Wang, L., and Schultz, P. G. (2005) Expanding the genetic code. *Angew. Chem. Int. Ed.* 44, 34-66.

- (25) Liu, C., and Schultz, P. G. (2010) Adding New Chemistries to the Genetic Code. *Annual Review of Biochemistry* 79, Online Advance March 9.
- (26) Holmes, M. A., Paulsene, W., Jide, X., Ratledge, C., and Strong, R. K. (2005) Siderocalin (Lcn 2) also binds carboxymycobactins, potentially defending against mycobacterial infections through iron sequestration. *Structure* 13, 29-41.
- (27) Goetz, D. H., Holmes, M. A., Borregaard, N., Bluhm, M. E., Raymond, K. N., and Strong, R. K. (2002) The neutrophil lipocalin NGAL is a bacteriostatic agent that interferes with siderophore-mediated iron acquisition. *Mol Cell* 10, 1033-1043.
- (28) Neilands, J. B. (1995) Siderophores: structure and function of microbial iron transport compounds. *J Biol Chem* 270, 26723-26726.
- (29) DiTusa, C. A., McCall, K. A., Christensen, T., Mahapatro, M., Fierke, C. A., and Toone, E. J. (2001) Thermodynamics of metal ion binding. 2. Metal ion binding by carbonic anhydrase variants. *Biochemistry* 40, 5345-5351.
- (30) DiTusa, C. A., Christensen, T., McCall, K. A., Fierke, C. A., and Toone, E. J. (2001) Thermodynamics of metal ion binding. 1. Metal ion binding by wild-type carbonic anhydrase. *Biochemistry* 40, 5338-5344.
- (31) Imlay, J. A. (2008) Cellular defenses against superoxide and hydrogen peroxide. *Annu Rev Biochem* 77, 755-776.
- (32) Kroncke, K. D., and Klotz, L. O. (2009) Zinc Fingers as Biologic Redox Switches? *Antioxidants & Redox Signaling* 11, 1015-1027.